



SPAWAR  
Systems Center  
San Diego

# ILIR 98

SSC SAN DIEGO

IN-HOUSE LABORATORY

INDEPENDENT RESEARCH

1998 ANNUAL REPORT

TECHNICAL DOCUMENT 3049  
April 1999

# **SSC SAN DIEGO IN-HOUSE LABORATORY INDEPENDENT RESEARCH 1998 ANNUAL REPORT**

Approved for public release;  
distribution is unlimited.



SSC San Diego  
San Diego, CA 92152-5001

# CONTENTS

<b>INTRODUCTION</b> .....	<b>1</b>
<b>SELECTED ILIR PROJECTS</b> .....	<b>5</b>
Development of Ultramicroelectrode (UME) Arrays for Use in a Remote Probe .....	7
Underwater Acoustic Array Processing in High-Slope Shallow-Water Environments .....	19
A New Sparse Complete Orthogonal Factorization Method as Applied to Bistatic Target-Strength Prediction .....	31
<b>PROJECT SUMMARIES</b> .....	<b>39</b>
<b>COMMAND AND CONTROL</b> .....	<b>41</b>
Algebraic Estimation of Multivalued Phenomena with Applications to Data Fusion .....	43
Using IMPORT to Implement Complex Behaviors in Simulations .....	48
Robust Control of Multiclass Queuing Systems for Command, Control, Communications, Computers, and Intelligence (C <sup>4</sup> I) .....	49
<b>COMMUNICATIONS</b> .....	<b>51</b>
Applications of Stochastic Nonlinear Dynamics to Communications .....	53
Performance Analysis of a Decision Feedback Equalizer for Line-of-Sight Digital Radio .....	56
Development and Analysis of Turbo Codes for Navy Applications .....	59
Resonantly Enhanced EHF Electroabsorption Modulator with a Novel N-P-I-N Diode Structure for Analog Fiber-Optic Link .....	62
Fiber-Optic Add/Drop Multiplexers Produced by Writing Gratings on Fused-Fiber Tapered Couplers .....	66
H <sup>∞</sup> Impedance Matching for Broadband Antennas .....	69
Telesonar Channel Models .....	72
<b>INTELLIGENCE, SURVEILLANCE, AND RECONNAISSANCE</b> .....	<b>77</b>
Generalized Higher Order Crossings Theory and Practice .....	79
Active Matched-Field Tracking .....	81
Solid-State Blue Laser Development .....	83
Pixon-Based Image Reconstruction from Inverse Synthetic Aperture Radar Data .....	86
3-D Propagation in Shallow Water Overlaying an Elastic Bottom .....	90
Impulsive Snap-through Acoustic Projector (ISnAP) .....	93
<b>OTHER LEADERSHIP AREAS</b> .....	<b>95</b>
Computational Modeling of Sediment Resuspension .....	97
Anti-Ice Coatings: New Low Surface Free Energy Coatings for Easy Ice-Release .....	100
Surface-Plasmon Flat-Panel Display .....	103
Propwash/Wake Resuspension in San Diego Bay (The Grand Plan III) .....	106
Biosonar Ensonification of Buried Mines .....	109
Exact Diagonalization of Large Sparse Matrices .....	113

<b>ACCOMPLISHMENTS AND IMPACTS .....</b>	<b>115</b>
Fiber-Optic Chemical Sensor Systems .....	117
Faster-Than-Real-Time Synthetic Forces (FTRT SF) Simulation .....	119
<b>FY 98 TRANSITIONED PROJECTS .....</b>	<b>121</b>
Applications of Stochastic Nonlinear Dynamics to Communications .....	123
Fiber-Optic Add/Drop Multiplexers Produced by Writing Gratings on Fused-Fiber Tapered Couplers .....	123
Surface-Plasmon Flat-Panel Display .....	124
Telesonar Channel Models .....	124
<b>PUBLICATIONS AND PRESENTATIONS .....</b>	<b>125</b>
REFEREED PAPERS (PUBLISHED OR ACCEPTED) .....	127
REFEREED PAPERS (SUBMITTED) .....	128
BOOKS/CHAPTERS .....	128
IN-HOUSE PUBLICATIONS .....	128
PROCEEDINGS .....	129
PRESENTATIONS TO PROFESSIONAL MEETINGS .....	131
<b>HONORS AND AWARDS .....</b>	<b>135</b>
<b>PATENT ACTIVITY .....</b>	<b>141</b>
<b>INDEPENDENT RESEARCH</b>	
Patents Issued .....	143
Claims Allowed; Notice of Allowance .....	144
Patent Applications Filed .....	145
Invention Disclosures Authorized .....	149
Invention Disclosures Submitted .....	150
<b>INDEPENDENT EXPLORATORY DEVELOPMENT</b>	
Patent Issued .....	154
Claims Allowed; Notice of Allowance .....	154
Patent Application Filed .....	154
<b>PROJECT TABLES .....</b>	<b>155</b>
SSC San Diego FY 98 ILIR Database .....	157
SSC San Diego FY 99 ILIR Database .....	160
<b>GLOSSARY .....</b>	<b>163</b>
<b>AUTHOR INDEX .....</b>	<b>173</b>



# INTRODUCTION

## INTRODUCTION

New and innovative ideas proposed by the scientists and engineers of the Space and Naval Warfare (SPAWAR) Systems Center, San Diego (SSC San Diego) are supported and encouraged through the In-house Laboratory Independent Research (ILIR) Program, which is administered by the Office of Naval Research (ONR). The ILIR program is implemented at SSC San Diego under the authority of the Deputy Executive Director for Science, Technology and Engineering and is managed by the Science and Technology Office. This program supports basic scientific research in several areas of interest to the Navy, including command and control, communications, surveillance, and navigation.

The FY 98 ILIR projects were selected under the direction of Dr. Eric Hendricks, Head, Science and Technology Office, and coordinated by Dr. Larry Flesner, Science and Technology Office. The selection process began with the 20 March 1997 call for proposals in four ILIR Thrust Areas. These areas are Command and Control; Communications; Intelligence, Surveillance, and Reconnaissance; and Other Leadership Areas. Scientists and engineers responded with 62 written proposals, which were screened for scientific merit and Navy relevance and then evaluated by panels of experts. These panels included Dr. Flesner; Dr. George Dillard, Scientist (Intelligence, Surveillance, and Reconnaissance Department); SSC San Diego technical experts; and line management for each principal investigator. Based on evaluations by these panels and an administrative review, 25 projects were selected, with a total funding of \$2,299,585.

This report describes the funding and accomplishments of the ILIR program for the period 1 October 1997 through 30 September 1998. Included are lists of publications and patents, honors and awards, and tables consisting of the SSC San Diego FY 98 and projected FY 99 ILIR databases. Four main sections are designated by focus area and include descriptions of the FY 98 ILIR projects, highlighting their objectives and accomplishments. In addition, three ILIR projects have been selected for emphasis and thus have more detailed descriptions because of the exemplary results obtained.

The three selected projects are

“Development of Ultramicroelectrode (UME) Arrays for Use in a Remote Probe” by Dr. Pamela A. Mosier–Boss and Dr. Stephen H. Lieberman. The authors demonstrated the use of microelectrode sensors to detect volatile organic compounds.

“Underwater Acoustic Array Processing in High-Slope Shallow-Water Environments” by Paul Baxley. The author investigates the localization errors and correlation degradations that occur when acoustic arrays are placed in shallow-water environments with sloping seafloors and when a two-dimensional propagation assumption is made.

“A New Sparse Complete Orthogonal Factorization Method as Applied to Bistatic Target-Strength Prediction” by Dr. Aram K. Kevorkian. This work presents a complete orthogonal factorization method that takes advantage of the structure and numerical properties in sparse, rank-deficient, overdetermined systems arising in bistatic target-strength prediction models.

The following table summarizes recent metrics for the SSC San Diego ILIR program.

	FY 94	FY 95	FY 96	FY 97	FY 98
Funding (\$K)	2,312	2,463	2,763	2,521	2,300
Number of projects	28	29	31	29	25
Professional work-years	14	15.3	15.6	14.5	13.3
Refereed papers (published or accepted)	13	26	19	19	15
Refereed papers (submitted)	10	9	9	10	5
Books/Chapters	—	—	—	—	3
In-house publications	5	3	4	2	2
Proceedings*	—	—	—	—	30
Presentations to professional meetings	25	60	38	50	42
Patents issued	7	5	6	7	5
Statutory Invention Registration	—	—	—	1	—
Claims allowed, pending issue	2	2	—	2	4
Patent applications filed	6	6	11	12	11
Invention disclosures authorized	—	5	6	4	3
Invention disclosures submitted	7	7	7	10	13

\* Counted within Presentations in previous years



## Development of Ultramicroelectrode (UME) Arrays for Use in a Remote Probe

Dr. Pamela A. Mosier-Boss and Dr. Stephen H. Lieberman

*We demonstrate the use of microelectrode sensors to detect volatile organic compounds (VOCs) in air. In general, VOCs that easily oxidize to form protons give a larger electrochemical response. We also study the use of voltammetry for speciation and the effect of electrode size on the electrochemical response. We show that surface-enhanced Raman spectroscopy (SERS) can be used to monitor the electrochemical reactions in situ and discuss its applicability in identifying the electroactive species.*

### INTRODUCTION

Ultramicroelectrodes (UMEs) can be made from any electrode material (gold [Au], platinum [Pt], carbon [C], etc.) in any geometrical arrangement (disks, rings, bands, etc.) and can be assembled into arrays. The choice of electrode material, size, and geometry depends on the field of application. The unconventional properties of UMEs make them attractive as sensitive electrochemical sensors and detectors in a variety of media [1–3]. In UMEs, the characteristic dimension that is given by the geometry of the electrode must be very small [4]. Reducing that characteristic dimension results in very small currents, decreased Ohmic losses due to the diminished current, reduced capacitive charging currents, and an increase in mass transport to and from the electrode. As a consequence of reduced capacitive charging currents and increased mass transport rates, ultramicroelectrodes exhibit excellent signal-to-noise (S/N) characteristics. Furthermore, the electrode potential can be changed rapidly, thus permitting voltammetric measurements on a submicrosecond time scale and measurements in highly resistive domains [5]. The reduced  $iR$  effect is particularly important because it allows measurements to be made on nonpolar solvents in the presence of appropriate support electrolytes, polar solvents and mixtures of polar and nonpolar solvents, in the absence of purposely added support electrolytes, low-temperature glasses and eutectics, and the gas phase [6].

The use of ultramicroelectrodes for the analysis of electroactive species in the gas phase was demonstrated first by Pons et al. [7–9]. In this initial investigation, it was shown that the sensitivity of the device was dependent upon the electrochemical properties of the analyte and on the properties of the surface separating the inner UME from the outer auxiliary electrode. Species selectivity of these microelectrode detectors arises from differences in the redox potentials of the analyte. Either constant potential or voltammetric techniques may be used. Since there is an interest in developing new technologies for environmental monitoring, we began investigating the feasibility of using these microelectrode sensors to detect and identify volatile organic compounds (VOCs) in the air, under ambient conditions. In particular, we examined the effect of electrode material and size on the magnitude of the electrochemical response, as well as the possibility of using the voltammetric response for speciation. We also demonstrated the use of surface-enhanced Raman spectroscopy (SERS) to monitor the electrochemical reactions *in situ* and discuss the applicability of SERS in species identification.

## ELECTROCHEMICAL RESPONSE OF MICROELECTRODE SENSORS TO VOCs IN THE GAS PHASE

Figure 1 shows a schematic of the microelectrode sensor used in this investigation to detect VOCs in the gas phase. The inner, working electrode consists of a metal wire that is epoxied inside the outer, auxiliary electrode. We were interested in determining how well these microelectrode sensors responded to VOCs in the air, since environmental monitoring devices must be able to operate in air under ambient conditions. There are two general categories of environmental monitoring devices. They either monitor a flowing stream, as is true of hand-held Photo Ionization Detectors (PIDs), or they monitor a relatively quiescent environment, such as smoke alarms or carbon monoxide detectors. The static and dynamic exposure tests used in this investigation simulate operation in a quiescent environment and in a flowing stream, respectively. Figure 2 summarizes the electrochemical response of a C/Au microelectrode assembly to acetonitrile in air. Similar results were obtained for other microelectrode sensors and other VOCs. Voltammetric curves (figure 2a) were obtained for acetonitrile as it evaporates. In air, a linear response is observed as a function of applied potential. The background current is on the order of 1 pA. Within minutes after an aliquot of acetonitrile is injected inside the sample chamber, an increase in current flow is observed. As the concentration of acetonitrile in air increases, the voltammograms begin to exhibit more curvature. Static and dynamic exposure tests yield the results shown in figures 2b and c, respectively. The results summarized in figure 2 indicate that the response of these sensors to an electroactive material in the gas phase is reversible. The sensors can be used in either a flowing stream or in a quiescent environment and can be used to monitor contaminants in air.

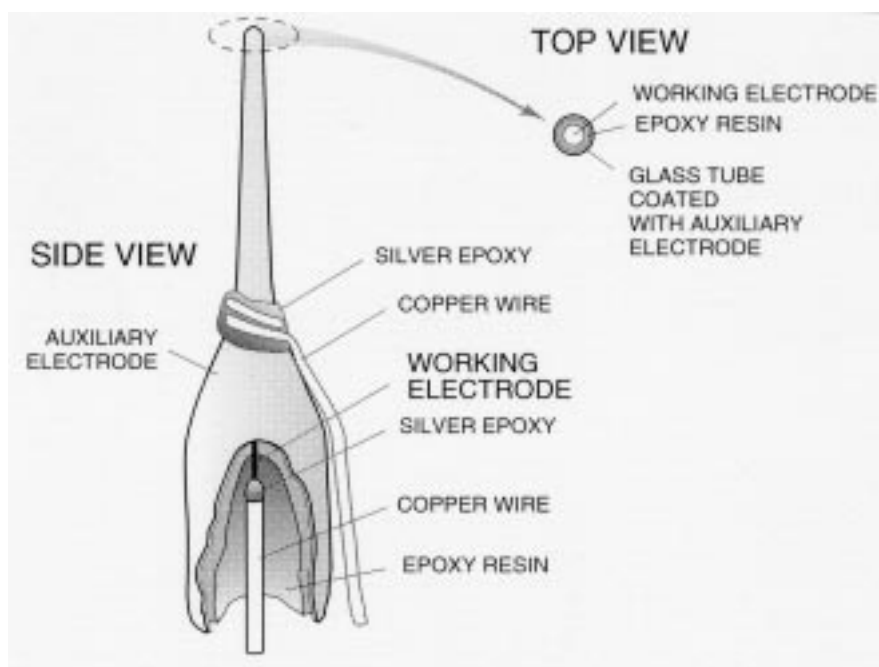


*Figure 1. Schematic of the microelectrode gas-phase detector for VOCs. The microelectrode assembly is constructed of a disk working electrode that is sealed in a glass tube coated with a thick gold metal film with epoxy resin. The working electrode is separated from the auxiliary electrode by a thin ring of glass and epoxy resin.*

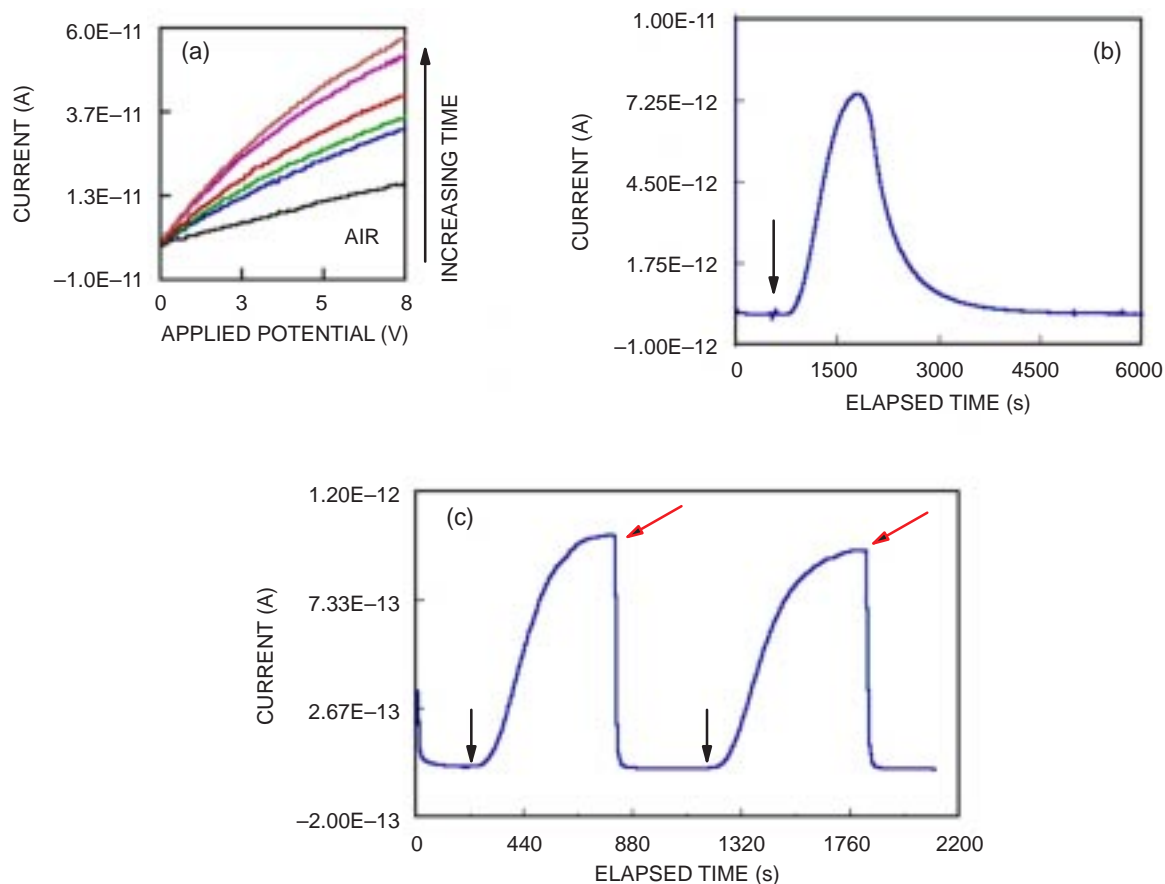


Figure 2. Electrochemical response of a C/Au disk microelectrode sensor to acetonitrile in the gas phase at room temperature. Diameter of the C working electrode is  $7\ \mu\text{m}$ .

(a) A  $25\text{-}\mu\text{l}$  aliquot of acetonitrile was injected into a glass flask. The evaporation of acetonitrile was monitored electrochemically by sweeping the voltage from 0 to 8 V at a sweep rate of  $100\ \text{mV s}^{-1}$ .

(b) Results of a static exposure test. The voltage was held constant at 3 V. An arrow indicates the time of injection of a  $2\text{-}\mu\text{l}$  sample of acetonitrile. The total volume of the sample chamber is 11.9 ml. When volatilized, the total concentration of acetonitrile in the sample chamber is  $0.132\ \text{mg ml}^{-1}$ .

(c) Dynamic response as a function of time for acetonitrile vapor. The potential was held constant at 8 V, and the argon (Ar) flow rate was  $10.9\ \text{ml min}^{-1}$ . The UME assembly is repeatedly exposed to analyte vapor and then to pure argon, yielding the differential response shown. The black arrows indicate when the C/Au assembly is exposed to argon bubbling through acetonitrile. The red arrows indicate purging with pure argon.

The results of static exposure tests for VOCs in air indicate that the electrochemical response is greatly dependent on the electrode material as well as the analyte. The largest electrochemical response is observed for compounds containing oxygen and nitrogen atoms, such as ethanol, acetonitrile, and 2-butanone. These materials are polar and have fairly large dipole moments and dielectric constants.

In contrast, the electrochemical response of the aromatic VOCs is very small, while that for the chlorinated hydrocarbons falls between these two extremes. Anodic oxidation of organic substances has been thoroughly investigated by using voltammetric techniques in aprotic solvents [10].

Aromatic hydrocarbons and their derivatives undergo oxidation to form radical cations that lose a proton rapidly to give the free radical. It was shown that substitution can increase the stability of aromatic cation radicals and that molecules capable of greater charge delocalization produce the more stable radicals. The anodic oxidation of aliphatic hydrocarbons generally proceeds by the transfer of two electrons and the loss of one proton to give a carbenium ion [11]:



These observations indicate that the ease of oxidation leading to the formation of protons directly correlates with the magnitude of the electrochemical response.

### EFFECT OF ELECTRODE SIZE ON THE ELECTROCHEMICAL RESPONSE

In the gas phase, where do the electrochemical reactions occur? Do they occur at the edges of the electrodes or on the surface of the working electrode? This information is necessary to determine which element of the sensor is critical to its performance. We began an investigation of the effect of electrode size on the electrochemical response. Figures 3a and b summarize static and dynamic exposure tests, respectively, for methylene chloride and silver/gold (Ag/Au) disk microelectrode sensors. The results indicate that the magnitude of the electrochemical response increases with

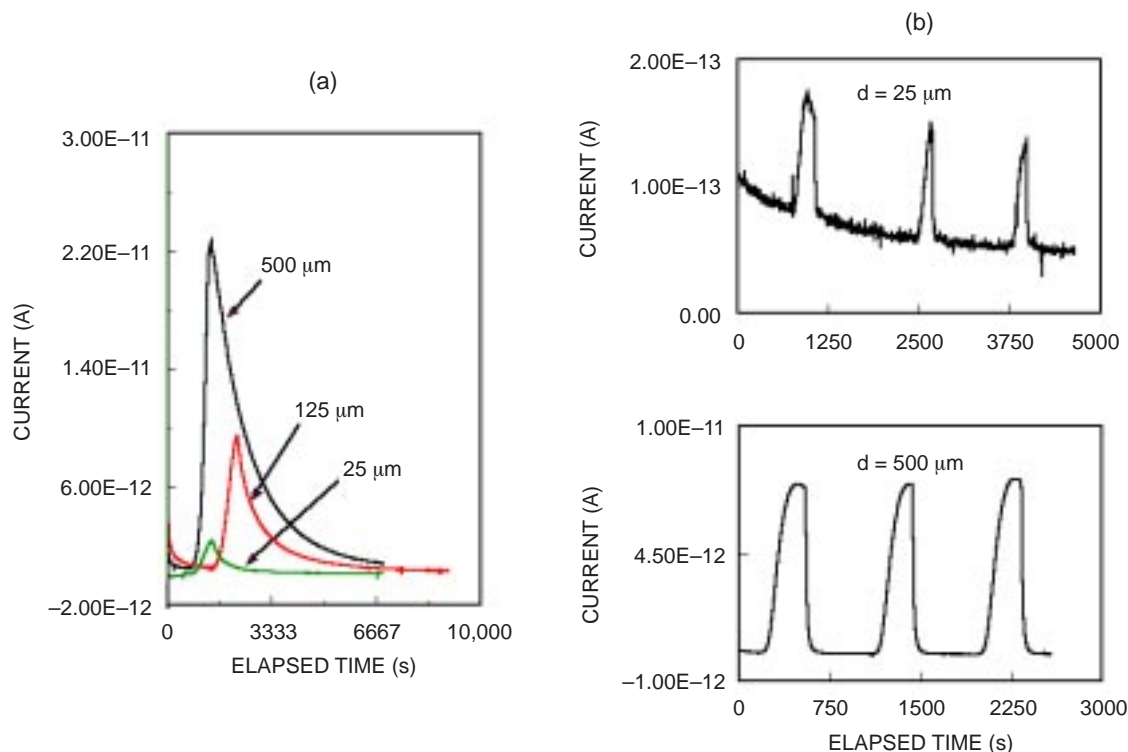


Figure 3. Static and dynamic exposure tests for methylene chloride and Ag/Au microelectrode sensors as a function of working electrode diameter.

(a) Static exposure tests using 500-, 125-, and 25- $\mu\text{m}$ -diameter Ag disk electrodes in the sensors. Sample size injected in the sample chamber is 25  $\mu\text{l}$ . The applied potential is 8 V. When volatilized, the total concentration of methylene chloride is 2.79  $\text{mg ml}^{-1}$ .

(b) Dynamic exposure tests using 25- and 500- $\mu\text{m}$ -diameter Ag disk electrodes in the sensors. The applied potential is 8 V, and the flow rate is 9  $\text{ml min}^{-1}$ .

increased electrode size as does the S/N ratio. Although the background current of the larger electrodes is slightly larger than the 25- $\mu\text{m}$ -diameter Ag disk microelectrode sensor, the background current for the larger sensors is still below 1 pA. The increase in size of the inner electrode does not dramatically affect the shape of the voltammograms. Since the magnitude of the response is proportional to the diameter of the inner electrode of the array and not its area, the electrochemical reactions occur at the electrode perimeters, and the critical dimension of these sensors is the spacing between the inner and outer electrodes and not the diameter of the inner electrode. These results also indicate that current flows over the surface of the insulating ring separating the two electrodes. Consequently, the insulator surface can be viewed as the selective layer. Modification of this insulating surface will affect the magnitude of the electrochemical response as well as the selectivity of the sensor.

### IDENTIFICATION OF THE ELECTROCHEMICALLY ACTIVE SPECIES

The microelectrode sensors used in this investigation proved to be very sensitive. However, an environmental monitoring device not only requires detection of a material but also identification.

Linear sweep voltammetry could allow speciation. The shape of the current/voltage reflects the specific set of events associated with the charge transfer reaction taking place under selected experimental conditions. The overall current-voltage relationship is complex and differs for various conditions. It is affected by the chemical nature and concentration of the electroactive species, by the chemical nature of the electrode material, and by the mode of transport. Figure 4 shows voltammograms obtained for ethanol in the gas phase using Pt, palladium (Pd), C, Ag, Au, nickel (Ni), and

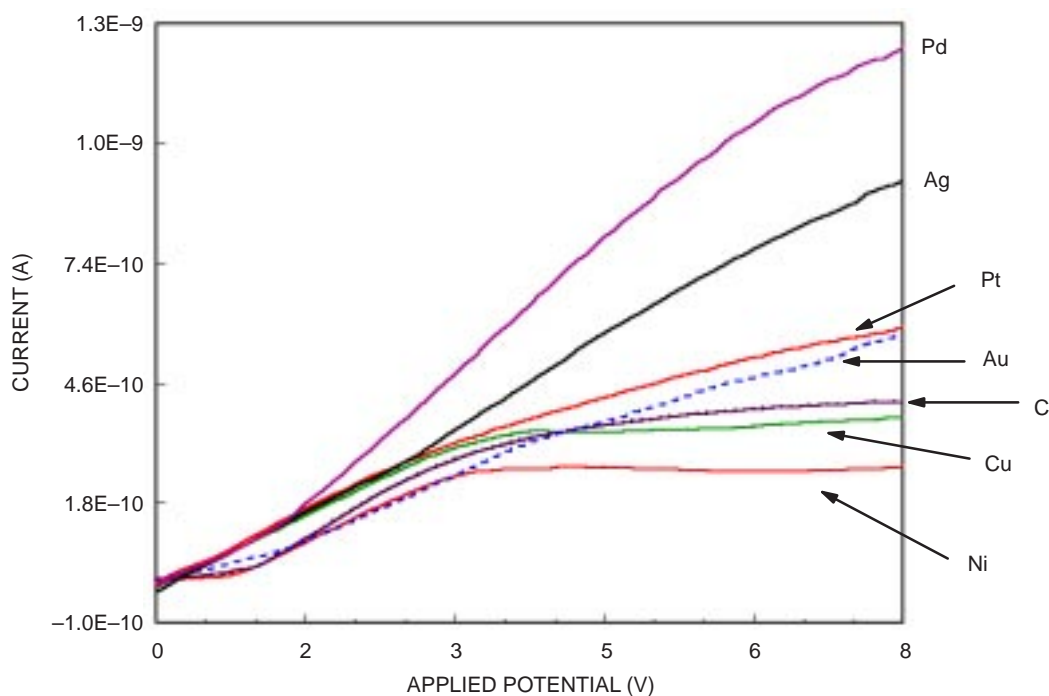


Figure 4. Voltammograms obtained for ethanol in the gas phase. The auxiliary electrode is Au. The working electrodes of the sensors are 25- $\mu\text{m}$ -diameter Ni, Au, Pt, Pd, and Ag disks; 7- $\mu\text{m}$ -diameter C disk; and 50- $\mu\text{m}$ -diameter Cu disk. Voltammograms were obtained at a sweep rate of  $100 \text{ mV s}^{-1}$ .

copper (Cu) microelectrode sensors. Although voltammograms can be obtained for these materials in the gas phase, their use in species identification is questionable for an environmental monitoring device. The voltammograms for acetonitrile obtained as a function of time using a C/Au assembly (figure 2a) indicate that the response is instantaneous. However, with time, as more acetonitrile molecules enter the gas phase, the voltammograms begin to exhibit more curvature, until the acetonitrile achieves its characteristic shape. Besides concentration issues, mixtures present an obvious difficulty in using voltammetry for speciation in an environmental monitoring device.

Since voltammetry is of limited use, another means of speciation needs to be found. One approach is to chemically modify the sensors so that they will respond to a particular compound or class of compounds. This approach has been applied to surface acoustic wave (SAW) devices [12]. A second approach is to package a number of these microelectrode sensors into one device. In this approach, multiple microelectrode sensors at different bias voltages will yield a pattern characteristic of a compound upon exposure. Neural networks or cluster-seeking routines can then be used to identify the components of a mixture. The usefulness of this latter approach has been demonstrated by Stetter et al. [13].

Another approach is to combine the specificity of spectroscopy with the sensitivity of electrochemistry. A device that combines both electrochemistry and spectroscopy would prove useful for environmental monitoring. In such a device, the microelectrode sensor would be used to continuously monitor the environment. Only when an increase in current flow is observed would the spectroscopic component of the device be activated to identify the electroactive species. For organic compounds, Raman spectroscopy is ideal for the purpose of speciation. Virtually all organic molecules display a characteristic Raman emission. Besides specificity, simultaneous multicomponent analysis is possible in Raman spectroscopy due to the high resolution of Raman spectra. Raman scattering from molecules adsorbed on such noble metals as silver, copper, and gold can be enhanced by as much as  $10^6$  to  $10^7$ . The phenomenon, surface-enhanced Raman spectroscopy [14,15], is still not fully understood despite intensive theoretical and experimental research. Raman spectra can be obtained remotely over optical fibers in real time, and there have been significant advances in the development of inexpensive, portable Raman spectrometers, charge-coupled device (CCD) detectors, and diode lasers.

Although the SERS phenomenon is not fully understood, it is known that SERS requires a roughened surface and that unprotected surfaces can undergo oxidation resulting in a decrease in the SERS response. Both alkanethiols and dialky disulfides react with Ag and Au to form self-assembled monolayers (SAMs). The alkyl group is attached to the surface by a metal-thiolate bond. Carron et al. [16,17] showed that octadecylthiol-coated Ag SERS substrates can be used to detect both aromatic compounds and chlorinated hydrocarbons in ground water. The coating also protects the SERS substrates from oxidation and fouling from atmospheric materials. This increases the lifetime of the SERS substrate from minutes or hours to months. Figure 5 shows SERS spectra of Ag/4-chlorothiophenol before and after exposure to methylene chloride in the gas phase. The coating itself has a characteristic SERS spectrum and can be used for calibration purposes. The vibrational peak due to methylene chloride at  $715.2\text{ cm}^{-1}$  is clearly visible in the SERS spectrum of 4-chlorothiophenol. The spectra shown in figure 5 indicate that these thiol-coated SERS substrates can also be used to detect VOCs in the gas phase.

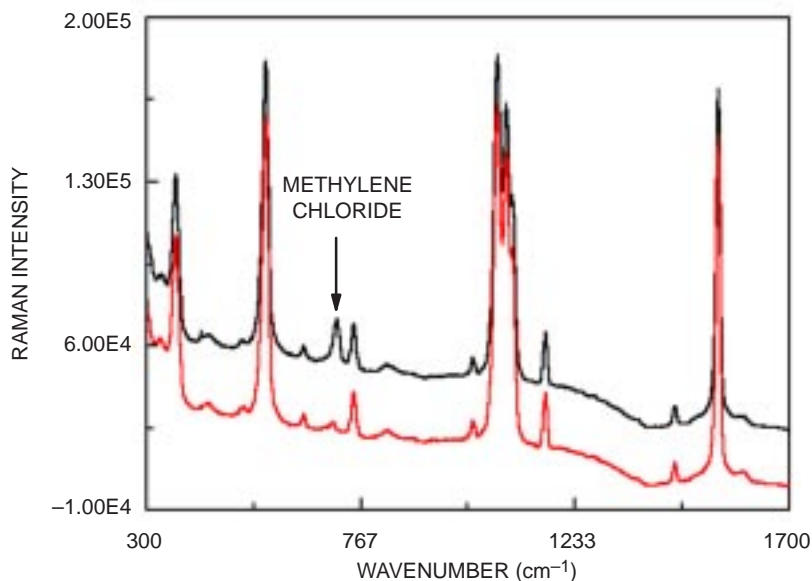


Figure 5. SERS spectra of Ag/4-chlorothiophenol and methylene chloride. The bottom spectrum is that of 4-chlorothiophenol on a chemically etched silver substrate. The top spectrum, obtained after the addition of methylene chloride to a cellulose sponge on the opposite side of the glass partition, clearly shows the emergence of the methylene chloride peak at  $715.2\text{ cm}^{-1}$  as methylene chloride interacts with the coating. Laser power at  $100\text{ mW}$  ( $780\text{-nm}$  excitation),  $100\text{-}\mu\text{m}$  slits,  $600\text{-g/mm}$  grating, CCD detector temperature at  $-58^\circ\text{C}$ , no binning of pixels, and  $100\text{-s}$  acquisition time.

Since the electrochemical reactions occur at the electrode perimeters in the gas phase, chemical modification of the surface of the working electrode should not appreciably affect the electrochemical response. Using the experimental configuration shown in figure 6, the electrochemical response of the microelectrode sensor can be measured while simultaneously obtaining SERS spectra of the surface of the working electrode. Both static exposure and dynamic exposure tests were conducted using Au/4-chlorothiophenol microelectrode sensors. Figure 7 shows the current/time curves obtained during static and dynamic exposure tests. The letters along the current/time curve indicate when a SERS spectrum was obtained. The  $650\text{ to }800\text{ cm}^{-1}$  spectral region of these spectra is shown. Although the 4-chlorothiophenol vibrational peak at  $703\text{ cm}^{-1}$  is more prominent on Au than on Ag (figure 5), it does not interfere with the detection of the methylene chloride peak at  $715\text{ cm}^{-1}$ . The results summarized in figure 7 show that the increase/decrease of current flow upon exposure of the microelectrode sensor to methylene chloride directly corresponds with the intensity of the methylene chloride peak in the SERS spectra. This indicates that the electroactive species is methylene chloride. These experiments demonstrate that *in situ* spectroelectrochemical measurements of these thiol-modified microelectrode sensors upon exposure to VOCs are feasible. It is possible to use the spectra to identify the electroactive species, and spectra can be obtained when the sensor is operated in both a flowing stream and in a quiescent environment.

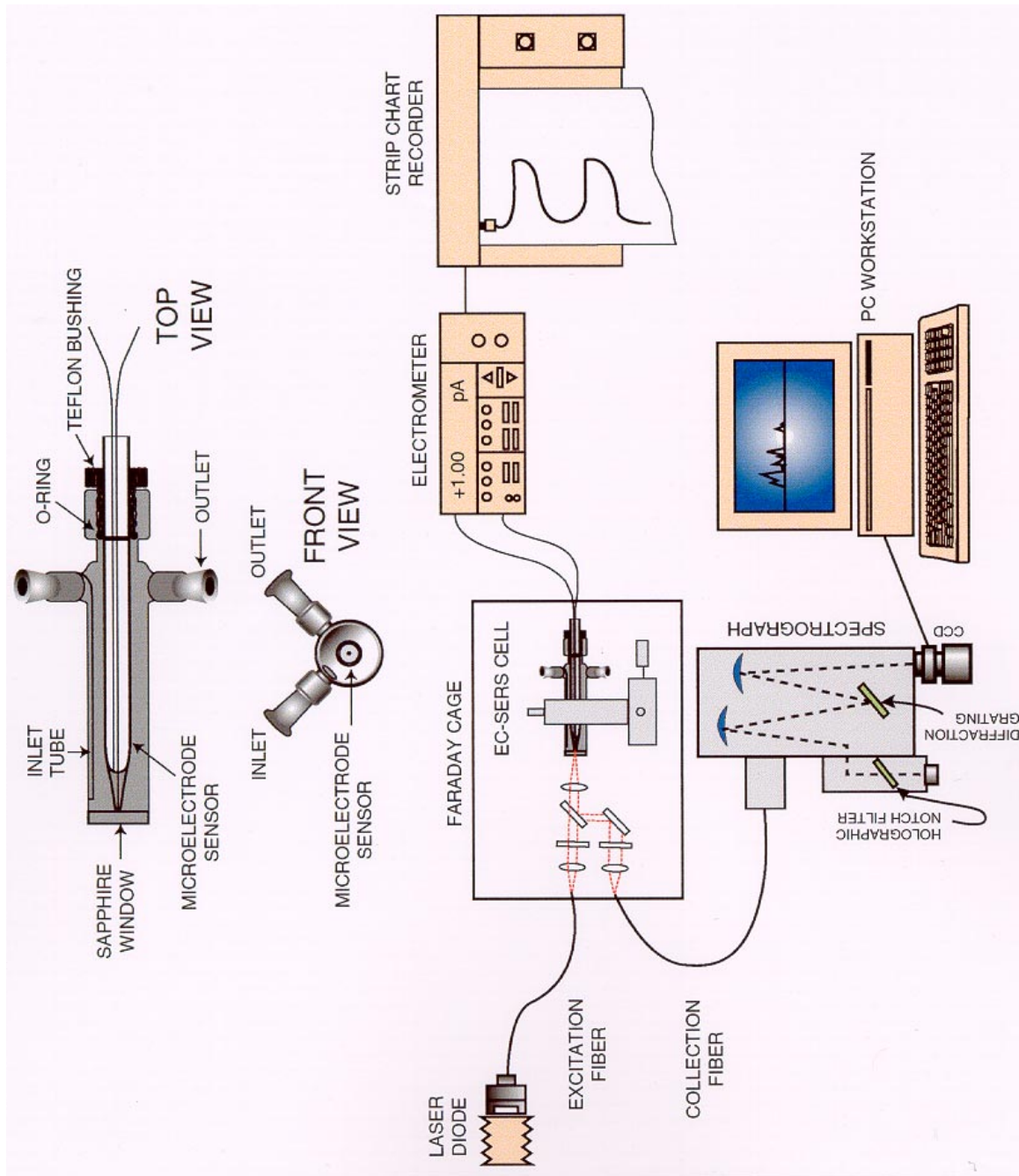


Figure 6. Schematic of the experimental arrangement used to simultaneously measure the electrochemical response of the microelectrode sensor while obtaining SERS spectra of the surface of the working electrode. This experimental arrangement combines the sensitivity of electrochemical detection with the specificity of spectroscopy.

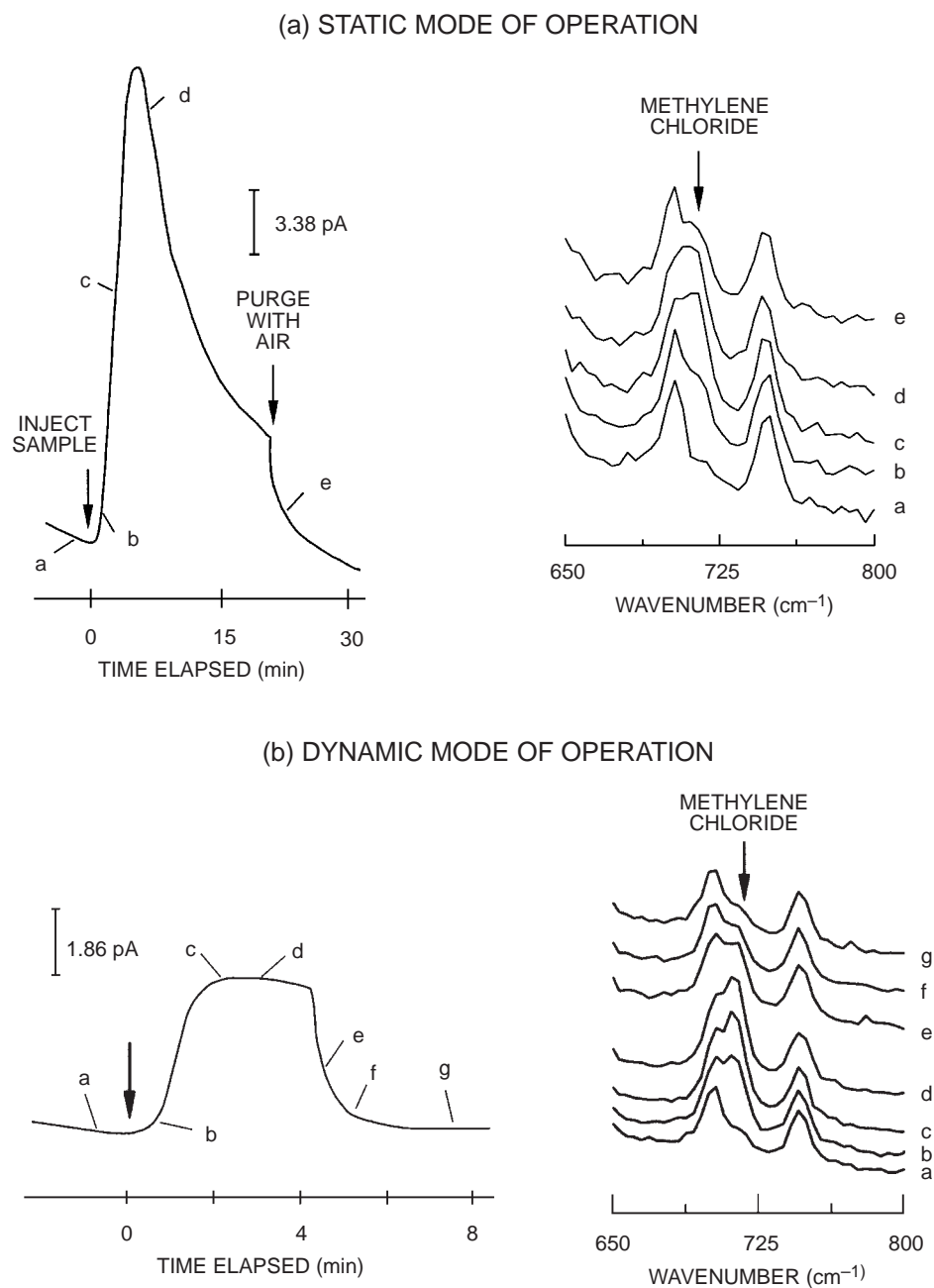


Figure 7. Current/time responses of Au/Au microelectrode sensor treated with 4-chlorothiophenol. Diameter of the working electrode is  $500\ \mu\text{m}$ . Applied potential is 8 V. Letters along the current/time curve indicate when SERS spectra were obtained. SERS spectra in the  $650$  to  $800\ \text{cm}^{-1}$  spectral region are shown. Laser power at  $63\ \text{mW}$  ( $852\text{-nm}$  excitation),  $100\text{-}\mu\text{m}$  slits,  $600\text{-grooves/mm}$  grating, detector temperature of  $-50^\circ\text{C}$ , binning three horizontal pixels of the CCD array. (a) Static mode of operation: Arrows indicate when a  $25\text{-}\mu\text{l}$  sample of methylene chloride is injected into the electrochemical cell and when the cell is purged with air. Spectra obtained using a  $10\text{-s}$  acquisition time. (b) Dynamic mode of operation: Arrow indicates when dry nitrogen is bubbled through a reservoir of methylene chloride and into the electrochemical cell. Spectra obtained using a  $30\text{-s}$  acquisition time.

## CONCLUSIONS

It has been shown that microelectrode sensors can be used to detect VOCs in air under ambient conditions. In the presence of VOCs, the electrode assemblies exhibit a good response time; they are reversible; and they can be used in either a flowing stream or in a quiescent environment. Although the microelectrode sensors used in this investigation are fairly large, it has been shown that micro-lithographic techniques can be used to prepare these sensors on chips, thereby drastically reducing their dimensions [18]. The magnitude of the electrochemical response is dependent on the electrode material and is related to the molecule's ease of oxidation leading to the formation of protons. We found that VOCs with high dielectric constants and net dipole moments generally gave a larger electrochemical response. Since explosive materials and drugs contain polar functional groups, these sensors can be used for their detection as well. Voltammograms of the VOCs can be obtained in the gas phase. The shape of the voltammogram is dependent upon the chemical nature of the electroactive species as well as the electrode substrate. However, the possibility of mixtures reduces the use of voltammetry for speciation in a device used for environmental monitoring.

In the gas phase, the electrochemical reactions occur at the perimeters of the electrodes making up the assembly. Therefore, the critical dimension that must be small is the spacing between the inner and outer electrodes of the assembly. Larger diameter wires can be used as long as this spacing is kept small, preferably under 100  $\mu\text{m}$ . The advantages of using larger diameter wires in these microelectrode sensors are an increase in sensitivity and better signal-to-noise ratios.

The microelectrode sensors used in this investigation proved to be very sensitive. However, an environmental monitoring device not only requires detection of a material but also identification. Since voltammetry is of limited use, another means of speciation needs to be found. One approach is to chemically modify the sensors so that they will respond to a particular compound or class of compounds. A second approach is to package a number of these microelectrode sensors into one device. In this approach, multiple microelectrode sensors at different bias voltages will yield a pattern characteristic of a compound upon exposure. Neural networks or cluster-seeking routines can then be used to identify the components of a mixture. Another approach combines spectroscopy with electrochemistry. The microelectrode sensors are used to continuously monitor the environment. When an increase in current flow between the two electrodes of the sensor occurs, spectroscopic techniques are used to identify the electroactive species. In this investigation, we have demonstrated the use of SERS to monitor the working electrode surface *in situ* during anodic oxidation.

## ACKNOWLEDGMENT

The authors would like to thank Prof. Keith Carron of the University of Wyoming for his assistance in preparing thiol-coated SERS substrates.

## REFERENCES

1. Pons, S. and M. Fleischman. 1987. "The Behavior of Microelectrodes," *Analytical Chemistry*, vol. 59, pp. 1391A–1399A.
2. Howell, J. O. and R. M. Wightman. 1984. "Ultrafast Voltammetry and Voltammetry in Highly Resistive Solutions with Microvoltammetric Electrodes," *Analytical Chemistry*, vol. 56, pp. 524–529.
3. Wightman, R. M. 1981. "Microvoltammetric Electrodes," *Analytical Chemistry*, vol. 53, pp. 1125A–1134A.
4. Heinze, J. 1993. "Ultramicroelectrodes in Electrochemistry," *Angewandte Chemie. International Edition in English*, vol. 32, pp. 1268–1288.
5. Wightman, R. M. 1988. "Voltammetry with Microscopic Electrodes in New Domains," *Science*, vol. 240, pp. 415–420.
6. Fleischmann, M. and S. Pons. 1991. "Electrochemistry in the Gas Phase," *Microelectrodes: Theory and Applications*; M. I. Montenegro, M. A. Queiros, and J. L. Daschbach, eds., NATO Advanced Study Institute (ASI) Series E; Kluwer Academic Publishers (Netherlands); pp. 357–375.
7. Ghoroghchian, J., F. Sarfarazi, T. Dibble, J. Cassidy, J. J. Smith, A. Russell, G. Dunmore, M. Fleischmann, and S. Pons. 1986. "Electrochemistry in the Gas Phase. Use of Ultramicroelectrodes for the Analysis of Electroactive Species in Gas Mixtures," *Analytical Chemistry*, vol. 58, pp. 2278–2282.
8. Brina, R., S. Pons, and M. Fleischmann. 1988. "Ultramicroelectrode Sensors and Detectors: Considerations of the Stability, Sensitivity, Reproducibility, and Mechanism of Ion Transport in Gas Phase Chromatography and in High Performance Liquid Phase Chromatography," *Journal of Electroanalytical Chemistry*, vol. 244, pp. 81–90.
9. Brina, R. and S. Pons. 1989. "The Use of Narrow Gap Microelectrodes as Sensitive and Species Selective Gas Chromatographic Detectors," *Journal of Electroanalytical Chemistry*, vol. 264, pp. 121–130.
10. Popovych, O. and R. P. T. Tomkins. 1981. *Nonaqueous Solution Chemistry*, John Wiley and Sons, Inc., New York, NY.
11. Cassidy, J., S. B. Khoo, S. Pons, and M. Fleischmann. 1985. "Electrochemistry at Very High Potentials: The Use of Ultramicroelectrodes in the Anodic Oxidation of Short-Chain Alkanes," *Journal of Physical Chemistry*, vol. 87, pp. 3933–3935.
12. Wells, M. and R. M. Crooks. 1996. "Interactions between Organized, Surface-Confined Monolayers and Vapor-Phase Probe Molecules. 10. Preparation and Properties of Chemically Sensitive Dendrimer Surfaces," *Journal of the American Chemistry Society*, vol. 118, pp. 3988–3989.
13. Stetter, J. R., P. C. Jurs, and S. L. Rose. 1986. "Detection of Hazardous Gases and Vapors: Pattern Recognition Analysis of Data from an Electrochemical Sensor Array," *Analytical Chemistry*, vol. 58, pp. 860–866.

14. Fleischmann, M., P. J. Hendra, and A. J. McQuillan. 1974. "Raman Spectra of Pyridine Adsorbed at a Silver Electrode," *Chemical Physics Letters*, vol. 26, pp. 163–166.
15. Jeanmaire, D. L. and R. P. van Duyne. 1977. "Surface Raman Spectroelectrochemistry Part I. Heterocyclic, Aromatic, and Aliphatic Amines Adsorbed on the Anodized Silver Electrode," *Journal of Electroanalytical Chemistry*, vol. 84, pp. 1–20.
16. Carron, K., L. Pietersen, and M. Lewis. 1992. "Octadecylthiol-Modified Surface-Enhanced Raman Spectroscopy Substrates: A New Method for the Detection of Aromatic Compounds," *Environmental Science and Technology*, vol. 26, pp. 1950–1954.
17. Mullen, K. and K. Carron. 1994. "Adsorption of Chlorinated Ethylenes at 1–Octadecanethiol-Modified Silver Surfaces," *Analytical Chemistry*, vol. 66, pp. 478–483.
18. Morita, M., M. L. Longmire, and R. W. Murray. 1988. "Solid-State Voltammetry in a Three Electrode Electrochemical Cell-on-a-Chip with a Microlithographically Defined Microelectrode," *Analytical Chemistry*, vol. 60, pp. 2770–2275.

Principal Investigator:

Dr. Pamela A. Mosier-Boss  
D363

0601152N

ZU30

Co-Investigator:

Dr. Stephen H. Lieberman  
D361

# Underwater Acoustic Array Processing in High-Slope Shallow-Water Environments

Paul A. Baxley

*Array processing on underwater acoustic arrays is traditionally performed without regard for the three-dimensionality of the acoustic propagation. In shallow-water environments with sloping seafloors, however, the path of the acoustic energy can “bend” out of the vertical plane containing the source and receiver, creating an acoustic field significantly different from that predicted with the two-dimensional propagation assumption. Consequently, array processors such as conventional beamformers (CBFs) or matched-field processors (MFPs) may suffer serious localization errors and correlation degradations when arrays are placed in these environments. This phenomenon is investigated by means of computer simulations for a theoretical wedge environment and by the analysis of vertical-line-array (VLA) source-tow data collected in a steep wedge-like environment near San Clemente Island during the Fourth Shallow-Water evaluation cell Experiment (SWelLEX-4).*

## INTRODUCTION

Acoustic analyses of underwater surveillance systems generally assume that the energy emitted from a source remains in the vertical plane containing the source and the receiver, which is referred to as two-dimensional (2-D) propagation. This assumption is true if the seafloor is perfectly flat, or for energy propagating in the upslope direction of an inclined-plane seafloor. It is only approximately valid in environments with nearly flat bathymetry or mild bathymetric gradients. However, if the gradients are large and are in directions other than the direction of propagation, the acoustic energy can be reflected out of the vertical plane, resulting in three-dimensional (3-D) propagation. If the gradients are steady over significant spatial dimensions, as in the case of a wedge-like ocean, then the path of acoustic propagation can experience a horizontal “bending” or “refraction,” creating a field significantly different from that predicted by the 2-D assumption [1–3]. This effect is illustrated in figure 1, which presents a computer simulation of a single ray path propagating over the sloping bathymetry near Kaneohe, Hawaii.

If an underwater acoustic array is placed in an environment that supports 3-D propagation, significant performance degradation may result if the 3-D effect is neglected. In particular, correlation levels will be degraded and source localization estimates (angle of arrival for conventional beamformers [CBFs], source range and depth for matched-field processors [MFPs] on a vertical line array [VLA]) will be in error. In cases of extreme bending, the acoustic energy may never reach the array, creating a type of horizontal shadow zone. The objective of this study is to (1) examine the effect of 3-D propagation on array processor performance when 2-D propagation is assumed, (2) quantify the limiting conditions for which the 2-D assumption may be used with confidence, and (3) investigate the performance improvement obtained by incorporating 3-D propagation into the array processor. This is accomplished via computer simulations for a theoretical wedge environment and the analysis of VLA source-tow data collected in a steep wedge-like environment near San Clemente Island during the Fourth Shallow-Water evaluation cell Experiment (SWelLEX-4).

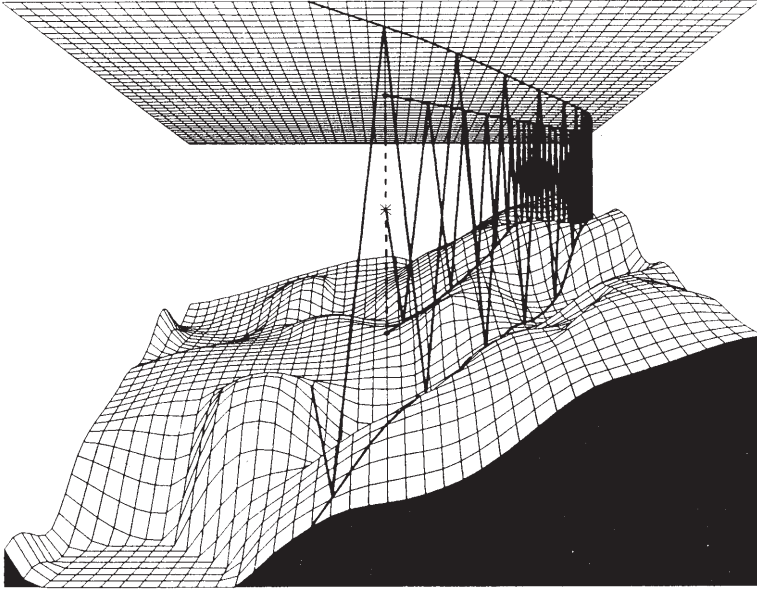


Figure 1. Horizontal “bending” of acoustic ray path propagating over a sloping bathymetry near Kaneohe, Hawaii. (Courtesy of Homer Bucker, SSC San Diego, D881.)

## ARRAY PROCESSING

The normalized Bartlett estimator [4] was selected as the array processing technique because of its simplicity and general utility. According to this technique, the measure of the match of correlation between the observed pressure  $p_n^o$  at each phone of an  $N$ -phone array and the predicted (or replica) pressure  $p_n(x)$  at the same phones for an assumed target location vector  $\mathbf{x}$  is given by

$$B_{BART}(x) = \frac{\sum_{n=1}^N \sum_{m=1}^N p_m^* R_{mn} p_n(x)}{\sum_{n=1}^N |p_n(x)|^2}$$

where  $R_{mn}$  is the normalized time-averaged cross-spectral matrix, given by

$$R_{mn} = \frac{\overline{p_m^o p_n^{o*}}}{\sum_{l=1}^N |p_l^o|^2}$$

For CBF on a line array with uniform weighting, the replica pressures  $p_m$  are given by a simple vertical planewave arrival model [5], namely,  $p_m(\theta) = \exp(ikd_n \sin\theta)$ , where  $k = 2\pi/\lambda$  is the wave-number,  $\lambda$  is the wavelength,  $d_n$  is the distance of element  $n$  from some reference location, and the source location parameter  $\mathbf{x}$  is reduced to the angle-of-arrival  $\theta$ . The highest value of  $B_{BART}$  should provide an estimate of the true angle of arrival.

For MFP, the replica pressures  $p_m$  are given by a solution to the acoustic wave equation for the environment being studied (e.g., pressures predicted by propagation models such as normal mode theory or 3-D Gaussian beams). For the case of a VLA in an azimuthally symmetric (range-independent) environment,  $\mathbf{x}$  is a two-dimensional vector with components  $r$  (source range) and  $d$  (source depth). Therefore, the Bartlett estimator applied to a VLA produces a surface, commonly referred to as an ambiguity surface, that plots correlation as a function of candidate source ranges and depths. The highest correlation should provide an estimate of the true source location. However, because of the repetitive nature of the modal-interference pattern in shallow water, high correlations will also occur at source locations that produce an acoustic field at the VLA resembling the field produced by the actual source at the true location. These false peaks, or sidelobes, can be quite large in shallow-water waveguides but will be lower than the true peak if the predicted pressures are calculated accurately.

## WEDGE SIMULATIONS

The study of 3-D propagation effects is difficult because of the high complexity of the resulting signal field. This is particularly true for experimental investigations. It is, therefore, useful to initially restrict the analysis to computer simulations of idealized problems, so that the effects can be systematically studied as a function of important parameters. The idealized environment selected for this study was the Acoustical Society of America (ASA) benchmark problem of a wedge-shaped waveguide with a penetrable lossy bottom [6], as shown in figure 2. This consists of a homogeneous water column (density = 1 g/cm<sup>3</sup>, sound speed = 1500 m/s) overlying a sloping planar homogeneous fluid half-space (density = 1.5 g/cm<sup>3</sup>, sound speed = 1700 m/s, attenuation = 0.5 dB/wavelength). A source was allowed to move along a track of constant bathymetry parallel to the wedge apex and away from well-sampled horizontal and vertical line arrays (HLAs and VLAs). Beam degradations and localization errors resulting from the sloping bathymetry were then determined as a function of wedge parameters and source range by comparing performance with that obtained for a source moving over a flat bottom of the same water depth. Acoustic pressures emitted by the source were simulated using Bucker's 3-D Gaussian Beam (3DGB) model [7], which was developed under the Independent Research funds in FY 91 through FY 93.

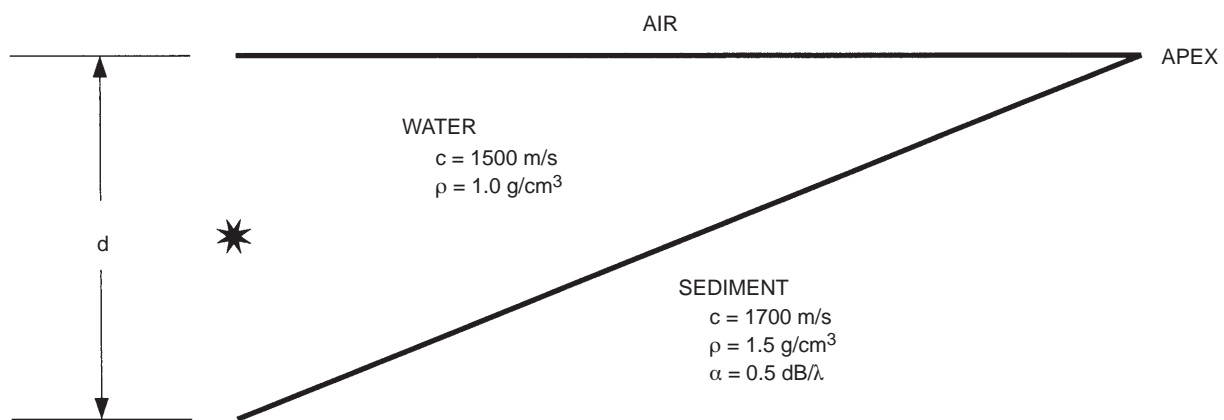


Figure 2. Acoustical Society of America benchmark wedge-shaped waveguide with penetrable lossy bottom;  $c$  is the compressional sound speed,  $\rho$  is density, and  $\alpha$  is the compressional attenuation.

Some typical effects are illustrated in figure 3, which compares transmission loss (figure 3a), HLA beam response ( $B_{BART}$  versus bearing; figure 3b), and VLA matched-field response (figures 3c and 3d), as a function of true source range, for a flat bottom with that for a  $5^\circ$ -slope wedge. In both cases, the water depth along the track is 100 m, the source depth is 10 m, and the frequency is 25 Hz. Figure 3c plots  $B_{BART}$  as a function of candidate source range and true range at a candidate source depth equal to the true depth (10 m). Figure 3d plots the maximum value of  $B_{BART}$  and the range and depth at the maximum as a function of true source range. The solid line in figure 3d represents the results for the flat bottom, which coincides with the true source track. Three distinct regions are clearly discernible in the wedge results. For true source ranges less than approximately 2.5 km, the results are similar to those for the flat bottom, except for a slight bending of the tracks in figure 3c. The similarity results from the fact that two modes are propagating in both cases. For true source ranges between 2.5 and 6.0 km, the field drastically changes because the higher mode has been stripped out as a result of the sloping bottom, leaving a single propagating mode. The HLA beam-former reports arrivals from other than the broadside direction in this region because each mode travels laterally to the receiver along hyperbolic paths, instead of along the track direction. While the matched-field correlation remains high in this region, the absence of the higher mode has degraded the main peak so that reliable range estimation is destroyed by the presence of the high sidelobes. While the source depth estimate is fairly stable in this region, it has shifted to a value around 60 to 70 m (figure 3d). The 6.5-km boundary marks the entrance into a horizontal shadow zone, where the remaining lowest mode is stripped out. Array responses in this region are meaningless and would normally be masked by the ambient noise.

The range boundaries defining modal cutoffs can be estimated easily by using simple algebraic expressions dependent on mode number, wedge angle, perpendicular distance of source and receiver from wedge apex, frequency, and critical angle. These expressions, termed the “caustic” equations, are provided by Deane and Buckingham [8] in the following form:

$$z_s^2 = \left( \frac{k\tilde{r}\tilde{r}'}{\mu} \right)^2 - \tilde{r}^2 - \tilde{r}'^2$$

where

$$\tilde{r} = r + \frac{\pi}{2k\alpha_w \sin \alpha_c}$$

$$\tilde{r}' = r' + \frac{\pi}{2k\alpha_w \sin \alpha_c}$$

and  $r$  is the distance of the source along the surface from the wedge apex,  $r'$  is the distance variable along the surface from the wedge apex,  $z_s$  is the distance variable along the wedge apex,  $k$  is the wavenumber,  $\alpha_w$  is the wedge angle,  $\alpha_c$  is the critical angle at the water/seafloor interface, and  $\mu = m\pi/\alpha_w$ , with  $m$  representing the mode number ( $m = 1, 2, 3, \dots$ ).  $r'$  plotted as a function of  $z_s$  for mode  $m$  is the caustic curve for mode  $m$ . This curve marks the boundary beyond which rays emitted from the source at a vertical launch angle corresponding to mode  $m$  (but at all azimuthal directions) will not travel. Although rays may be launched in all azimuthal directions, the sloping seafloor causes the

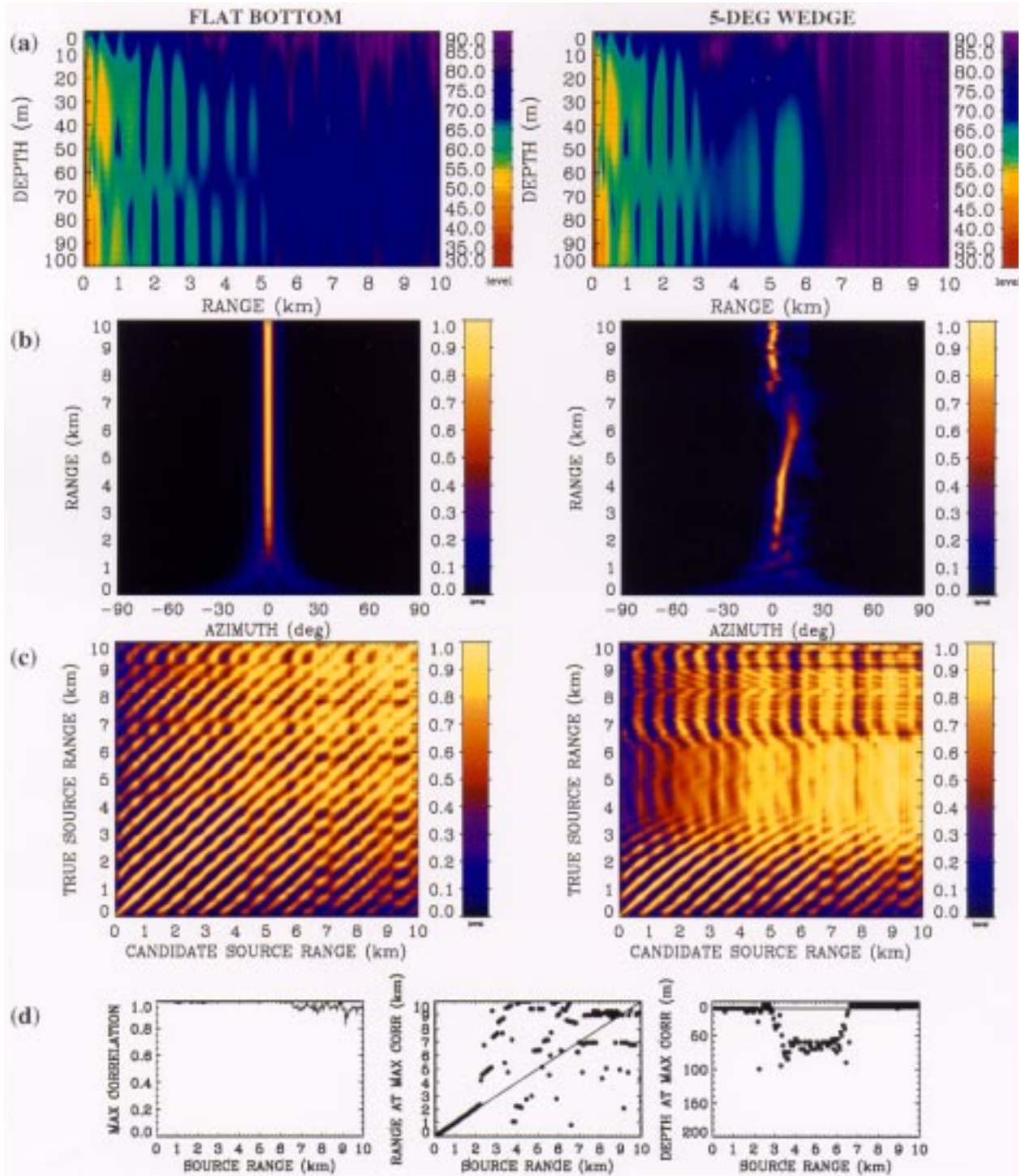


Figure 3. Typical 3-D bathymetric effects on (a) signal field, (b) HLA beam response, and (c and d) VLA matched-field response. Frequency = 25 Hz. Source depth = 10 m. Water depth along track = 100 m. In (a) through (c), the left column is for a flat bottom while the right column is for a 5° wedge. In (b), source track is in broadside direction to HLA aperture. All matched-field results use replicas obtained for flat bottom. In (c), candidate source depth = 10 m, and main peak track begins near zero candidate source range (near diagonal in left column). Large sidelobes occur in (c) because only a few modes propagate at this frequency and water depth. In (d), the maximum correlation, and the candidate range and depth of that maximum, for the full range-depth ambiguity surfaces, are plotted over the duration of the track. In (d), the light solid line represents results for flat bottom, for which the maximum correlation is always unity (no mismatch) and which coincides with the true source location.

rays to bend along hyperbolic paths, creating a shadow zone bounded by the caustic line. Figure 4 presents the caustic curves corresponding to the  $5^\circ$ -slope wedge discussed in reference to figure 3. Moving a receiver along the  $r' = r$  (where  $r$  is the distance from wedge apex at which the water depth is 100 m) is, by reciprocity, equivalent to fixing the receiver and moving the source along the same line, as was the case in figure 3. Clearly, as  $z_s$  increases along the  $r' = r$  line, the crossings of caustic curves is seen to correspond with the points of modal cutoffs observed in figure 3. The caustic equations provide a convenient means of predicting if 3-D effects will be important in a given scenario.

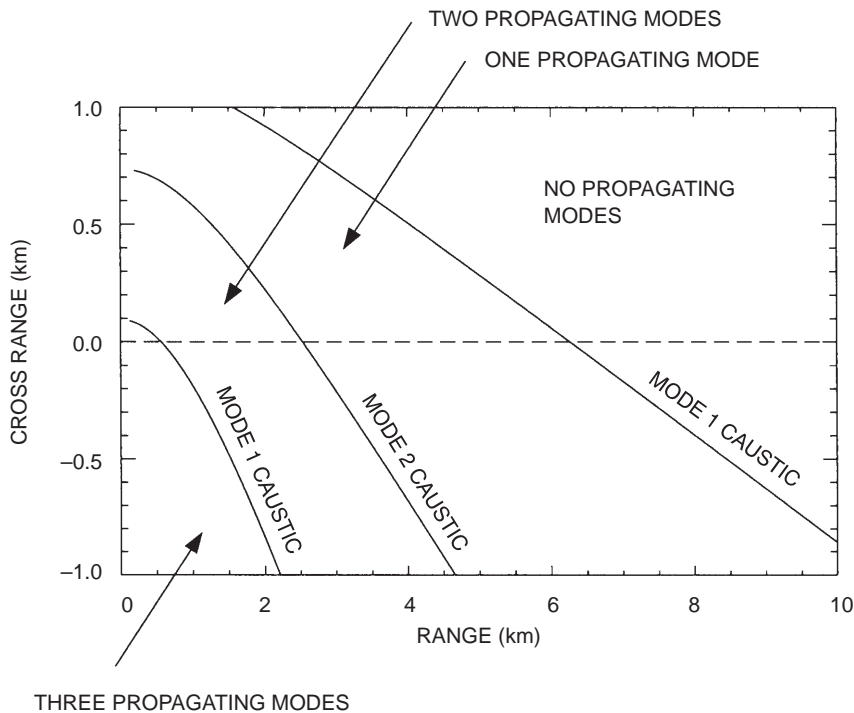


Figure 4. Theoretical 25-Hz caustic curves for  $5^\circ$  wedge water depth at zero cross range (environment used for wedge results in figure 3). For a source located at the origin, the caustic curves mark boundaries beyond which particular modes are stripped out. Intersection of caustic curves with zero cross range marks range of mode cutoff for a receiver moving along the zero-cross-range line. These mode cutoffs agree with those observed in the simulation results of figure 3.

MFP localization performance can be enhanced if 3-D effects are included in the matched-field processor. Figure 5 compares the 100-Hz matched field obtained for a  $4^\circ$  wedge with that obtained for a flat bottom. For the wedge result, the water depth is 100 m at the zero-cross-range axis, decreasing in the positive cross-range direction. For the flat-bottom case, the water depth everywhere is 100 m. In both cases, the VLA is located at the origin, while the source is located at a range of 5 km and a cross range of 0 km, and the source depth is 10 m. The wedge results exhibit the expected azimuthal discrimination, absent from the flat-bottom case (the arcs in figure 5a are actually segments of distorted circles), with the maximum correlation occurring at the true source location. Notice, however, the presence of regions of distinct interference patterns. These regions differ because a different number of modes are surviving in each, as demonstrated by the corresponding

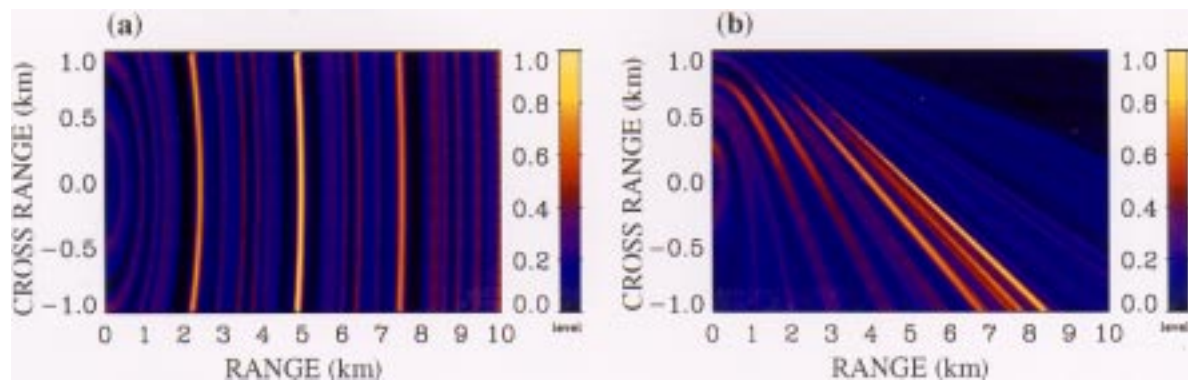


Figure 5. Simulated 100-Hz matched-field range-cross range (at 10-m candidate source depth) ambiguity surface for (a) 100-m water depth flat bottom, and (b) 4° wedge with 100-m water depth at zero cross range. VLA located at origin. Source range = 5 km. Source cross range = 0 km. Source depth = 10 m.

theoretical caustic curves in figure 6. By reciprocity, a source located in a region between the caustics will produce energy containing the stated number of modes for that region at a receiver located at the origin. The higher correlations in the region containing the true source location in figure 5 (which clearly corresponds to the region propagating modes 1 through 4 in figure 6) results from the fact that the true and replica pressures contain the same number of modes. The interference pattern in that region is characteristic of that produced by that number of modes.

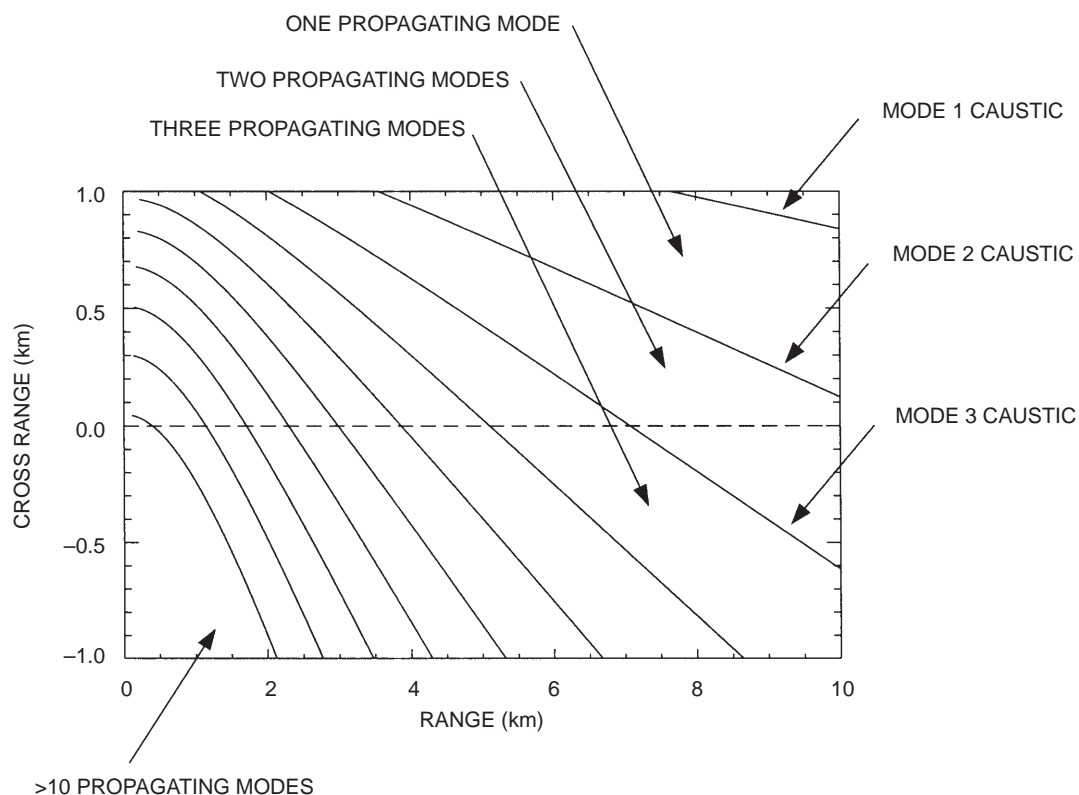


Figure 6. Theoretical 100-Hz caustic curves for 4° wedge with 100-m water depth at zero cross range (environment used for wedge results in figure 5).

## SWelIEX-4 DATA ANALYSIS

Experimental evidence for the presence of 3-D bathymetric effects was obtained via the analysis of VLA source-tow data recorded in a steep wedge-like environment during SWelIEX-4. SWelIEX-4 took place in March 1995 offshore San Clemente Island, an area characterized by steep bottom slopes (as high as  $6^\circ$  to  $7^\circ$ ). A 64-phone VLA was suspended beneath the research platform FLIP in approximately 218 m of water. Source tows, transmitting 10 narrowband frequency tonals from 52 to 187 Hz at 15-Hz increments, were performed in the vicinity of the VLA by the Canadian research vessel CFAV *Endeavour*. Figure 7 shows the source-tow track considered in this analysis, along with the bathymetry of the region and the location of the VLA (at the origin). Nineteen elements of the original 64-element VLA were used in this analysis, with a spacing of 5.626 m and an aperture of 101.25 m positioned in the upper half of the water column.

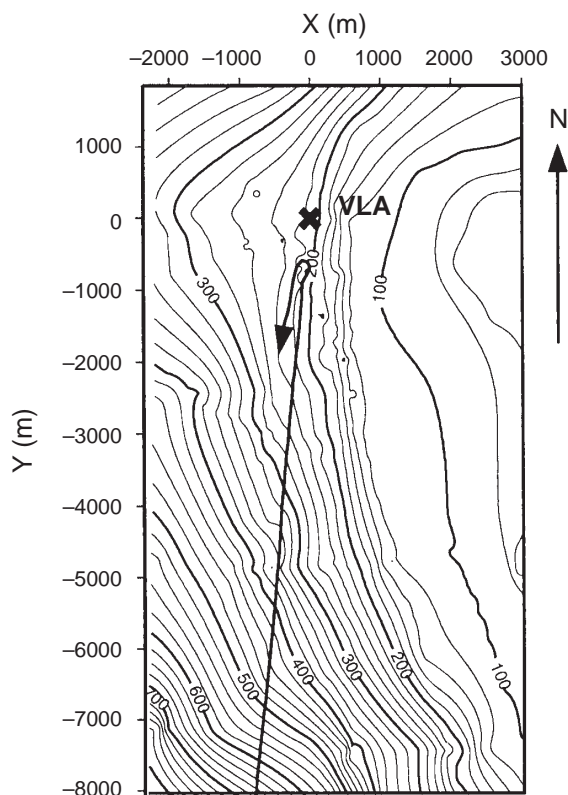


Figure 7. SWelIEX-4 environment, VLA location, and source-tow track analyzed.

## Multi-Frequency Signal Analysis

Possible evidence for the presence of horizontal “refraction” is provided via an examination of multi-frequency single-phone signal power versus time (or source range) over the source-tow interval. Figure 8 presents such an analysis for the 67-, 82-, 97-, and 112-Hz tonals on channel 10. Note that the field is “stretched” as frequency is increased. The diagonal line identifies an apparent modal cutoff point that occurs at earlier times as frequency increases. These results are in agreement with theoretical observations for wedge environments [1,3]. Modal caustic lines tend to flatten toward

straight lines parallel to the wedge apex as frequency increases. This reduction in the degree of horizontal “bending” results in the moving of modal cutoff points to larger ranges, as observed in figure 8.

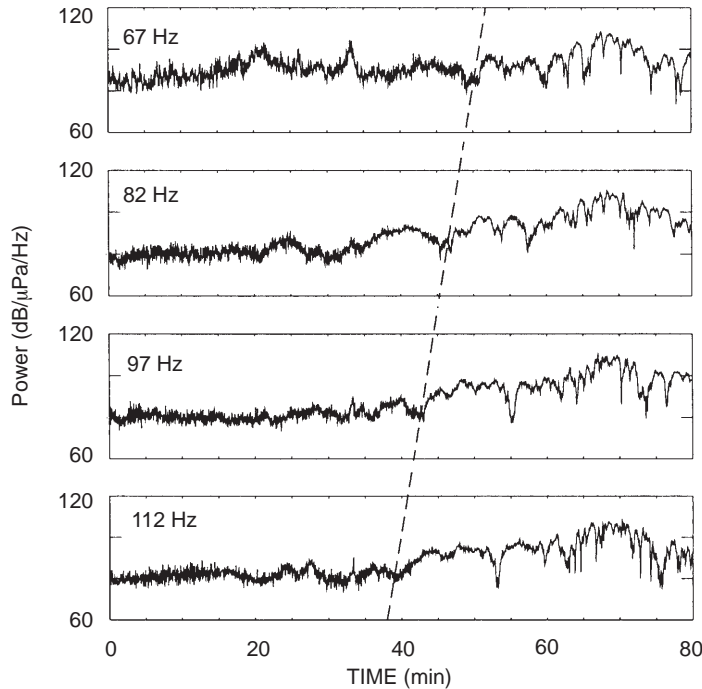


Figure 8. Single-phone (channel 10) power at 67, 82, 97, and 112 Hz versus time (or source range) over source-tow interval.

### Matched-Field Localization Errors

Prior to performing a matched-field analysis, inversions for optimal geoacoustic parameters and array configuration parameters were performed at short range so that mismatch in these parameters would not be misinterpreted as a 3-D effect. The optimized array configuration possessed an array tilt component of  $4.2^\circ$  in the direction away from the source, with a top phone depth of 20.625 m. Modeling the bottom as a simple fluid half-space, an optimal compressional sound speed in the bottom was determined to be 1586.0 m/s.

Matched-field processing was applied to the SWelLEX-4 data by using a 2-D assumption (adiabatic normal mode theory) to generate the predicted or replica pressures. The presence of 3-D effects will then be manifested as errors in the MFP localization estimates. Figure 9 presents frequency-averaged matched-field results as a function of time for the source-tow track. These were obtained by incoherently averaging the matched-field ambiguity surfaces for nine tonals (67, 82, 97, 112, 127, 142, 157, 172, and 187 Hz). Figure 9a presents  $B_{BART}$  as a function of range and time, with the candidate source depth following the depth of maximum correlation over time. Figure 9b plots the maximum correlation and the range and depth of the maximum as a function of time. The dashed curves indicate the true range and depth versus time obtained from navigation data. At short range (up to approximately 2 km), the range/depth estimates are observed to agree well with the true values. However, between source ranges of 2 and approximately 5 km, the MFP range estimate shifts to

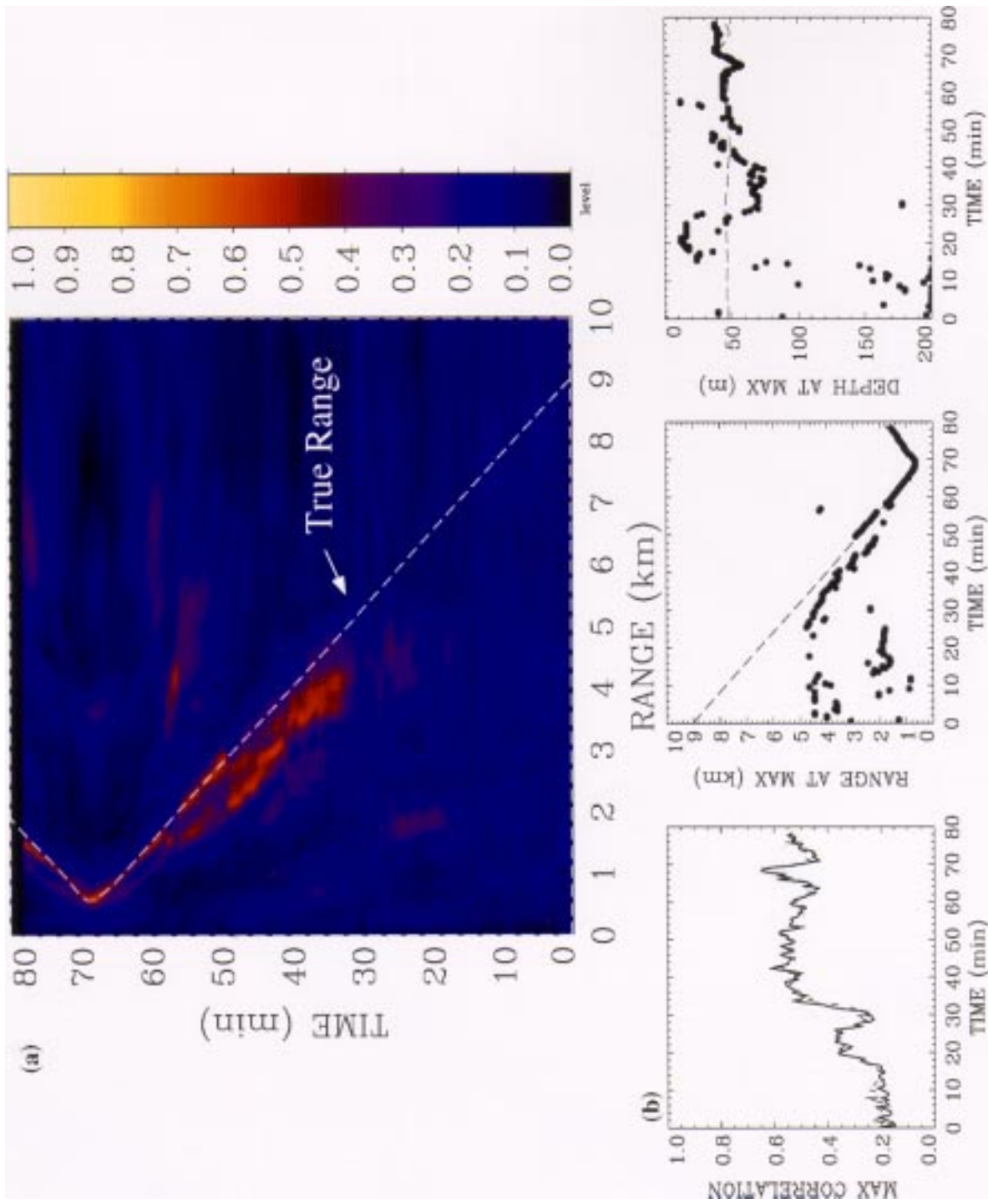


Figure 9. Frequency-averaged matched-field results for SWellEX-4 source-tow data. (a) Correlation versus range and time with source depth following depth at maximum correlation. (b) Maximum correlation, range at maximum, and depth at maximum, versus time. Dashed curves indicate true range and depth from navigation data. 2-D adiabatic normal-mode theory used to generate replica pressures. Results obtained by incoherently averaging ambiguity surfaces for nine frequencies (67, 82, 97, 112, 127, 142, 157, 172, and 187 Hz).

values significantly lower than the true values, and the depth estimate shifts to a value approximately 20 m greater than the true depth. This is strong evidence that the sloping seafloor has significantly altered the signal field and that modes have been eliminated as a result of horizontal “refraction.” An examination of echo-sounder data did not reveal any distinct changes in the seafloor geoacoustic properties that might provide an alternative explanation for this behavior. Beyond a source range of 5 km, the correlation drops drastically and the localization estimates exhibit a random character. This suggests that this region may either be a shadow zone caused by the sloping seafloor, or that the geoacoustic properties of the seafloor have changed such that attenuation is greatly increased in this region.

## CONCLUSIONS

Evidence supporting the hypothesis that 3-D propagation effects can adversely affect the performance of underwater acoustic arrays has been provided via computer simulation and experimental results. The neglect of 3-D effects can result in significant errors in localization estimates and correlation degradation. This may be caused by a change in the phase relationship between modes, resulting from the fact that different modes travel different horizontal paths in sloping environments. In addition, the horizontal bending of paths may cause modes to be stripped out. The caustic equations provide a useful “rule-of-thumb” for determining if 3-D effects may be important for a given environment. Inclusion of 3-D effects into the MFP can restore or improve localization performance and provide azimuthal discrimination. The experimental observation of 3-D effects with the SWelLEX-4 data is notable since the complexity of real environments and the large number of parameters impacting the problem render the study of these effects extremely difficult.

## ACKNOWLEDGMENTS

Homer Bucker of SSC San Diego provided technical assistance with the implementation of the 3-D Gaussian beam propagation model. Richard Bachman of SSC San Diego provided a reconstructed bathymetric grid for the SWelLEX-4 environment. Ross Chapman and Ronald Kessel of the University of Victoria provided the bathymetry data and many useful insights into the analysis.

## REFERENCES

1. Harrison, C. H. 1979. “Acoustic Shadow Zones in the Horizontal Plane,” *Journal of the Acoustical Society of America*, vol. 65, no. 1, pp. 56–61.
2. Doolittle, R., A. Tolstoy, and M. Buckingham. 1988. “Experimental Confirmation of Horizontal Refraction of CW Acoustic Radiation from a Point Source in a Wedge-Shaped Ocean Environment,” *Journal of the Acoustical Society of America*, vol. 83, no. 6, pp. 2117–2125.
3. Glegg, S. A. L. and J. R. Yoon. 1990. “Experimental Measurements of Three-Dimensional Propagation in a Wedge-Shaped Ocean with Pressure-Release Boundary Conditions,” *Journal of the Acoustical Society of America*, vol. 87, no. 1, pp. 101–105.
4. Tolstoy, A. 1993. *Matched-Field Processing for Underwater Acoustics*, World Scientific, Singapore.
5. Steinberg, B. D. 1976. *Principles of Aperture and Array System Design*, John Wiley & Sons, Inc., New York.

6. Jensen, F. B. and C. M. Ferla. 1990. "Numerical Solutions of Range-Dependent Benchmark Problems in Ocean Acoustics," *Journal of the Acoustical Society of America*, vol. 87, no. 4, pp. 1499–1510.
7. Bucker, H. P. 1994. "A Simple 3-D Gaussian Beam Sound Propagation Model for Shallow Water," *Journal of the Acoustical Society of America*, vol. 95, no. 5, pp. 2437–2440.
8. Deane, G. B. and M. J. Buckingham. 1993. "An Analysis of the Three-Dimensional Sound Field in a Penetrable Wedge with a Stratified Fluid or Elastic Basement," *Journal of the Acoustical Society of America*, vol. 93, no. 3, pp. 1319–1328.

Principal Investigator:  
Paul Baxley  
D881

0601152N  
ZU25

# A New Sparse Complete Orthogonal Factorization Method as Applied to Bistatic Target-Strength Prediction

Dr. Aram K. Kevorkian

*In this work, we present a complete orthogonal factorization method that takes advantage of the structure and numerical properties in sparse, rank-deficient, overdetermined systems arising in bistatic target-strength prediction models. The sparse overdetermined matrices in these models belong to a class called row-bordered block diagonal matrices. Applying this decomposition method to highly ill-conditioned bistatic target-strength prediction models, we have obtained between nine-fold and fifteen-fold improvement over the compute time required by the Linear Algebra PACKage (LAPACK) for a range of models. Further speedups can be realized by exploiting a variety of parallelisms inherent in the models. Algorithmic speedup of this magnitude will enable the extension of the frequency range in bistatic target-strength prediction models to regions of greater interest to the Navy. All computer runs were done on the SSC San Diego Distributed Center Convex Exemplar SPP 1600.*

## INTRODUCTION

Knowledge of bistatic target strength is of increasing importance in sonar systems. Full-scale measurements of monostatic target strength are expensive and difficult and become impractical for general bistatic geometries. Usually one is limited to measurements at a limited number of monostatic angles and, perhaps, a few bistatic angles in a single plane. Extending the value of this measured data by using it to estimate the full bistatic target-strength pattern is extremely desirable. Previous efforts to do this have severe limitations or restrictions in their applicability.

A method has been developed [1] that relies on measured monostatic and limited bistatic data, and uses a numerical model to estimate the surface field and propagate it to the farfield for full bistatic geometries. The crux of this method is to construct the farfield propagator matrix that relates the farfield scattered pressures to some surface quantity. A singular value decomposition of the propagator matrix is used to eliminate nonradiating surface modes. Then, the radiating part of the surface values is determined by least-squares approximation from knowledge of the measured monostatic and limited bistatic scattering data and from the principle of reciprocity, which requires the scattering matrix to be symmetric. The least-squares problem involves a large, sparse, rank-deficient matrix. Although the solution of this least-squares problem is non-unique, it appears that the minimum norm solution gives good results when the surface values are used to reconstruct the full bistatic scattering pattern. Available conventional algorithms, such as those contained in LAPACK, deal with the rank deficiency but take no advantage of the sparsity. Therefore, they are very time-consuming, and this severely limits the frequency range of applicability.

## SPARSITY STRUCTURE OF MATRIX IN THE BISTATIC TARGET-STRENGTH PREDICTION MODEL

Large, sparse, overdetermined systems of equations  $Mx = b$  arise in numerous scientific and engineering applications. In the bistatic target-strength prediction (btsp) model, the sparse overdetermined matrix  $M$  is rank-deficient, and also, for some permutation matrix  $P$ ,  $PM$  is a 2-by-1 block matrix

$$PM = \begin{pmatrix} A \\ G \end{pmatrix},$$

where  $A = [A_{ij}]$  is a  $k$ -by- $k$  block diagonal matrix whose diagonal blocks are overdetermined matrices with identical dimensions and sparsity structure, and  $G = [G_{ij}]$  is a 1-by- $k$  block matrix in which every block is nonzero. We will refer to a matrix that has the form in  $PM$  as a row-bordered block diagonal matrix, and use  $\delta$  to denote the number of rows of  $G$ . Figure 1 shows the row-bordered block diagonal form of a 935-by-300 matrix  $M$  obtained from one of four btsp applications we have investigated so far. This matrix has 7620 nonzeros (less than 4 percent of the total number of entries in  $M$ ) and  $\delta = 35$ .

## A LINEAR LEAST-SQUARES SOLUTION WITHOUT TAKING ADVANTAGE OF BLOCK DIAGONAL FORM OF A

When the overdetermined matrix  $M$  is of full rank, the QR factorization can be used for the solution of the linear least-squares problem

$$\min_x \|Mx - b\|_2.$$

For the more difficult case where  $M$  is not of full rank, QR factorization with column pivoting is the most common method [2, 3] for the solution of the rank-deficient linear least-squares problem. The main objective in the QR factorization with column pivoting is to determine an  $n$ -by- $n$  permutation matrix  $S$  so that  $MS$  takes the form

$$MS = Q \begin{pmatrix} R_{11} & R_{12} \\ 0 & 0 \end{pmatrix},$$

where  $Q$  is an  $m$ -by- $m$  orthogonal (or unitary) matrix, and  $R_{11}$  is an  $r$ -by- $r$  nonsingular upper triangular matrix with  $r = \text{rank}(M)$ . A critical component in this factorization step is to determine the numerical rank of  $M$ . This is usually done by applying a good condition estimator to  $R_{11}$ .

In terms of the matrices  $S$  and  $Q$ , the overdetermined system  $Mx = b$  takes the equivalent form

$$(Q^TMS)(S^Tx) = (Q^Tb).$$

Combining these two equations gives the linear least-squares solution

$$x = S \begin{pmatrix} R_{11}^{-1}(c - R_{12}z) \\ z \end{pmatrix},$$

where  $c$  consists of the first  $r$  elements of  $Q^Tb$  and  $z$  consists of the last  $n - r$  elements of  $S^Tx$ . Setting  $z = 0$  in this relation for  $x$  gives the “basic” solution to the linear least-squares problem

$$x_B = S \begin{pmatrix} R_{11}^{-1}c \\ 0 \end{pmatrix}.$$

Note, if  $R_{12} \neq 0$ , then the basic solution  $x_B$  is not the minimum norm solution to the rank-deficient linear least-squares problem, and so to obtain the minimum norm solution we need to do additional orthogonal transformations on the  $r$ -by- $n$  upper trapezoidal matrix  $(R_{11} \ R_{12})$ .

Let  $Z$  be an  $n$ -by- $n$  orthogonal (or unitary) matrix such that

$$(R_{11} \ R_{12}) Z = (T_{11} \ 0),$$

where  $T_{11}$  is an  $r$ -by- $r$  upper triangular matrix and nonsingular. Making use of this relation in  $Q^TMS$  gives the so-called complete orthogonal factorization

$$MS = Q \begin{pmatrix} T_{11} & 0 \\ 0 & 0 \end{pmatrix} Z^T.$$

In terms of the orthogonal matrices  $Q$  and  $Z$  and the permutation matrix  $S$ , the overdetermined system  $Mx = b$  has the equivalent form

$$(Q^TMSZ)(Z^TS^Tx) = (Q^Tb).$$

Combining these last two equations gives

$$x = SZ \begin{pmatrix} T_{11}^{-1}c \\ 0 \end{pmatrix},$$

which is the minimum norm solution to the rank-deficient linear least-squares problem as computed in LAPACK [3].

## A LINEAR LEAST-SQUARES SOLUTION THAT TAKES ADVANTAGE OF THE BLOCK DIAGONAL FORM OF A

When QR factorization with column pivoting is applied to the row-bordered block diagonal matrix  $PM$ , the leading block  $A$  in  $PM$  loses its block diagonal form after only a few Householder updates. This deformation in the block diagonal form of  $A$  is a direct consequence of the fact that each row and each column in every block of the  $1$ -by- $k$  block matrix  $G$  in  $PM$  contains at least one nonzero entry.

In this section, we present a new method [4] that takes advantage of the block diagonal form of  $A$  to compute a linear least-squares solution of the overdetermined system  $Mx = b$ . The first step uses QR factorization with column pivoting to factorize each of the  $k$  rank-deficient diagonal blocks of  $A$  individually. At the completion of this step, we obtain an orthogonal (or unitary) matrix  $Q^{(i)}$  and an  $n$ -by- $n$  permutation matrix  $S^{(i)}$  such that

$$A_{ii}S^{(i)} = Q^{(i)} \begin{pmatrix} U_{11}^{(i)} & U_{12}^{(i)} \\ 0 & 0 \end{pmatrix},$$

where  $U_{11}^{(i)}$  is an  $s_i$ -by- $s_i$  nonsingular upper triangular matrix with  $s_i = \text{rank}(A_{ii})$ , for  $i = 1, \dots, k$ . If block  $A_{ii}$  is of full rank, then we have

$$A_{ii}S^{(i)} = Q^{(i)} \begin{pmatrix} U_{11}^{(i)} \\ 0 \end{pmatrix}.$$

Since the original matrix  $M$  in the btsp model is rank-deficient, at least one diagonal block of  $A$  must be rank-deficient. In practice, we have observed that each and every diagonal block of  $A$  is rank-deficient, and so we will assume henceforth that all diagonal blocks of  $A$  are rank-deficient.

Let us define

$$G_{1i}S^{(i)} = \begin{pmatrix} U_{21}^{(i)} & U_{22}^{(i)} \end{pmatrix}, \quad i = 1, \dots, k,$$

and use the orthogonal matrices  $Q^{(i)}$  and permutation matrices  $S^{(i)}$  to form the following matrices

$$Q_1 = \begin{bmatrix} Q^{(1)} & & \\ & \ddots & \\ & & Q^{(k)} \\ & & & I_\delta \end{bmatrix} E,$$

and

$$H = \begin{bmatrix} S^{(1)} & & \\ & \ddots & \\ & & S^{(k)} \end{bmatrix} F,$$

where  $I_\delta$  is a  $\delta$ -by- $\delta$  identity matrix and  $E$  and  $F$  are  $m$ -by- $m$  and  $n$ -by- $n$  permutation matrices, respectively. Then it can readily be shown that for some  $E$  and  $F$ , the matrix  $PMH$  takes the following block form

$$PMH = Q_1 \begin{bmatrix} U_{11} & U_{12} \\ U_{21} & U_{22} \\ 0 & 0 \end{bmatrix},$$

where

$$U_{1j} = \begin{bmatrix} U_{1j}^{(1)} & & \\ & \ddots & \\ & & U_{1j}^{(k)} \end{bmatrix},$$

and

$$U_{2j} = \begin{pmatrix} U_{2j}^{(1)} & \cdots & U_{2j}^{(k)} \end{pmatrix}, \quad j = 1, 2.$$

The construction of the Householder update  $Q_1^T(PM\Pi)$  completes the first step in our algorithm. Figure 2a shows the Householder update  $Q_1^T(PM\Pi)$  of the 935-by-300 matrix considered in figure 1. The leading block  $U_{11}$  in this Householder update consists of the three (full) upper triangular matrices shown in figure 2a. Each of these three upper triangular matrices is a 90-by-90 matrix which makes the block  $U_{11}$  a 270-by-270 upper triangular matrix.

### COMPLETE ORTHOGONAL FACTORIZATION OF $PM\Pi$

Let  $s$  denote the order of the upper triangular matrix  $U_{11}$  in the Householder update  $Q_1^T(PM\Pi)$ . The algorithmic details in the next two steps of our method are as follows. First, we use  $(\delta+1)$ -by- $(\delta+1)$  Householder reflections to zero the  $\delta$ -by- $s$  block matrix  $U_{21}$  in  $Q_1^T(PM\Pi)$ . At the completion of this step, we have

$$PM\Pi = Q_1 Q_2 \begin{pmatrix} R & B \\ 0 & D \\ 0 & 0 \end{pmatrix},$$

where  $Q_2$  is an  $m$ -by- $m$  orthogonal (or unitary) matrix,  $R$  is an  $s$ -by- $s$  upper triangular matrix and nonsingular,  $B$  is an  $s$ -by- $(n-s)$  nonzero block, and  $D$  is a  $\delta$ -by- $(n-s)$  nonzero block.

Next, we apply QR factorization with column pivoting to the  $\delta$ -by- $(n-s)$  block  $D$  in the Householder update  $(Q_1 Q_2)^T(PM\Pi)$ . This gives

$$PM\Pi = Q_1 Q_2 Q_3 \begin{pmatrix} R_{11} & R_{12} \\ 0 & 0 \end{pmatrix},$$

where  $Q_3$  is an  $m$ -by- $m$  orthogonal (or unitary) matrix,  $R_{11}$  is an  $r$ -by- $r$  upper triangular matrix and nonsingular with  $r = s + \text{rank}(D)$ .

At this stage, we compute the  $n$ -by- $n$  orthogonal (or unitary) matrix  $Z$  defined previously, giving us the complete orthogonal factorization

$$PM\Pi = Q_1 Q_2 Q_3 \begin{pmatrix} T_{11} & 0 \\ 0 & 0 \end{pmatrix} Z^T.$$

Subsequently, the use of the Householder update  $(Q_1 Q_2 Q_3)^T(PM\Pi)Z$  produces the desired minimum norm solution

$$x = \Pi Z \begin{pmatrix} T_{11}^{-1} c \\ 0 \end{pmatrix},$$

where  $c$  consists of the first  $r$  elements of the column vector  $(Q_1 Q_2 Q_3)^T(Pb)$ .

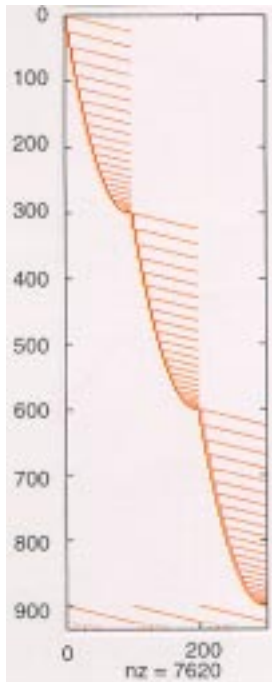
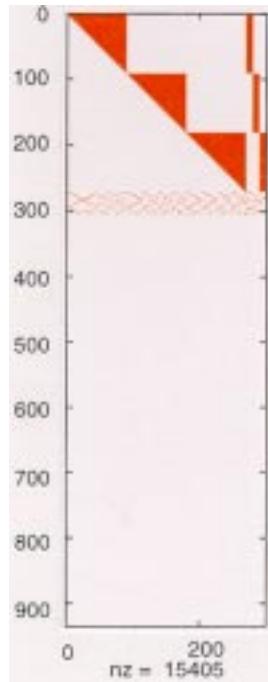
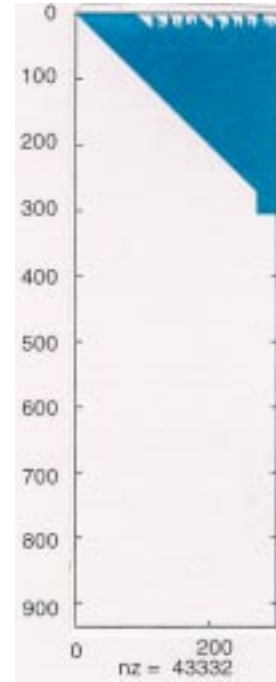


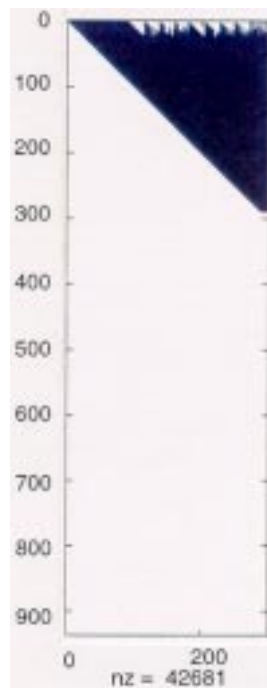
Figure 1. Row-bordered block diagonal form  $PM$  of a 935-by-300 matrix  $M$ .



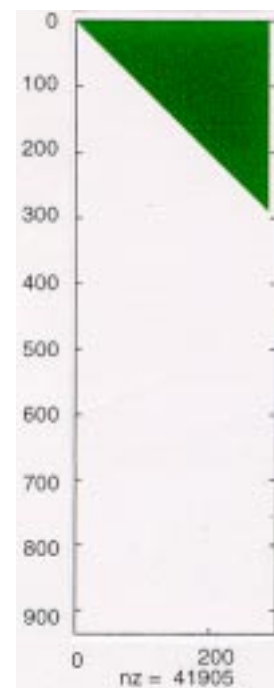
(a)



(b)



(c)



(d)

Figure 2. (a) Householder update  $Q_1^T(PM_\mu)$ . (b) Householder update  $(Q_1Q_2)^T(PM_\mu)$ . (c) Householder update  $(Q_1Q_2Q_3)^T(PM_\mu)$ . (d) Householder update  $(Q_1Q_2Q_3)^T(PM_\mu)Z$ .

Figures 2b and 2c show the Householder updates  $(Q_1Q_2)^T(PM\Pi)$  and  $(Q_1Q_2Q_3)^T(PM\Pi)$  of the 935-by-300 matrix considered in figure 1. The leading block  $R_{11}$  in the Householder update  $(Q_1Q_2Q_3)^T(PM\Pi)$  is a 289-by-289 nonsingular upper triangular matrix while  $R_{12}$  is a 289-by-11 nonzero matrix. Figure 2d shows the Householder update at the conclusion of the complete orthogonal factorization.

## TAKING ADVANTAGE OF THE PARALLEL AND VECTOR CAPABILITIES IN A HIGH-PERFORMANCE COMPUTER

Suppose we let  $\Psi_0 = PM\Pi$ , and let  $Q_1, Q_2, Q_3$ , and  $Z$  be the orthogonal matrices defined earlier. Then, our sparse complete orthogonal factorization algorithm takes the following compact form:

---

```

procedure cofd (complete orthogonal factorization by decomposition)
begin
  for  $i \leftarrow 1$  until 3 do
    compute Householder update  $\Psi_i = Q_i^T \Psi_{i-1}$ 
  end;
  compute Householder update  $\Psi_4 = \Psi_3 Z$ ;
  solve triangular system  $\Psi_4 y = w$  for the minimum norm solution of  $Mx = b$ ;
  comment  $x = (\Pi Z)y$  and  $w = (Q_1 Q_2 Q_3)^T (Pb)$ 
end

```

---

In what follows, we highlight the steps we have taken, and plan to take, to get greater efficiency on modern high-performance computers.

### COMPUTATION OF HOUSEHOLDER UPDATE $\Psi_1$

This step is ideally suited for parallel computation. Since  $Q_1$  consists of  $k$  orthogonal (or unitary) matrices  $Q^{(i)}$  that are independent of each other, all  $k$  Householder updates  $(Q^{(i)})^T A_{ii} S^{(ii)}$  can be computed independently and on different processors. Also, each of these  $k$  Householder updates is rich in level-2 operations of matrix-vector multiplications followed by an outer product update.

### COMPUTATION OF HOUSEHOLDER UPDATE $\Psi_2$

Since the QR factorization performed in this step does not involve column pivoting, we are able to represent a product of  $\alpha$  elementary Householder reflections in a block form of Householder reflection. With this block formulation, the computation of the Householder update  $\Psi_2$  becomes rich in level-3 operations of matrix-matrix multiplications. The parameter  $\alpha$  used in the block representation of Householder reflections is dependent on the amount of floating point numbers that a given cache can hold [2]. The larger the cache, the better are the results obtained from the block algorithm.

### COMPUTATION OF HOUSEHOLDER UPDATE $\Psi_3$

This step involves QR factorization with column pivoting, and so the computation of the Householder update here is rich in level-2 operations of matrix-vector multiplications.

## COMPUTATION OF HOUSEHOLDER UPDATE $\Psi_4$

Again, the QR factorization performed in this step does not involve column pivoting, and so we are able to represent a product of  $\alpha$  elementary Householder reflections in a block form. This means that the computation of Householder updates  $\Psi_2$  as well as  $\Psi_4$  are rich in level-3 operations of matrix-matrix multiplications.

## COMPUTATIONAL RESULTS

Table 1 summarizes the results obtained from the application of cofd and LAPACK to the four btsp models we have investigated thus far. In all four models,  $A$  was a 3-by-3 block diagonal matrix. The first four columns in table 1 give the number of rows, number of columns, number of border rows, and number of nonzeros in each of the four overdetermined matrices, respectively. The fifth column gives the ratio of LAPACK execution time to cofd execution time without any parallelization. The sixth and last column shows speedups obtained by exploiting the parallelism inherent in step 1 of cofd. All computer runs were done on the SSC San Diego Distributed Center Convex Exemplar SPP 1600.

Table 1. Results from application of cofd and LAPACK to four btsp models.

Overdetermined Matrix M				LAPACK/cofd	LAPACK/cofd (Step 1 Parallelized)
m	n	$\delta$	# nonzeros		
935	300	35	7620	6.45	14.57
935	900	35	22860	5.92	10.61
2046	666	48	24840	5.67	14.48
2046	1998	48	74520	5.31	9.53

## REFERENCES

1. Schenck, H. A., G. W. Benthien, and D. Barach. 1995. "A Hybrid Method for Predicting the Complete Scattering Function from Limited Data," *Journal of the Acoustical Society of America*, vol. 98, pp. 3469–3481.
2. Golub, G. H. and C. Van Loan. 1989. *Matrix Computations*, Second Edition, The Johns Hopkins University Press, Baltimore and London.
3. Anderson, E. et al. 1995. *LAPACK Users' Guide*, Second Edition, Society for Industrial and Applied Mathematics, Philadelphia.
4. Kevorkian, A. K., D. Barach, and G. W. Benthien. 1997. "Sparse Complete Orthogonal Factorization as Applied to Bistatic Target-Strength Prediction," *Proceedings of the DoD HPCMP High-Performance Computing Users Group Meeting*, 23 to 27 June, San Diego, CA.

Principal Investigator:  
Dr. Aram K. Kevorkian  
D714

0601152N  
ZU35





## Algebraic Estimation of Multivalued Phenomena with Applications to Data Fusion

*Objective(s):* Using conditional and relational event algebra, establish a sound and unified algebraic basis, compatible with all corresponding probability evaluations, for the combination of disparate information in data fusion.

*Accomplishment(s):* During FY 98, we achieved a prime objective by establishing an algebraic (or event)-based loss function as one of the building blocks for a new algebraically oriented decision structure. With this accomplishment and the results of FY 97 employing the newly emerging mathematical tools of conditional and relational event algebra, a sound and unified decision theory—for both hypotheses testing and estimation—can now be developed with respect to a number of classes of models of information (termed “probability-functional”), which hitherto were not seen to be comparable or combinable directly as events. To this end, quantitative measures of improvement were implemented (involving the Fréchet–Hailperin interactive logical structure bounds) for these classes. In addition, another useful aspect of conditional event algebra was demonstrated by showing that the well-known, but highly controversial, “Adams’ high probability” deduction scheme is actually equivalent to ordinary conjunctive deduction in an appropriate conditional event algebra setting. Still another deduction breakthrough was shown via the two equally well-known “penguin triangle” (or generalized syllogism) and the “Judy Benjamin updating” problems being amenable to analysis via both second-order probability and conditional event algebra considerations. Finally, the scope of relational event algebra itself and tie-ins with the random set representations of fuzzy logic were greatly expanded and improved in form during FY 98 with the new treatment of several basic numerical functions.

Using some previous ILIR results derived during FY 97 (summarized in [1]), this FY 98 work is a key step toward the establishment of a logically sound, comprehensive, and numerically feasible-to-implement theory of decision making. (FY 97 work has contributed greatly to the hypotheses testing end of the theory, while present FY 99 work is directed toward the deduction and final conclusion aspect of the theory.) All of this work is centered around the newly developing fields of conditional event and relational event algebra.

In brief, conditional event algebra provides, in a sound, consistent manner, without violating any of the well-known *Lewis triviality conditions* (explained in [2], part 3), a probability space of events extending any given probability space of unconditional events and containing, as well, those special distinct events that, when evaluated probabilistically, yield conditional probabilities. In that extended space, one can first obtain any desired finite logical combination of such “conditional events” (especially those with differing antecedents), and then obtain fully implementable probability evaluations of such combinations. (See, e.g., [3] for background on conditional event algebra.) In turn, these evaluations allow, for the first time, natural probability-based metrics (such as the well-known Boolean symmetric difference probability and the newly proposed Boolean symmetric difference conditioned on disjunction probability—see again [2], part 3) to be fully evaluated. In particular, these evaluations depend nontrivially on the determination of the probabilities of logical conjunctions. Noting that conditional probabilities are nothing more than arithmetic divisions of nested events,

relational event algebra more generally provides a probability space for logically combining and evaluating probabilistically not only the identified unconditional events, but those “relational events” as well, corresponding to possibly complicated functions of probabilities, such as powers, exponents, analytic functions, and polynomials in several variables. For the same reason, in turn, natural probability metrics can be fully evaluated for the first time relative to pairs of models based on various functions of probabilities (not just divisions, as in the case of conditional probabilities). This can be implemented by use of reasonable “second-order” probability assumptions (involving the relative atomic probabilities of the relational events involved) so that the evaluations of such metrics can be used to test hypotheses of similarity of models). (See again [2], part 3 for details.) In brief, conditional event algebra—and more generally, relational event algebra—are new mathematical tools showing that probability can be extended greatly in a homomorphic-like way for evaluating previously unknown hidden logical relations between models of information, improving upon traditional numerical-only based approaches. (See figure 1 for a simple illustration.)

In particular, since rules of inference are most naturally evaluated via conditional probabilities, all of the above are applicable to the problem of determining similarity, or dually, approximate inconsistency of inference rules. Other potential applications of this work include comparisons and combinations of models that represent forced linear weighted expert opinion, as well as many types of linguistic descriptions that are initially modeled via fuzzy logic. (See, e.g., [4–6] for a listing of various data-fusion examples for which conditional or relational event algebra is applicable.)

The establishment of a new, comprehensive approach to decision making involving models of information in general probability-functional form requires three aspects, usually in the following given sequence of implementation: hypotheses testing, combination of information/estimation, and deduction or conclusion processes. In addition to determining similarity measures for testing of hypotheses where required (as developed in FY 97), the two other aspects must also be treated. FY 98 work was aimed at the estimation aspect, while FY 99 work is concerned with the deduction aspect. One basic goal of the FY 98 work was achieved with the derivation of a new loss function, compatible with conditional and relational event algebra, analogous in form to the standard numerical-based loss function of weighted sums of squares—or more generally, weighted quadratic forms. This algebraic-based loss function is a natural analogue of the well-known weighted sum of squares loss function, where, in particular, the numerical weights are replaced by “constant-probability” events (developed in FY 97), which yield constant evaluations under all probability measures. In turn, this leads to, analogous to the weighted sample mean being characterized as that entity minimizing the weighted sum of squares relative to a fixed collection of numbers, an algebraic weighting of events that, at least, yields a smaller loss (in a sense both algebraic and numerical, compatible with all probability evaluations) than either the conjunction or disjunction of a fixed collection of events. In fact, this algebraic weighting always lies event-wise between iterated conjunction and disjunction of events. (See, e.g., [7, 8].) Relations between such algebraic weighted means of events and Minkowski (or functional image) averaging of events have also been established. Ongoing numerical work is being conducted to demonstrate both the implementability and quantitative improvement in using both hypotheses testing/similarity measures and estimation techniques based on the above algebraic approach, compared to standard numerical-only approaches to modeling of information [9].

**Goals: Given Models  $M_1, M_2$  as below, determine following in sequence:**

1. Given Probability Space  $(\Omega, B, P)$ , with Ordinary (Unconditional) Events  $a, b, c$  in Sigma Algebra  $B$ , Part of  $(\Omega, B, P)$ , Obtain Product Probability Space  $(\Omega_o, B_o, P_o)$ , extending  $(\Omega, B, P)$  with Imbeddings  $(a|\Omega), (b|\Omega), (c|\Omega)$  in  $B_o$  of  $a, b, c$ , respectively, and Nontrivial Relational Events  $f_o(a,b,c), g_o(a,b,c)$  in Sigma Algebra  $B_o$ , Satisfying commutative—or equivalently, homomorphic-like—relations below
2. Determine Computable Logical Combinations, including  $f_o(a,b,c)$  &  ${}_o g_o(a,b,c)$ , over  $B_o$ , extending conjunction & over  $B$
3. Obtain Probability Evaluations  $P_o(f_o(a,b,c) \& {}_o g_o(a,b,c))$
4. Obtain full evaluations of Probability Metrics  $d(f_o(a,b,c), g_o(a,b,c))$  for comparing or testing hypotheses for  $M_1$  vs.  $M_2$
5. If desired, or appropriate, algebraically average  $M_1$  and  $M_2$  via  $f_o(a,b,c) \oplus g_o(a,b,c) = f_o(a,b,c) \times \theta(w) \vee g_o(a,b,c) \times (\theta(w))'$
6. Deductions with respect to  $M_1, M_2$ , via  $f_o(a,b,c), g_o(a,b,c), f_o(a,b,c) \oplus g_o(a,b,c)$ , interpreting weak deduction as a conditioning

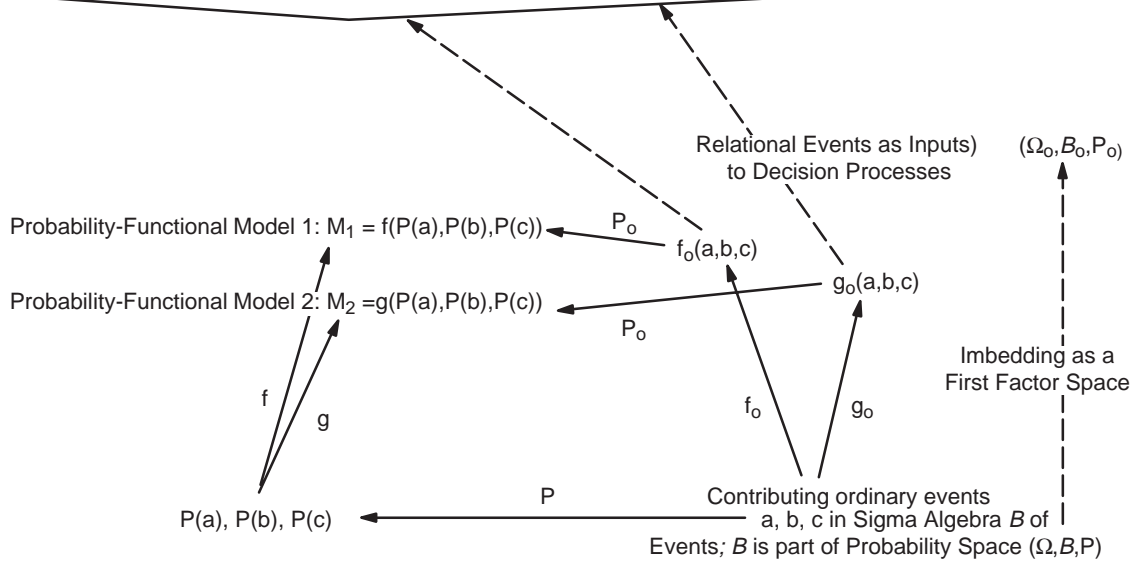


Figure 1. Summary of issues that the FY 98 project addresses for the case of two competing probability-functional models of information.

Note 1. The general mathematical issues addressed here are (1) Extend the homomorphic properties of probability with respect to the three simple arithmetic operations of addition, subtraction, and multiplication (for appropriately restricted events) to not only arithmetic division but other more complex operations. This goal is achieved via the development of the new tools of conditional and relational event algebra, whereby certain product probability spaces are constructed, extending also the original/given space of unconditional events in a natural sense. (2) Use these homomorphisms (or homomorphic-like properties) to establish measures of similarity, test hypotheses, combine information, and deduce results. Consequently, all of the above is accomplished in a more unified, feasible-to-implement, and fundamental way than previous numerical-only based *ad hoc* approaches to these issues.

Note 2. In figure 1, all of the solid arrows are “commutative,” representing the homomorphic-like relations  $M_1 = P_o(f_o(a,b,c))$ ,  $M_2 = P_o(g_o(a,b,c))$ . In achieving any of the above goals, one must be able to obtain, in reasonable closed-form, logical combinations such as  $f_o(a,b,c) \& {}_o g_o(a,b,c)$ , as well as their probability evaluations  $P_o(f_o(a,b,c) \& {}_o g_o(a,b,c))$ , where  $\&_o$  is the conjunction operator over  $B_o$  extending the given conjunction operator  $\&$  over  $B$ .  $\theta(w)$  is a “constant-probability” event in the sense that  $P_o(\theta_o(w)) = w$ , for all  $P$  of interest, for any real  $w, 0 \leq w \leq 1$ .

It was also demonstrated during FY 98 that conditional and relational event algebra are valid tools for enhancing the scope of probability in surprising new ways, while at the same time avoiding the introduction of such nonstandard concepts of *nonmonotonic logics* and related concepts. (See, e.g., Pearl's introduction to nonmonotonic logic [10].) Specifically, this was accomplished in essentially three different ways: First, it was shown, once and for all, that the well-known *Adams' High Probability* deduction scheme is actually equivalent to ordinary conjunctive deduction for an appropriate product space conditional event algebra setting (first discussed in presentation [11] and partially documented in [8]; more complete documentation is forthcoming in [12]). Second, the equally well-known *Penguin Triangle (or generalized syllogism) problem* was successfully addressed through use of second-order probabilities, as well as through interpreting—and weakening—deduction in terms of conditional probability, followed by application of conditional event algebra [8], [12]. Third, in a related direction, recent work has shown that the updating of information problem (in the form of the well-known *Judy Benjamin updating problem*) can also be successfully analyzed via the use of both second-order probabilities and conditional event algebra [13].

Also, a breakthrough was achieved in both simplifying the forms of a number of different types of relational events, as well as expanding the list of functions having relational event representations, including infinite series and polynomials in several variables (with restricted coefficients), min, max, absolute value, and bounded sum and difference, among others (see, e.g., [8], section 4).

Moreover, much progress has also been achieved in developing a compatible extension [14–16] of the now well-established one-point random set coverage representation of aspects of fuzzy logic (see, e.g., [4], sections 4–6, as well as the recent survey of the basic controversies between fuzzy logic and probability [17]).

## REFERENCES

1. Goodman, I. R. and G. F. Kramer. 1997. "Decision Theory Augmented by Natural Metrics with Applications to Data Fusion," *Independent Research 1997 Annual Report (IR '97) TD 2987* (April), SSC San Diego, CA, pp. 29–48.
2. Goodman, I. R., R. P. Mahler, and H. T. Nguyen. 1997. *Mathematics of Data Fusion*, Kluwer Academic Press, Dordrecht, Holland.
3. Goodman, I. R. and H. T. Nguyen. 1995. "Mathematical Foundations of Conditionals and Their Probabilistic Assignments," *International Journal of Uncertainty, Fuzziness and Knowledge-Based Systems*, vol. 3, no. 3, (Sept.), pp. 247–339.
4. Goodman, I. R. and G. F. Kramer. 1997. "Extension of Relational and Conditional Event Algebra to Random Sets with Applications to Data Fusion," in *Random Sets: Theory and Applications* (J. Goutsias, R. P. Mahler, and H. T. Nguyen, eds., Institute of Mathematics and its Applications [IMA] Monograph #97), Springer-Verlag, New York, pp. 209–242.
5. Goodman, I. R. 1998. "New Perspectives on Deduction in Data Fusion," *Proceedings of the 1998 (Open) Symposium on Multisensor Data Fusion* (held March 30–31, 1998, at Georgia Tech. Research Institute, Marietta, GA), pp. 79–96.
6. Goodman, I. R. and G. F. Kramer. 1998. "Recent Use of Relational Event Algebra, Including Comparisons, Estimations and Deductions for Probability-Functional Models," *Proceedings*

1998 *IEEE International Symposium on Intelligent Control* (held Sept. 14–17, 1998, National Institute of Standards and Technology (NIST), Gaithersburg, MD), pp. 543–548.

7. Goodman, I. R. 1998. “Applications of Fréchet and Other Random Set Averaging Techniques to Fusion of Information,” *Proceedings of SPIE Signal Processing, Sensor Fusion and Target Recognition VII*, vol. 3374, (I. Kadar, ed.), (held April 13–15, 1998, Orlando, FL), pp. 108–118.
8. Goodman, I. R. and H. T. Nguyen. 1998. “Adams’ High Probability Deduction and Combination of Information in the Context of Product Probability Conditional Event Algebra,” *Proceedings of the International Conference on Multisource-Multisensor Information Fusion (Fusion’98)*, vol. 1, (held July 6–9, 1998, Las Vegas, NV), pp. 1–8.
9. George, M. J. and I. R. Goodman. “Numerical Studies of Conditional and Relational Event Algebra, Illustrating Use and Comparison with Other Approaches to Modeling Information,” to be submitted for publication.
10. Pearl, J. 1998. *Probabilistic Reasoning in Intelligent Systems: Networks of Plausible Inference*, Morgan Kaufmann Publishers, San Mateo, CA. See especially sections 1.5, 10.1, and 10.2.
11. Goodman, I. R. 1998. “New Results on High Probability Deduction and Combination of Information,” presented at the 36<sup>th</sup> Annual Bayesian Research Conference (held Feb. 19–20, 1998, Los Angeles, CA).
12. Goodman, I. R. and H. T. Nguyen. “Probabilistic Transitivity, Higher Order Probability, and Product Space Conditional Event Algebra,” to be submitted for publication.
13. Goodman, I. R. and H. T. Nguyen. “Probability Updating Using Second Order Probabilities and Conditional Event Algebra,” submitted for publication in *Information Sciences*.
14. Goodman, I. R. and G. F. Kramer. 1999. “Homomorphic-Like Random Set Representations for Fuzzy Logic Models Using Exponentiation with Applications to Data Fusion,” *Information Sciences*, vol. 113, pp. 85–112.
15. Goodman, I. R. 1997. “Can a Fuzzy Analogue Be Developed Relative to Adams’ High Probability Deduction Logic?,” invited presentation to the Berkeley Information and Soft Computing (BISC) Seminar, University of California at Berkeley (Nov).
16. Goodman, I. R. and H. T. Nguyen. “Fuzziness and Randomness,” invited Chapter 1 for book *Statistical Modeling, Analysis, and Management of Fuzzy Data* (D. A. Ralescu, C. Bertoluzza, and M. A. Gil, eds.), Springer–Verlag, New York, to appear 1999.
17. Goodman, I. R. “Random Set and Fuzzy Sets: A Special Connection,” *Proceedings of the International Conference on Multisource-Multisensor Information Fusion (Fusion’98)*, vol. 1 (held July 6–9, 1998, Las Vegas, NV), pp. 93–100.

Principal Investigator:  
Dr. I. R. Goodman  
D44215

0601152N  
ZU58

## Using IMPORT to Implement Complex Behaviors in Simulations

*Objective(s):* Improve the fidelity and efficiency of warfare modeling through research on computer languages that combine imperative and declarative language structure.

*Accomplishment(s):* The Integrated Modular Persistent Objects and Relations Technology (IMPORT) is a computer language used for warfare simulation. During the course of this program, significant advancements were made in incorporating adaptive and fuzzy logic into the agent-based approach to simulation present in IMPORT.

The Declarative Object Management Environment (DOME) is the declarative sublanguage of the Integrated Modular Persistent Objects and Relations Technology (IMPORT) computer language. DOME implements a logic programming language that allows the description of complex behaviors. DOME can also be used to create “shallow models” where the programmer needs only a very rough model of some very complex object (e.g., modeling the economy based on various statistical indexes).

In principle, logic programs can perform any computation. In practice, they are inefficient at performing arithmetic and most algorithmic computations. The objective of this research was to discover an optimal language structure by combining an imperative and declarative language structure.

During the course of this project, we developed and demonstrated a synthetic-forces-level demonstration and a framework of classes that explicitly model thought process and illustrate several principles (executed simultaneously):

- (a) Multiple levels of fidelity in the course of modeling the same entities in the synthetic battlespace;
- (b) Multiple levels of resolution used to model the same set of entities in the synthetic battlespace (on-the-fly aggregation and deaggregation); and
- (c) A consistent method of behavior control in both of the above circumstances modeling C<sup>4</sup>I processes and hardware (command center, communications, and sensors).

Results from this research will be incorporated into the Joint Simulation System (JSIMS). JSIMS is a \$600M program and is currently the largest military-forces simulation program.

Principal Investigator:  
Jeffrey W. Wallace  
D44201

0601152N  
ZU64

## **Robust Control of Multiclass Queuing Systems for Command, Control, Communications, Computers, and Intelligence (C<sup>4</sup>I)**

*Objective(s):* Use modern control theory and stochastic analysis methods to design scheduling methods for multiclass queuing systems arising in heterogeneous computer networks.

*Accomplishment(s):* By using an impulse control method, we found a novel way to devise scheduling strategies. Optimal scheduling instants and schedule actions were obtained by an entirely off-line calculation involving quasi-variational inequalities.

A novel technique to devise scheduling strategies was completed by using a multidimensional stochastic point process model and impulse and stopping-time control techniques. Optimal scheduling instants and schedule actions were obtained by analyzing the optimality system, which is an entirely off-line calculation involving quasi-variational inequalities (QVI). The solution gives the optimal action to be taken at any given state in the system. The results for a two-dimensional (2-D) QVI (i.e., two queues, two processors) were plotted, and decision boundaries were determined. The possible actions were (1) transfer a job from queue-1 to queue-2, (2) no action, and (3) transfer a job from queue-2 to queue-1. These graphs were generated for many different values of the following parameters: (1) cost functional (cost for jobs to stay in the queue), (2) processor speed and arrival rate of jobs modeled as a Markov point process, (3) queue size, (4) stopping cost, and (5) switching cost. As we varied certain parameters, the system behaved as we expected. For example, if we increased the processor speed on queue-1, jobs were more readily transferred from queue-2 to queue-1.

In addition to the 2-D QVI, we also extended the results to a 3-D model. The results of this model are harder to visualize because they are 3-D boundary spaces. We did view slices of the results, and they did match our expectations with respect to changes in parameter values.

A static task scheduler was also implemented. Here, we were given a certain number of tasks and processors and needed to determine the optimal solution. This problem was deterministic as opposed to the above QVI problem, which was stochastic. We worked on this problem in the hope of supporting and possibly getting funding with the multi-modal watch station (MMWS) project.

A third task we completed with extra funds at the end of FY 98 was to implement a demonstration of a miniature Network Centric Warfare System. Our demo system includes Java code that is run on a heterogeneous network of computers and a web page to track the system. We attempted to incorporate a system that could process jobs in a secure, efficient, and reliable manner. To this end, computers can pass jobs between each other; the job states are periodically saved; and they can be transferred in encrypted mode. On our web page, you can launch a certain number of jobs, watch them being distributed, then simulate central processing unit (CPU) or power failure, and observe the robustness of the system.

Principal Investigator:  
Dr. Richard F. Freund (retired)  
(over for Associates)

0601152N  
ZU56

Associate Investigators:  
Dr. Michael J. Gherrity  
D44208

Dr. Sri Sritharan  
D313

Eric W. VonColln  
D44213

Rob Morris  
D44213

Jeff Waters  
D44213



# COMMUNICATIONS

## Applications of Stochastic Nonlinear Dynamics to Communications

*Objective(s):* Control and optimize electronic communication systems and devices via nonlinear dynamics. Specifically, the nonlinear model of the analog phase-locked loop (PLL) benefits from the optimization of the system noise at low signal-to-noise ratios (SNRs). This intriguing cooperative effect arises out of the coupling between deterministic and random dynamics in a nonlinear system and is known as “stochastic resonance” (SR). There are two distinct application areas in which nonlinear dynamics might immediately improve PLL-based communication systems. The first application area is at the component level by tuning the amount of noise present in an individual phase-locked loop. Here, the cycle slip problem (the sudden noise-induced jump from one stable state to the next) is recast as a time-dependent shot noise process that exhibits SR. The second application area occurs when nonlinear elements form arrays. By employing nonidentical oscillator theory, then “tuning” the *spatial* disorder, the SNR of an array of PLLs improves as well as the frequency and phase locking across the array. Beam steering is accomplished simply by adjusting the spatial disorder. Complementing the analytical and numerical studies of noise in nonlinear arrays is a series of experiments on microelectronic coupled dynamic elements.

*Accomplishment(s):* We formulated noise-induced cycle slipping in the analog PLL as a stochastic resonance phenomenon. As the device SNR decreases, the cycle slip rate grows until the PLL is useless. The average number of slips is a measure of noise-induced system degradation. A familiar result for nonlinear loops, specifically second-order loops with sinusoidal phase detector characteristics, is that the probability distribution of cycle slips is a Poisson process. To combat this problem, the optimization of noise may induce control over the slip rate. This involves using a time-dependent shot noise description of the cycle slip rate, which is based on the theory of single-threshold SR. In the model, the signal is too weak to induce a transition, but noise stimulates an output after which the system relaxes back to its quiescent state. No energy is required to return to the rest state. The key modeling assumption is that the phase error variance depends on the input noise level.

Equation 1 describes the evolution of the phase error ( $\theta$ ) of a second-order phase-locked loop (PLL) driven by a periodic signal ( $T_D = 2\pi/\Omega$ ) and additive Gaussian white noise. The free-running frequency of the voltage-controlled oscillator is  $\omega_o$ , and dissipation is controlled by the damping factor  $\gamma$ .

$$\ddot{\theta} + \gamma \cos \theta \dot{\theta} + \omega_o^2 \sin \theta = A \sin(\Omega t) + \eta(t). \quad (1)$$

The probability of  $q$  slips ( $2\pi$  jumps in either direction) is given by,

$$P(q) = \frac{(\nu T)^q e^{-\nu T}}{q!}, \quad (2)$$

where  $\nu$  is the average rate of slips in the measurement interval  $T$ . To formulate this as a stochastic resonance (SR) problem, the constant rate  $\nu$  is replaced by a time-dependent rate  $\nu(t)$ .

$$vT \rightarrow \int_0^T v(t)dt. \quad (3)$$

The probability distribution is now

$$P(q, t) = \frac{\left(\int_0^T v(t)dt\right)^q e^{-\int_0^T v(t)dt}}{q!}. \quad (4)$$

Since the slip rate is a Poisson process, the PLL produces a train of  $N$  uncorrelated events (slips) that are randomly distributed over the measurement interval.

$$i_T(t) = \sum_{i=1}^N f(t - t_i) \quad (5)$$

The power spectral density is computed after taking the square of the Fourier transform of equation (5), then time, ensemble, and phase averaging are applied. The incoming signal provides the periodic modulation of the cycle slip rate of the form

$$v(t) = A + B \cos(\Omega t + \varphi). \quad (6)$$

Calculating the power spectral density for the train of random slips produced by the PLL yields

$$S(f) = \left\{ 2A|F(\omega)|^2 + |F(\omega)|^2 B^2[\delta(\omega - \Omega) + \delta(\omega + \Omega)] \right\}. \quad (7)$$

Clearly, the periodic modulation of the shot noise results in the recovery of the periodic input signal  $\Omega$ .

The second area of study involves arrays of PLLs employing spatial disorder. Areas in which this could play an important role are sensor arrays, beam steering, and beam-forming problems. As a first step toward applying these results to the beam-steering problem, a one-dimensional chain of analog PLLs is simulated. Figure 1 dramatically illustrates this point. This is a numerical simulation of a one-dimensional array of 64 analog phase-locked loops. The PLLs are coupled via linear nearest neighbor with each element receiving a globally applied signal  $A \sin(\omega_D t)$ : the equation of motion is

$$\ddot{\theta}_n + \gamma \cos \theta_n \dot{\theta}_n = -\omega_{0n}^2 \sin \theta_n + A \sin(\omega_D t) + \kappa(\theta_{n-1} + \theta_n) + \kappa(\theta_{n+1} - \theta_n) \quad (8)$$

where  $\theta_n$  is the phase error of the  $n^{\text{th}}$  phase-locked loop in the chain,  $\omega_{0n}$  is the natural frequency of the  $n^{\text{th}}$  PLL, and  $\omega_D$  is the frequency of the global alternating current (AC) driving. Spatial disorder is introduced through variations in the natural frequency ( $\omega_0$ ) of each PLL. When all the elements are identical ( $\Delta\omega_0 = 0$ ), the resulting motion is chaotic, i.e., no *long-term* frequency or phase coherence. If *spatial* disorganization is introduced into an array, then ordered motion emerges. The center and bottom panels demonstrate different schemes for spatial variation. While random spatial disorder produces periodic motion, the highest degree of coherence occurs when every other element in the array (alternate binary disorder) is spatially disordered. The idea is straightforward: When a collection of limit-cycle oscillators is coupled via nearest neighbor, the oscillators become frequency locked but not phase locked. A phase gradient is created across the chain by changing the limit cycles of the elements. Simply put, altering the oscillator produces a different limit cycle and, hence,

phase. Nearest neighbor interactions transmit the change in phase down the chain forming a constant gradient. Beam steering is accomplished by continually adjusting the disorder parameter. The notion of spatial disorder improving temporal symmetry is a tantalizing result. So, can practical nonlinear arrays, such as phased-array antennas or synchronized transmitters, exploit spatial disorder to improve frequency and phase locking?

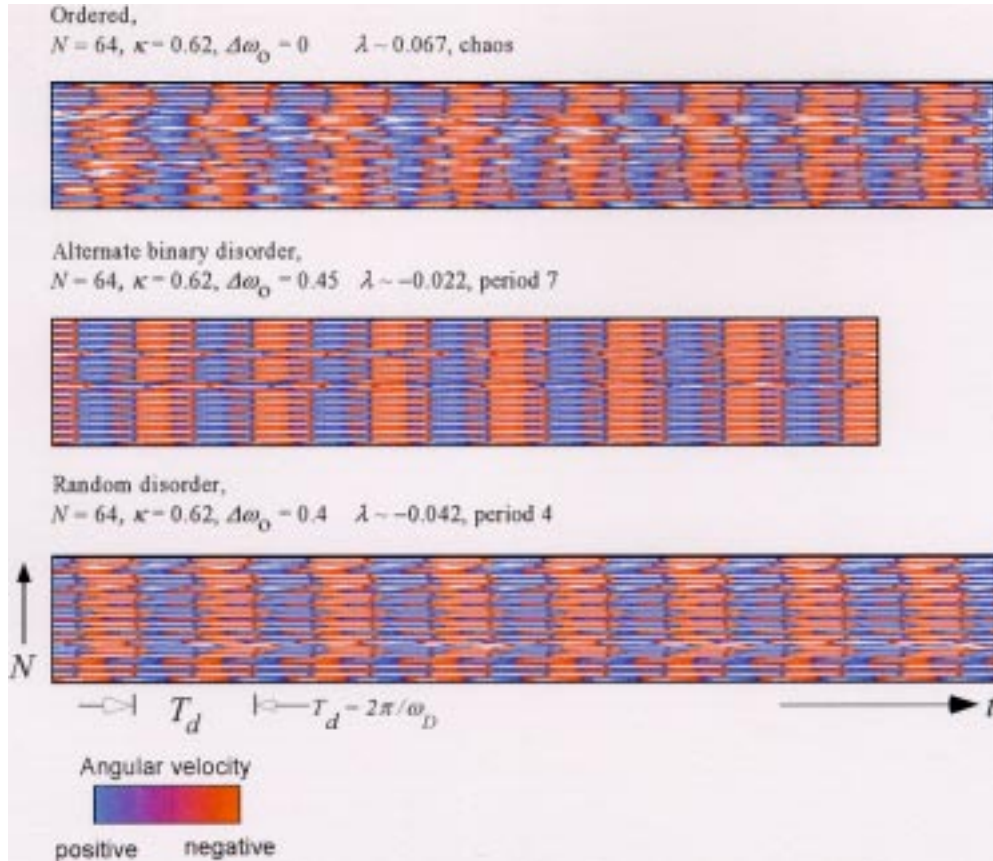


Figure 1. Time evolution (horizontally) of a chain of 64 locally coupled analog phase-locked loops. Blue and red colors code angular velocities of the spatiotemporal evolution of the array. The top panel is a collection of identical oscillators that evolve with chaotic motion. The center panel illustrates the effect of disordering every other element in the chain. The binary disorder converts the motion from chaotic to periodic. Finally, the bottom sequence illustrates the effect of randomly changing the natural frequency of every PLL. This results in periodic motion, but the phase dispersion is larger than in the previous case. The parameters used in the figure are  $\mu = 2.00$ ,  $A = 3.00$ ,  $\omega_0 = 1.54949$ , and  $\omega_D = 1.22$ .

Principal Investigator:  
Dr. Adi R. Bulsara  
D364

Co-Investigator:  
Dr. Brian K. Meadows  
D364

0601152N  
ZU65

## Performance Analysis of a Decision Feedback Equalizer for Line-of-Sight Digital Radio

*Objectives(s):* Provide an approximate analysis approach to the computation of probability of symbol error and mean-burst-error length in a decision feedback equalizer (DFE) that takes into account feedback error. Propose a new DFE design that mitigates the effects of feedback error.

*Accomplishment(s):* We have proposed an approximate analysis approach to the computation of probability of symbol error and mean-burst-error length in a DFE, taking into account the propagation of feedback error. We have also developed a new DFE design that incorporates soft decisions into the feedback mechanism and a constraint on the norm of the feedback filter. By using the proposed analysis approach and supporting it with extensive simulations, we have shown that this DFE structure can significantly mitigate the effects of feedback error.

The decision feedback equalizer (DFE) is an important component in many modern digital communication receivers and is used to mitigate the intersymbol interference (ISI) effects of channel-induced distortion of a communication signal. The DFE incorporates a feedforward filter that performs initial linear equalization of the received signal, with a feedback component that filters previously detected information symbols and subtracts the result from the output of the feedforward filter. The feedforward and feedback filter taps are jointly optimized by minimizing the minimum mean-square error (MSE) between the input and the output of the symbol detector. The DFE generally outperforms the traditional linear equalizer, particularly when the channel has deep spectral nulls in its response. The Navy has an interest in implementing the DFE structure in digital wireless modems, which must operate in a time-varying propagation environment with dispersion on the order of several communication symbols.

A potential source of degradation in DFE system performance occurs when incorrectly detected symbols are fed back through the feedback filter. Then, instead of mitigating ISI from the input to the symbol detector, the DFE enhances the ISI. The probability of symbol error and the mean-burst-error length emanating from the equalizer increase. This has been a notoriously difficult problem to analyze. The burstiness of the errors has implications for error-correction coding and interleaver depth that may be incorporated into the modem design.

In this work, we present an approximate analysis approach to the computation of probability of DFE symbol error and mean-burst-error length, taking into account feedback error. We also propose a new DFE design that mitigates the effects of feedback error. Figure 1 shows the proposed structure. A soft-decision device is included into the feedback mechanism. The intent is to feed back hard decisions of reliable symbol estimates that have small Euclidean distance to a component of the symbol constellation. Unreliable estimates that are farther away are fed back in the form of intermediate or soft decisions. Also, the feedforward and feedback filters are jointly optimized with an additional constraint on the square of the norm of the feedback filter taps. Large taps in the feedback filter result in significant ISI if decision errors are fed back. The norm constraint on the feedback filter causes more responsibility of equalization to be placed on the feedforward filter. If the norm constraint is set to zero, the linear equalizer results.

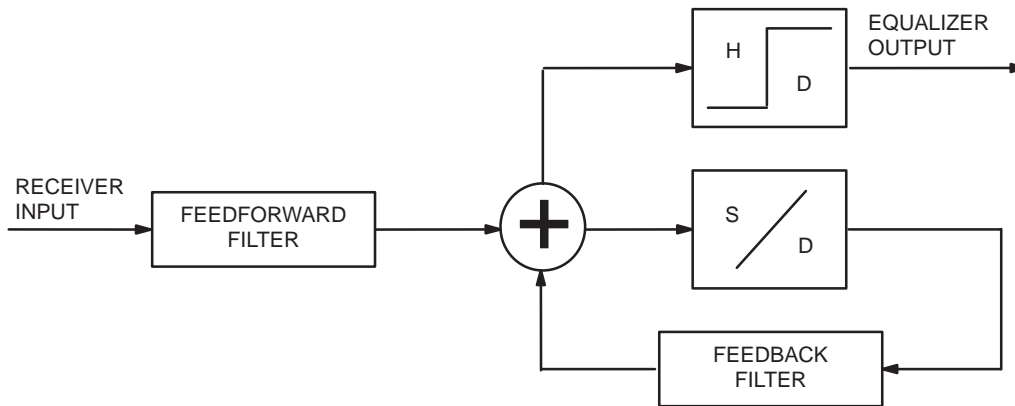


Figure 1. Decision feedback equalizer structure used to mitigate the effects of feedback error.

As an example, we equalize a channel with a delay spread of 4 quadrature phase shift keying (QPSK) symbols and 12-dB signal-to-noise ratio. We use an equalizer with 10 half-rate-spaced pre- and post-cursor taps in the feedforward filter and four rate-spaced taps in the feedback filter. The 21 taps in the feedforward filter are also used to provide matched filtering to the known transmitted waveform. Figure 2 is a plot of probability of symbol error versus mean-burst-error length for various soft-decision regions and no constraint on the feedback filter norm. The soft-decision region is defined for the QPSK symbol constellation as a pie-shaped slice with angle  $\theta$ , placed between neighboring QPSK symbols. If the input to the soft-decision device is within this region, an average of the corresponding neighboring symbols is fed back instead of a QPSK symbol. Results of the theoretical

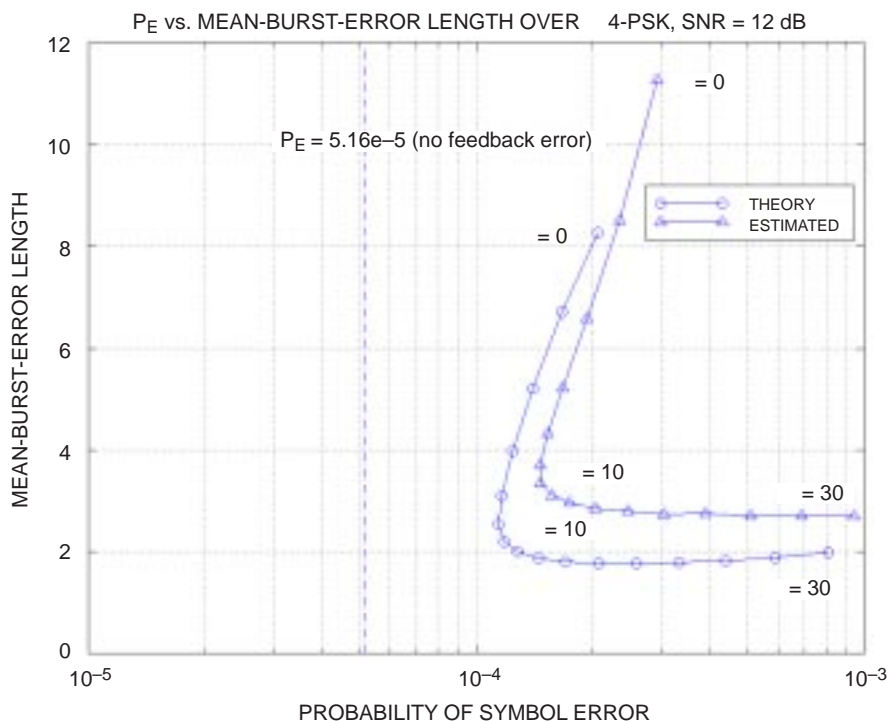


Figure 2. Probability of symbol error versus mean-burst-error length for various soft-decision regions.

analysis as well as simulation are shown. Also shown is the ideal, theoretical probability of symbol error, assuming no feedback error. This has been the traditional performance measure used for the DFE. We see that with no soft-decision region ( $\theta = 0$  degree), there is almost an order of magnitude difference between the ideal probability of error and both the theoretical and estimated error. This indicates that for this radio channel, the error feedback mechanism contributes to DFE performance degradation. Also, the average burst-error length is about 10 symbols. However, as we incorporate the soft-decision region by increasing  $\theta$ , we see that the mean-burst-error length and the probability of symbol error dramatically decrease until  $\theta = 10$  degrees. For angles greater than 10, the number of short bursts increases to the extent that the probability of error begins to degrade. Figure 3 is a similar plot for various constraints on the norm of the feedback filter with  $\theta = 10$ . The values are plotted for consecutively stronger constraints starting with 1.0 times the unconstrained norm (no constraint) to 0.05 times the unconstrained norm. We see that we can gain additional performance in terms of mean-burst-error length and probability of symbol error by incorporating into the DFE design both soft-decision feedback and a constraint on the feedback filter norm.

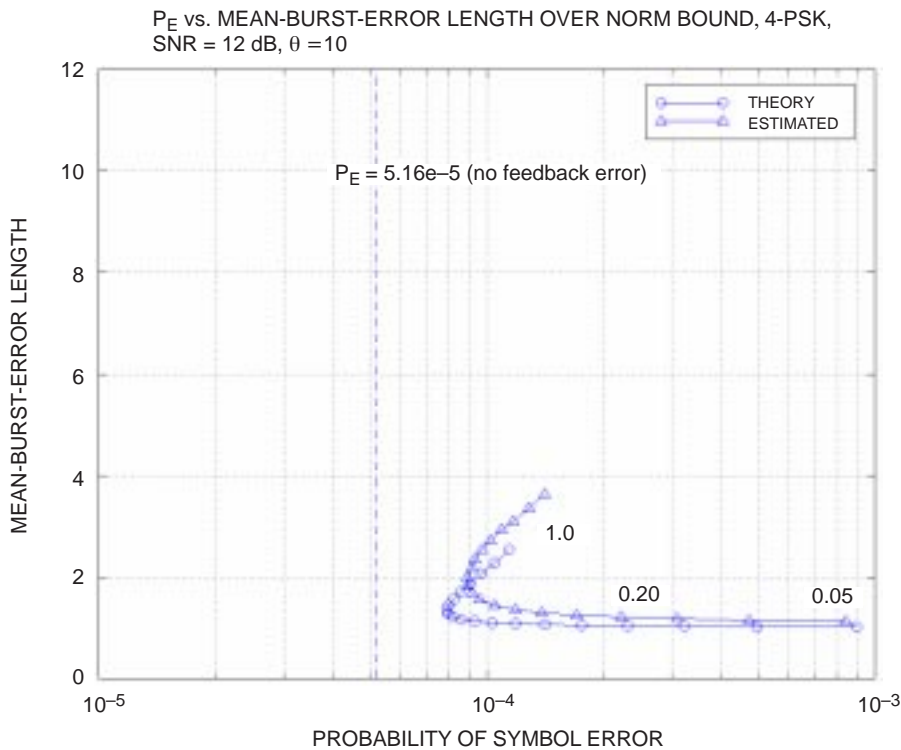


Figure 3. Probability of symbol error versus mean-burst-error length for various constraints on the norm of the feedback filter with soft-decision angle of 10 degrees.

Principal Investigator:  
 Michael Reuter  
 D855

0601152N  
 ZU60

## Development and Analysis of Turbo Codes for Navy Applications

*Objective(s):* Develop turbo coding techniques and evaluate their performance in digital radio communications channels common to Navy environments.

*Accomplishment(s):* We investigated the use of the powerful turbo coding technique combined with the bandwidth-efficient method known as trellis-coded modulation (TCM), with applications that included the 5- and 25-kHz UHF SATCOM channels. We finished a survey report comparing various methods of turbo-coded TCM, and we provided MATLAB<sup>®</sup> simulation software and a report of our results. In simulations, our turbo-coded TCM realized coding gains of 1 to 2 dB, at a bit error rate of  $10^{-5}$ , relative to an implementation of TCM known as pragmatic TCM. These gains were achieved with comparable computational complexity but greater delay than with pragmatic TCM. Actual implementation of turbo-coded TCM will require an analysis of the trade-off between the benefits of large coding gain achieved at reasonable complexity and the costs of increased delay. A table of delay as a function of interleaver length and bit rate is provided for use as a preliminary analysis of this trade-off.

SSC San Diego and the Defense Information Systems Agency (DISA) Joint Interoperability and Engineering Organization (JIEO) have been investigating methods to increase data throughput rates to 12 kbps and 64 kbps over the 5- and 25-kHz UHF SATCOM channels, respectively. There are, however, many challenges to bandwidth-efficient communication over the UHF SATCOM channel. Such challenges include (1) the hard-limiting transponder on DoD UHF satellites, which has the dual effect of removing all amplitude modulation from the transmitted signal and producing spectral regrowth, and (2) the nonlinear amplifiers often used in earth station and satellite high-power amplifiers, which can significantly distort the transmitted signal.

In view of these challenges, two well-known bandwidth-efficient techniques, known as trellis-coded modulation (TCM) and continuous phase modulation (CPM), were proposed as methods to increase UHF SATCOM data rates. TCM achieves coding gain, and therefore, higher data rates, without increasing transmitted power or required bandwidth by combining convolutional coding with higher order modulation schemes. This research investigated turbo-coded TCM (TCTCM), i.e., the application of turbo codes to TCM, in which the standard convolutional codes typically used in TCM are replaced with more powerful turbo codes.

First introduced in 1993, turbo codes are concatenated systems of two or more recursive systematic convolutional (RSC) codes, joined by one or more pseudo-random interleavers. The introduction of randomness and the use of suboptimal iterative decoding algorithms enable turbo codes to achieve near Shannon-limit performance with reasonable decoding complexity.

The application of turbo codes to TCM has received considerable attention in the literature. For our application of turbo codes to TCM, we chose to combine turbo codes with Pragmatic TCM, creating what we call turbo-coded Pragmatic TCM (TCPTCM). Pragmatic TCM (PTCM) was described in [1] and has been implemented in hardware by Qualcomm, Inc., as the Q1900 Single Chip Viterbi/Trellis Decoder [2].

---

MATLAB is a registered trademark of The MathWorks, Inc.

We began the research by writing a survey report [3] comparing various methods of TCTCM as described in the published literature. Subsequently, we developed MATLAB simulation software, including a general-purpose toolbox and a forward error-correction encoding and decoding toolbox. Finally, we performed simulations of TCTCM systems and plan to submit a report of our results [4] for publication.

We compared the performance of our TCPTCM method with that of PTCM in our own simulations and with the published simulation results of a turbo-coded TCM method of Benedetto, Divsalar, Montorsi, and Pollara [5] called parallel concatenated trellis-coded modulation (PCTCM). Figure 1 shows the results for the following comparable 2 bits/s/Hz systems: (1) uncoded quadrature phase shift keying (QPSK); (2) a rate-2/3 PTCM system comprising a single 64-state convolutional encoder; (3) a rate-2/3 TCPTCM system comprising two 16-state RSC encoders, a 1024-bit interleaver, and five decoding iterations; (4) a rate-2/3 TCPTCM system comprising two 16-state RSC encoders, an 8192-bit interleaver, and five decoding iterations; and (5) a rate-2/3 PCTCM system of Benedetto et al. [5] comprising two 16-state RSC encoders, four 4096-bit interleavers, and eight decoding iterations.

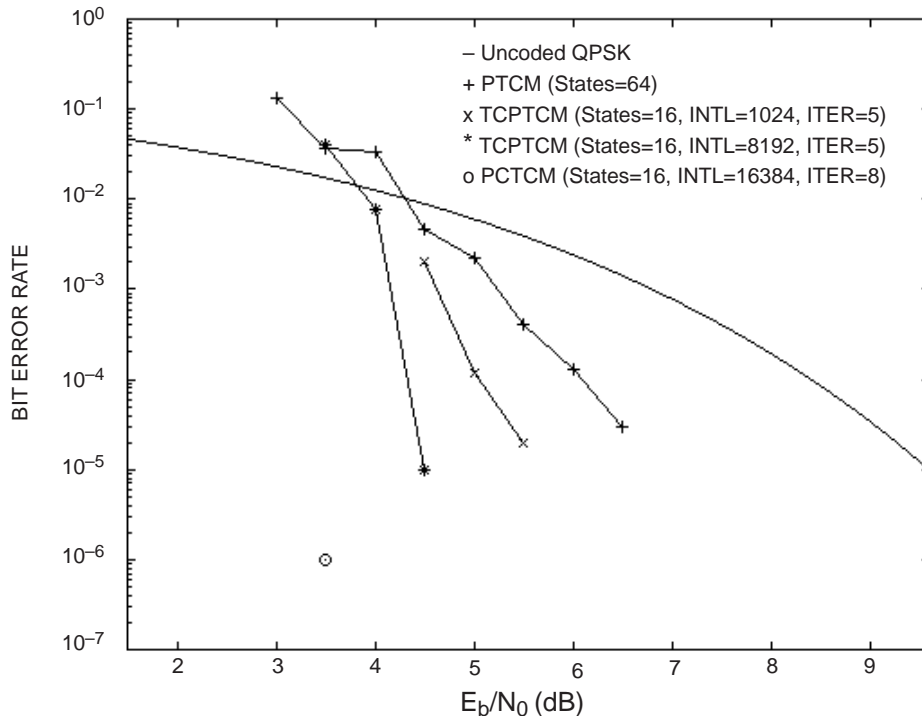


Figure 1. Bit-error-rate performance comparison between PTCM, TCPTCM, and PCTCM.

At a bit error rate (BER) of  $10^{-5}$  (figure 1), the PTCM simulation demonstrated coding gain of approximately 3 dB relative to the 9.6 dB attained theoretically by uncoded QPSK in additive white Gaussian noise. At the same BER, the two TCPTCM simulations, with computational complexity comparable to the PTCM system but greater delay, achieved increased gains of 4 and 5 dB depending on interleaver length. Extrapolating the TCPTCM curve with 8192-bit interleaver to a BER of  $10^{-6}$ , it appears that this TCPTCM system is only about 1 dB from the 3.5-dB performance point

recorded for the PCTCM system, which is itself within 1.7 dB of Shannon's limit for 2 bits/s/Hz systems.

It is encouraging that our TCPTCM system, with simpler design complexity and shorter interleaver, achieved performance nearly comparable to the PCTCM system. These results provide an example of the trade-off between the benefits of very large coding gain achieved at reasonable complexity and the costs of increased delay related to interleaver length. Figure 1 and table 1 show delay as a function of interleaver length (INTL) and bit rate (R) and can be used to provide a preliminary analysis of this trade-off. Finally, the TCPTCM system represents a simple modification of PTCM, which has already been implemented in hardware; hence, it seems likely that, with an efficient hardware implementation of turbo encoding and decoding, a hardware implementation of the TCPTCM system itself could be developed.

Table 1. Delay for selected values of interleaver length and bit rate.

R (bits/s)	INTL (bits)		
	1024	8192	16384
2400	0.427	3.413	6.827
9600	0.107	0.853	1.707
12000	0.085	0.683	1.365
32000	0.032	0.256	0.512
64000	0.016	0.128	0.256

## REFERENCES

1. Viterbi, A. J., J. K. Wolf, E. Zehavi, and R. Padovani. 1989. "A Pragmatic Approach to Trellis-Coded Modulation," *IEEE Communications Magazine*, vol. 27, no. 7 (July), pp. 11-19.
2. Qualcomm, Inc. 1998. "Q1900 Viterbi/Trellis Decoder," *Forward Error Correction Products Data Book*, vol. 80-24128-1 (February), pp. 1-1-1-77.
3. Wahlen, B. 1997. "Survey of the Application of Turbo-Codes with Trellis-Coded Modulation to Medium Data Rate UHF SATCOM," <http://bobcat.spawar.navy.mil/hdrlos>, 23 September.
4. Wahlen, B. E. and C. T. Mai. 1998. "Turbo Code Decoding Applied to Trellis-Coded Modulation," <http://bobcat.spawar.navy.mil/hdrlos/tctcm.pdf>, 5 October.
5. Benedetto, S., D. Divsalar, G. Montorsi, and F. Pollara. 1996. "Parallel Concatenated Trellis Coded Modulation," *Proceedings of the IEEE International Conference on Communications*, Dallas, TX, 23 to 27 June, pp. 974-978.

Principal Investigator:  
Dr. Bruce E. Wahlen  
D855

0601152N  
ZU63

## Resonantly Enhanced EHF Electroabsorption Modulator with a Novel N-P-I-N Diode Structure for Analog Fiber-Optic Link

*Objective(s):* Develop frequency-tuned electrical driving circuits for semiconductor optical modulators and detectors, operating up to 50 GHz.

*Accomplishment(s):* We developed a microwave tuning circuit integrated with an electroabsorption modulator to extend the modulator frequency response from 20 to 44 GHz. A modulator/detector with N-P-I-N diode structure achieved a 16-A/W detector responsivity, exhibiting phototransistor gain behavior.

### BACKGROUND

Analog fiber-optic links offer many advantages for shipboard antenna remoting as well as radio frequency (RF) distribution and control of active phased-array signals. Size, weight, bandwidth, and electromagnetic interference (EMI) immunity are the chief advantages of using fiber-optic technology and are critical topside design-engineering issues. These photonic links are applicable for future shipboard (e.g., SC 21) communication, radar, and electronic warfare systems spanning the high frequency (HF) to extremely high frequency (EHF) range. In the ILIR project, we proposed an optoelectronic monolithic-microwave-integrated-circuit (MMIC) module that uses an electroabsorption (EA) modulator with an RF tuning circuit. This MMIC module extends the present RC limited modulator response into EHF range with fractional transmission bandwidth, where  $R$  is the line impedance and  $C$  is the modulator capacitance. The MMIC module fabricated on semi-insulating substrate provides modulator and transmission-line tuning circuit integration. One of the challenging issues in the FY 97 study was the high modulator series resistance,  $R_s$ , degrading the tuned modulator response. Thus, in this FY 98 effort, we proposed an N-P-I-N diode structure to reduce  $R_s$  and to improve the modulator tuning response.

### APPROACH

A discrete EA modulator with low drive voltage generally suffers high RF loss ( $\sim 9$  dB) at EHF frequencies due to diode capacitive shunting. Reducing modulator length will reduce diode capacitance but will increase drive voltage. Another way to recover capacitive loss is to use microwave tuning for fractional bandwidth. A tuning circuit shown in figure 1(a) used LC resonance to recover the capacitive loss ( $\sim 9$  dB), where  $L$  can be a short transmission line connected in parallel to the diode. The shunting capacitor at the end of the transmission line served as a direct current (DC) block for the diode bias and an RF short to the ground for tuning. In FY 97, we proposed a resonant tuning circuit shown in figure 1(b) by adding a resonant section in front of the tuned modulator to further enhance the tuning efficiency by 6 dB.

The FY 97 report addressed the initial MMIC layout for the resonantly tuned modulator. After several iterations in our device fabrications, the first working unit was achieved in early FY 98. The microwave property of this unit was evaluated by measuring the device return loss ( $S_{11}$ ). However, contrary to the simulation, the measured  $S_{11}$  results indicated no tuning around the designed 44 GHz due to large parasitic inductance contributed by the interdigitated fingers above 20 GHz. Our measurement also indicated a large transmission-line resistance ( $>10 \Omega$ ) in the resonant section due to narrow transmission-line width. Large resistance also contributed to tuning degradation (as discussed in the FY 97 report).

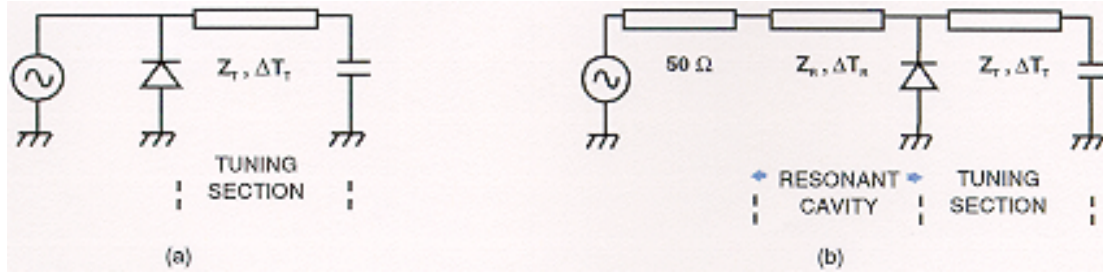


Figure 1. (a) Circuit schematics of the tuned modulator and (b) circuit schematics of the resonantly tuned modulator.

To achieve a tuned modulator at 44 GHz, we redesigned the MMIC layout (figure 2). This modified circuit layout improves the previous design by replacing the interdigitated shunt capacitor with a silicon-dioxide ( $\text{SiO}_2$ ) parallel-plate capacitor, eliminating the resonant section, and reducing the overall modulator size. The compact  $\text{SiO}_2$  capacitor eliminates the parasitic inductance of the interdigitated fingers, enabling tuning at 44 GHz. Sacrificing the resonant section, the overall modulator series resistance can be reduced to enhance the tuning response. The reduced modulator waveguide length improves the waveguide optical loss.

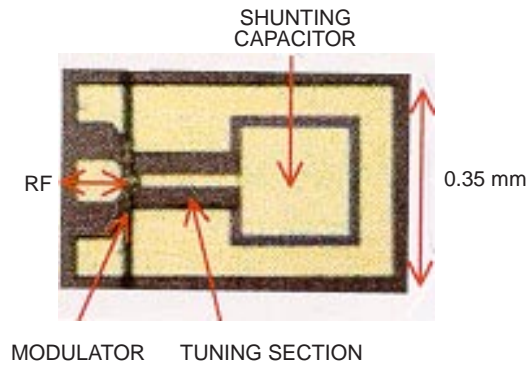


Figure 2. Modified MMIC layout for tuning at 44 GHz.

We proposed investigating the modulator with an N-P-I-N structure for reducing the modulator series resistance. This structure is designed by forward-biasing the N-P junction while reverse-biasing the P-I-N junction. By changing the waveguide from  $\text{P}^+$  layer- $\text{P}^+$  contact to  $\text{P}^+$ -N layer- $\text{N}^+$  contact, we expect to reduce  $R_s$  substantially.

## MMIC MODULE DESIGN AND FABRICATION

Using the modified MMIC design, a tuned modulator was fabricated and tested up to 50 GHz. Figure 3 shows the measured modulator S11 data and the S11 data obtained from simulated results; both are in close agreement. The S11 data indicate that the modulator is tuned at 44 GHz as specified by the design goal. Based on parameters extracted from the S11 measurements, the tuned and untuned modulator responses were simulated (figure 4). From figure 5, a 6-dB RF capacitive loss in the RC limited response was recovered by using the tuned circuit. The tuned modulator exhibits a 3-dB bandwidth of ~30 GHz.

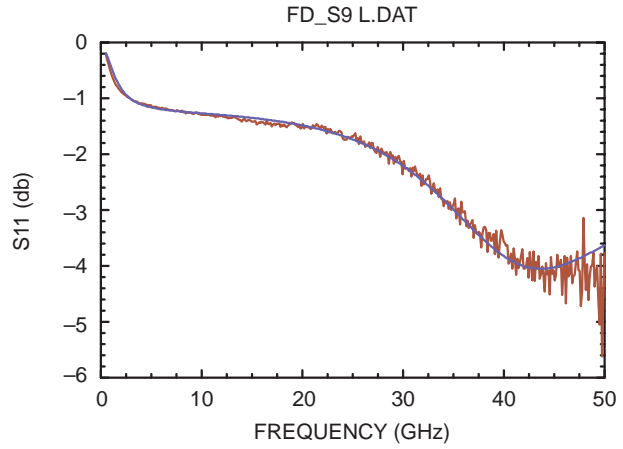
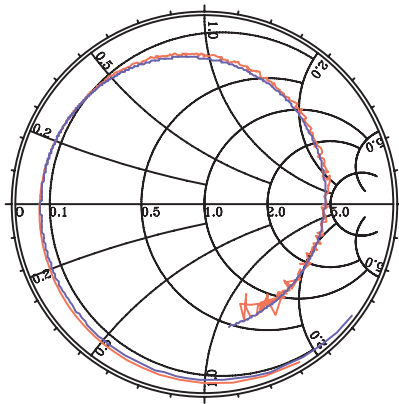


Figure 3. Measured and simulated modulator  $S_{11}$  responses of the modified MMIC design, displayed in Smith Chart and logarithm format with frequencies ranging from 0.5 to 50 GHz. The red line represents the measured results, and the blue line represents the simulated results.

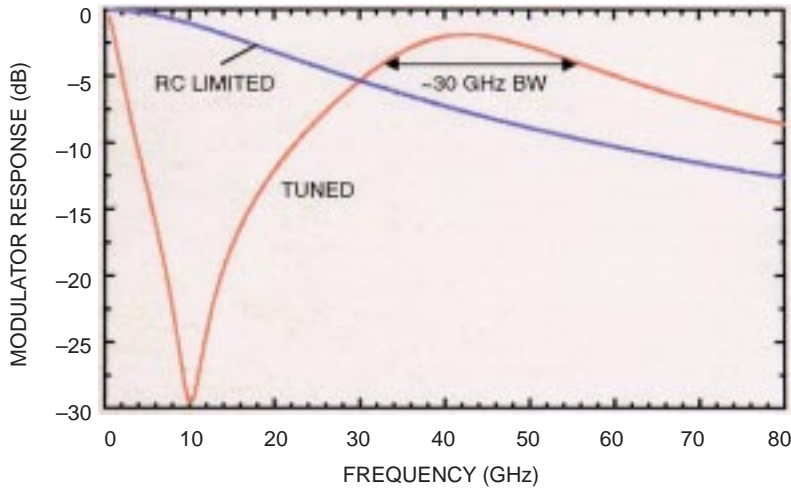


Figure 4. Simulated tuned and untuned modulator response, based on the measured  $S_{11}$  data.

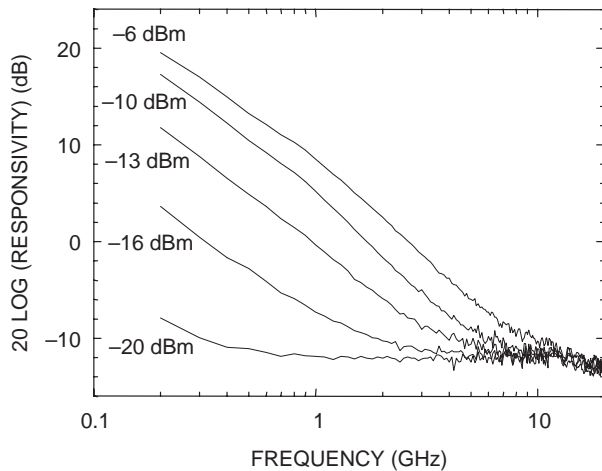


Figure 5. Frequency response of the N-P-I-N modulator/detector at different total optical powers. In the measurements, only the DC optical power is varied and the modulated optical power is fixed at  $-20$  dBm.

## MODULATOR WITH N-P-I-N STRUCTURE

The proposed N-P-I-N diode structure for reducing the modulator series resistance demonstrated phototransistor behavior in the EA photocurrent output. Due to this photocurrent generated through absorption, the EA modulator was reported useful as a waveguide P-I-N photodiode [1] with 0.47-A/W responsivity. By adding an extra N layer to the existing P-I-N structure, the responsivity of the modulator/detector can be further increased. The DC photocurrent of the modulator was measured as a function of incident optical power from a 1.32- $\mu\text{m}$  wavelength light source. A DC responsivity of 16 A/W was obtained in the range of 0.1 to 0.4 mW, due to phototransistor amplification.

The frequency response of the N-P-I-N modulator/detector at  $-6$  V bias was measured from 0.2 to 20 GHz, with a fixed RF-modulated optical power of  $-20$  dBm combined with various DC optical powers. Figure 5 depicts the measured results corresponding to cases where the combined optical powers reaching the modulator are  $-20$ ,  $-16$ ,  $-13$ ,  $-10$ , and  $-6$  dBm, respectively. It can be seen that the detector RF response increases as the DC optical level is raised. At 0.2 GHz, a factor of 23.5 increase in RF responsivity is obtained at  $-6$ -dBm total power (with a corresponding responsivity of  $\sim 10$  A/W) compared with that at  $-20$  dBm. From 0.2 to  $\sim 10$  GHz, the frequency response drops at an initial rate of  $\sim 6$  dB/octave, similar to that of a transistor behavior [2]. Enhancement of the detector responsivity with the optical power is understood in terms of the saturation of the recombination centers at the nonideal carrier-injecting emitter-base junction at high device current [3]. The saturation causes both injection efficiency and detector responsivity to increase, as is commonly observed in phototransistors.

## REFERENCES

1. Welstand, R. B., S. A. Pappert, C. K. Sun, J. T. Zhu, Y. Z. Liu, and P. K. L. Yu. 1996. "Dual-Function Electroabsorption Waveguide Modulator/Detector for Optoelectronic Transceiver Applications," *IEEE Photonics Technology Letters*, vol. 8, pp. 1540–1543.
2. Asbeck, P. M., M. F. Change, K. C. Wang, and D. L. Miller. 1990. "Heterojunction Bipolar Transistor Technology," *Introduction to Semiconductor Technology*, C. T. Wang, ed., Wiley, New York, pp. 170–230.
3. Chand, N., P. A. Houston, and P. N. Robson. 1985. "Gain of a Heterojunction Bipolar Phototransistor," *IEEE Transactions on Electron Devices*, vol. ED-32, pp. 622–627.

Principal Investigator:  
Dr. Chen-Kuo Sun  
D895

0601152N  
ZU39

Associate Investigators:  
Dr. Stephen Pappert  
D895

Prof. Paul Yu  
University of California, San Diego (UCSD)

## **Fiber-Optic Add/Drop Multiplexers Produced by Writing Gratings on Fused-Fiber Tapered Couplers**

*Objective(s):* Demonstrate a novel method for producing add/drop (A/D) multiplexers that may be used in fiber-optic systems employing multiple wavelengths of light to carry information.

*Accomplishment(s):* During FY 98, a laboratory was established for the creation of fiber-optic Bragg gratings. An excimer laser capable of creating the necessary index of refraction changes in glass fibers was procured, and an optic system using phase masks was developed for the writing of gratings. Reflective gratings were demonstrated with strengths greater than 10% in standard telecommunications fiber, and up to 95% in a special photosensitive fiber.

SSC San Diego, D895, has an established expertise in the area of fused-fiber biconical tapered couplers and has used this technology to demonstrate a variety of wavelength division multiplexers (WDMs), devices capable of combining multiple wavelengths of light onto a single optical fiber. One of the most promising devices developed has been the polarization-independent narrow channel (PINC) WDM, which has proved useful as a means of multiplexing or demultiplexing wavelengths of light that are relatively closely spaced to each other. These couplers have very low loss (typically <0.2 dB), are environmentally stable (~0.01-nm/deg C channel shift), exhibit polarization insensitivity leading to low-channel cross-talk with unpolarized light (>20-dB isolation), have been packaged to tolerate high pressures (tested to 10 kpsi), and have a small size (1/8-inch diameter, <2.5-inches long). However, these devices cannot be made with arbitrarily close wavelength spacings and, due to the condition for maintaining polarization independence, they are limited in the number of channels with which they can be used. In addition, higher channel counts require multiple PINC WDMs to be cascaded together, even if one wishes to separate only a single wavelength of light from the fiber link. This becomes important for most naval systems that will use such devices since cost, component count, and packaged size are all important issues. Thus, it is highly desirable to develop a more compact, inexpensive device.

The add/drop (A/D) wavelength division multiplexers being developed in this project are based on a combination of tapered, fused optical fiber and fiber-optic Bragg grating technologies. Fused-fiber couplers are produced such that light that was originally in one fiber is transferred entirely into a second fiber. This process is done by laying two optical fibers side by side and heating and fusing them together. The ends are then pulled so that the fibers form a tapered region in which light can transfer from the guiding region of one optical fiber to the other. Fused couplers can be made from a variety of different types of optical fibers such that the light in a very broad wavelength band in the 1550-nm region will undergo 100% coupling. A reflective region will then be created in the center of the fused coupler, which will reflect a single narrow band of light of a given wavelength. Light that has been shifted from the original optical fiber into the second one will have undergone a phase shift of 90 degrees. If the reflective region is placed in the center of the fused coupler, then light will accumulate a phase shift of 45 degrees as it travels through the coupler to the reflective region. Another 45-degree phase shift will accrue as it is reflected and travels backwards through the fiber coupler. Thus, the reflected light will also be coupled over 100% into the second optical fiber, only this time the light will emerge from the input side of the device. Thus, if many wavelengths of light

are input to the coupler on one optical fiber, most of them will be coupled over to the second optical fiber on the output end. However, the one wavelength that is reflected will emerge from the input side of the second fiber. This process will provide a mechanism for dropping a single wavelength of light off a fiber link that is carrying multiple wavelengths of light. If the grating is properly designed, it is conceivable that the device could be capable of operating similarly with light traveling in the opposite direction as well. In this way, a signal can be added to a fiber link. Thus, a single device may be capable of providing both the add and drop functions simultaneously. Figure 1 is a diagram depicting the operation of the A/D multiplexer.

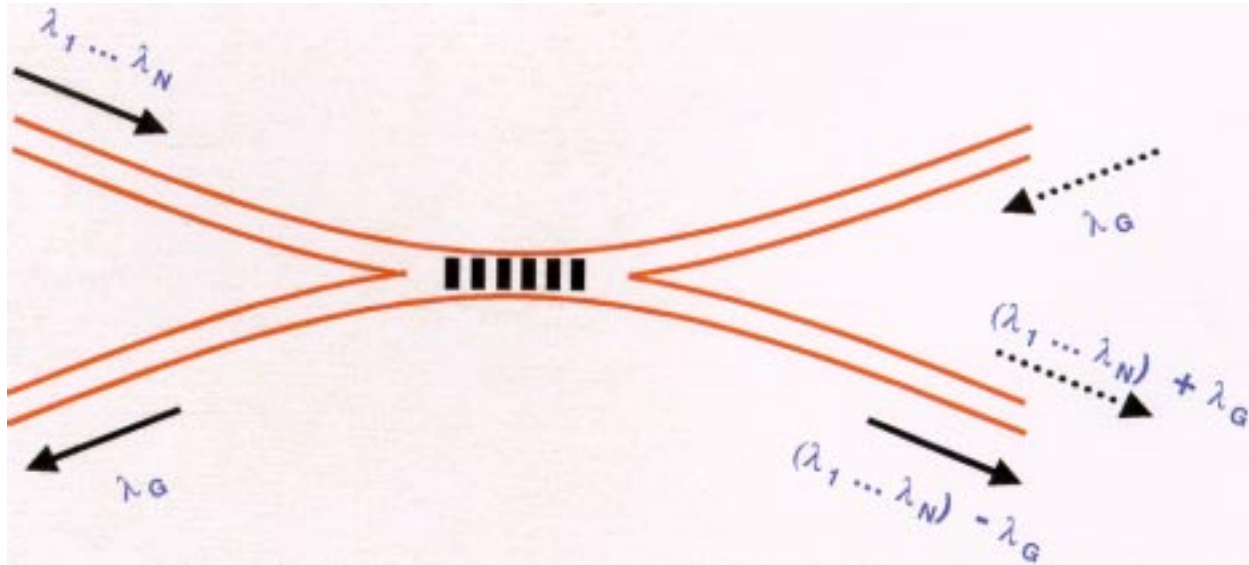


Figure 1. Schematic showing operation of the multiplexer in both the add (dashed arrow) and drop (solid arrow) configurations.

Key to the success of this task is the ability to create the narrowband reflective region in the center of the fused region of the coupler. In recent years, a technique for creating periodic changes in the index of refraction of an optical fiber has been developed. This technique causes light traveling through a fiber to be reflected when it hits this region of index modulation only if the wavelength is correct relative to the period of the index modulation. These devices, known as fiber Bragg gratings, are created by exposing periodic regions of the fiber to high-intensity ultraviolet (UV) light, which has the effect of raising the index of refraction of the exposed region. In this effort, an excimer laser, emitting at a wavelength of 248 or 193 nm, is used to create the grating. In past work with PINC WDMs, such a laser has been used to tune the wavelength response of WDMs, and index of refraction changes on the order of  $10^{-3}$  have been achieved in the fused region of couplers without damaging them. Such results are more than adequate to produce a Bragg grating. Of the various possible methods for creating the periodic exposure of the glass, the phase mask technique has been chosen due to the more relaxed fabrication requirements. Technical issues to be explored include the strength and duration of the UV beam, length and placement of the Bragg grating within the fused region, the effect of the grating writing process on the optical properties of the fused-fiber WDM, and mechanical/alignment issues regarding the placement of a phase mask in close proximity to a fused coupler.

Early work on this task has been geared toward developing the capability of creating fiber Bragg gratings. These initial tests have been performed on optical fibers, not fused-fiber devices. Preliminary results have demonstrated reflective grating strengths of better than 10% in standard telecom optical fibers and up to 95% in specially developed photosensitive optical fibers. Improvements in the mechanical and optical setup now being implemented are expected to significantly improve these results. Once high-quality Bragg gratings can be routinely produced in fibers, investigations into writing them in the fused region of fiber couplers will begin. Efforts will be directed at altering the Bragg grating facility to allow the writing of gratings on pre-packaged tapered, fused-fiber couplers. Bragg gratings fall into two different categories, labeled Type I and Type II gratings, which mainly differ on the UV fluence used when writing these gratings. These two gratings have different properties, and investigations will be made to determine which type is best suited for writing in fused-fiber couplers. Once a device has been demonstrated that indicates that gratings have been successfully written in the fused region of a fiber coupler, a series of experiments will be conducted to optimize the operation of the device as an add/drop multiplexer. Device parameters that will be addressed include insertion loss, channel isolation, directivity, and channel bandwidth. Operation for a specific function (wavelength dropping) will be investigated first, and then the process for allowing simultaneous A/D functionality will be addressed. Process variables that will be considered in the device optimization stage include UV fluence, UV wavelength, writing times, grating length and placement within the coupler, fiber photosensitivity, and grating angular tolerances, along with investigations into using various types of fused-fiber couplers. Methods will be developed to ensure repeatable, high-yield production of A/D multiplexers at specific and well-defined wavelengths. Devices will be tested over temperature to measure their environmental sensitivity, and efforts will be made to ensure that the packaged multiplexers perform in a manner consistent with the known optical fiber index of refraction temperature dependence. A successful conclusion to this work is expected to provide high-quality, robust, and inexpensive fiber-optic A/D multiplexers ideally suited for inclusion in the next generation of Navy communications and surveillance systems.

Principal Investigator:  
Richard J. Orazi  
D895

0601152N  
ZU59

## $H^\infty$ Impedance Matching for Broadband Antennas

*Objective(s):* Improve the design of impedance matching networks for broadband antennas.

*Accomplishment(s):* To maximize the power radiated from a broadband antenna, we designed a matching network to minimize the impedance mismatch between the power source and the antenna. There are standard techniques for minimizing the mismatch at a single frequency, but none solve the broadband problem. Previous methods lack any method of computing the performance of an “optimum” matching network. Thus, synthesis methods lacked a standard for evaluating their proposed matching networks. The main accomplishments of this project are fourfold: (1) We developed an algorithm and code to compute the performance of the optimum matching network; (2) We calculated this optimum performance from impedance data; (3) We calculate one component of the matrix-valued function representing the optimum matching network; and (4) We produced a collection of low-order matching circuits and explored the complexity versus optimality trade-off.

This project was motivated by two papers. A Naval Ocean Systems Center (NOSC) Technical Document by S. T. Li and D. W. S. Tam [1] set forth the Navy’s problem of designing a network to match a shipboard antenna to a 50-ohm transmission line for the high-frequency (HF) frequency band. This document provided the motivation. Also, in 1981, J. W. Helton wrote *Broadbanding: Gain Equalization Directly from Data* [2]. This paper described an approach to optimum impedance matching by using an analytic  $H^\infty$  method. The development of this  $H^\infty$  method provided the basis for this project.

Figure 1 depicts the problem setup. Given impedance data for an antenna  $z_A$  over a frequency band  $\Omega$  and line impedance  $z_G$ , find the *best* performance possible from *any* lossless matching network connecting them. The goal is to maximize the transducer power gain or, equivalently, minimize the voltage standing wave ratio (VSWR) uniformly over  $\Omega$ . *The major result of our  $H^\infty$  approach is a code that computes the performance of the optimum matching network from samples of  $z_A$ .*

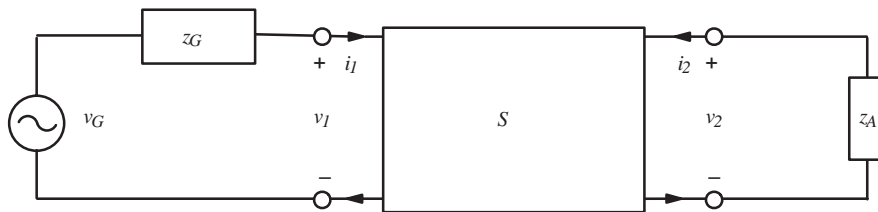


Figure 1. The matching problem. Given  $z_A$  and  $z_G$ , find a lossless two-port with scattering matrix  $S$  maximizing the transducer power gain.

Knowing the optimal performance thus provides a standard for evaluating proposed matching circuits. An example of this follows: If the optimal VSWR is 2.5 and a given matching circuit delivers a VSWR of 2.6 over the frequency band, then the circuit may be accepted as nearly optimal and quantifiably so. Conversely, if the specifications call for a VSWR not to exceed 3.0, but the optimal VSWR is 3.5, then the engineer should explore alternative designs because no matching network will suffice.

In addition to the performance bound, our  $H^\infty$  code also produces a starting point for constructing matching networks. If the scattering matrix  $S$  for a lossless 2-port is

$$S = \begin{bmatrix} s_{11} & s_{12} \\ s_{21} & s_{22} \end{bmatrix}, \quad (1)$$

the  $H^\infty$  method produces  $s_{11}$  corresponding to an optimal matching network. However,  $s_{11}$  is given only as numerical samples over the frequency band  $\Omega$ —not in the traditional rational function form. Thus, a further direction of this project is to exploit this novel  $s_{11}$  data for the construction of a practical matching network. The example below illustrates our method.

**Example.** The data in this example are 401 impedance samples measured at the SSC San Diego model range and labeled AOC21B. The frequency band  $\Omega$  is 2 to 8 MHz. Figure 2 plots the data as reflectances. The results of our  $H^\infty$  code for an optimum matching network are a VSWR = 3.378,  $s_{11}$  plotted in figure 3, and the terminated reflectance in figure 4. The  $H^\infty$  method establishes that, for an optimum matching network, the terminated reflectance will have constant magnitude over  $\Omega$ . This appears as a circle in figure 4. Using a basic optimization approach, we have constructed a simple matching circuit composed of two LC-tanks. The terminated reflectance of this suboptimal circuit is also plotted in figure 4. As the performance of these matching circuits improves, the magnitudes of their terminated reflectance converge the optimal VSWR over  $\Omega$ .

AOC21B: ANTENNA REFLECTANCE DATA

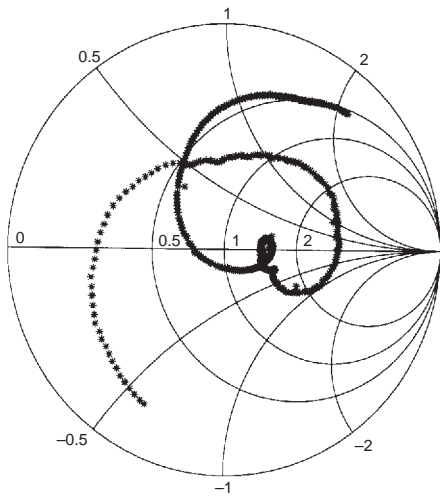


Figure 2. Reflectance measured over 2 to 8 MHz for antenna AOC21B from the SSC San Diego model range.

AOC21B: OPTIMAL MATCHING REFLECTANCE

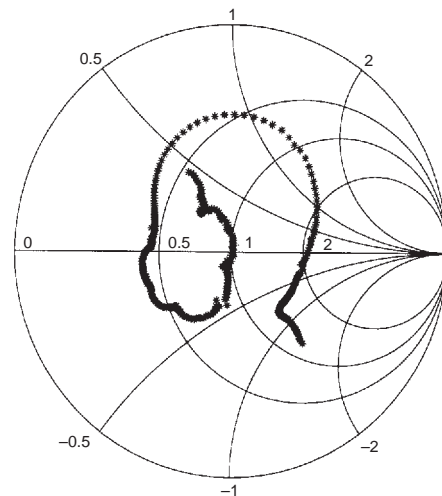


Figure 3.  $s_{11}$  from optimal matching circuit for antenna AOC21B.

AOC21B T-CIRCUIT WITH LC TANKS;  $L(\mu H) = [0 \ 4.22 \ 0.25]$ ;  
 $C(pF) = [0 \ 520 \ 1270]$

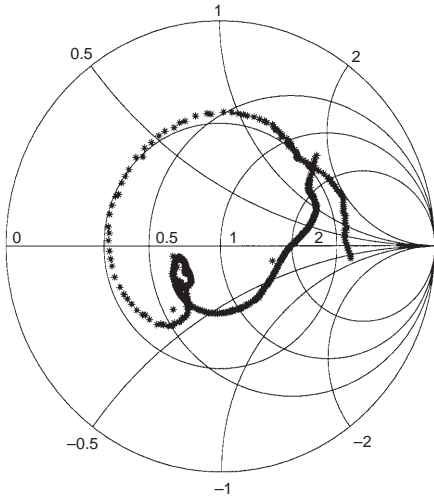


Figure 4. Terminated reflectance for suboptimal matching LC "T" with optimal VSWR = 3.378 circle.

## REFERENCES

1. Li, S. T. and D. W. S. Tam. 1987. "The Design of Impedance-Matching Networks for Broadband Antennas," NOSC TD 1148 (September), Naval Ocean Systems Center,\* San Diego, CA.
2. Helton, J. W. 1981. "Broadbanding: Gain Equalization Directly from Data," *IEEE Transactions on Circuits and Systems*, vol. CAS-28, no. 12, pp. 1125–1137.

Principal Investigator:  
Dr. David F. Schwartz  
D721

0601152N  
ZU21

---

\* now SSC San Diego

## Telesonar Channel Models

*Objective(s):* Understand undersea acoustic communication channels through theoretical and numerical modeling of the propagation physics.

*Accomplishment(s):* “Telesonar” is an undersea acoustic signaling for wireless networks of distributed sensors in shallow and very shallow water. Telesonar technology relies on modern digital signal processors (DSPs) and digital communication theory to overcome deleterious aspects of the physical channel and exploit advantageous channel features. Typically, telesonar employs various spread-spectrum modulation techniques with signal energy in the 8- to 16-kHz acoustic band. Propagation of acoustic communication signals in shallow-water environments is impaired by a complex multipath structure and the nonhomogeneous, nonstationary nature of the medium and its boundaries. The resulting multipath spread and Doppler spread can significantly disperse and distort received signals. This project is developing a physics-based numerical propagation model that attempts to account for these effects.

Research on the adverse transmission channel is essential for developing, optimizing, and using telesonar technology. The physical channel is seawater—a refractive, nonhomogeneous medium depicted in figure 1. The channel is bounded by an absorptive, range-dependent seafloor and a reflective, time-varying sea-surface. The transmitter broadcasts the signal, generally in an omnidirectional pattern. Signal propagation is via pressure waves and includes forward scattering from the channel boundaries. Signal energy arrives at the receiver amidst a background of nonwhite noise, including jammers and co-channel interference. This ILIR project addresses the need for numerical propagation models in support of telesonar-link simulation, environment-dependence assessment, performance prediction, and mission planning. Basic research for these physics-based and statistics-based models has already aided signal design, sea-test planning, and data analysis for several 6.2 and 6.3 telesonar efforts.

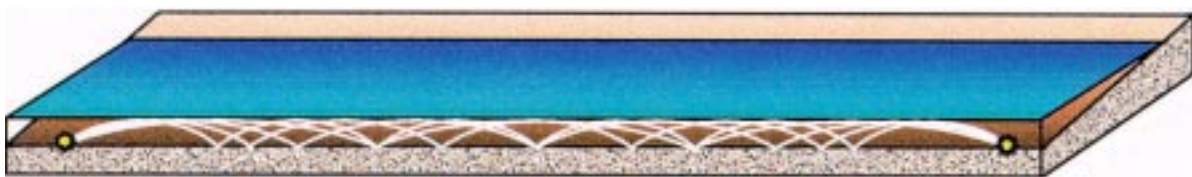


*Figure 1. Bounded, time-variant, undersea channels can spread received signal energy in both time and frequency. Analysis of this doubly dispersive propagation yielded certain necessary assumptions for channel-tolerant signal design. The transmission channel must be assumed to be Rayleigh faded and overspread, with reception impaired by nonwhite noise, including jammers and multi-access network activity.*

FY 98 was the initial year of this telesonar channel project. The research complements and supports ONR-funded 6.2 telesonar technology development initiated at SSC San Diego in FY 96. Every effort is being made to purposefully integrate the channel-research and technology-development projects to their mutual benefit. The research and technology efforts, in fact, have become co-dependent. The technology sea trials provide channel-scattering functions and channel-noise

statistics needed for the channel research. The channel research provides an understanding of the channel needed for design and development of teleseismic signaling strategies. This ILIR project has funded selected technology studies involving channel exploitation, and these efforts are the subject of continuing investigation in FY 99.

The emphasis of this project is theoretical and numerical modeling of the channel. During FY 98, available channel-response data were analyzed, and propagation theory for dispersive communications channels was examined and extended. This understanding of the acoustic propagation physics has led to the selection of an appropriate modeling philosophy based on a hybrid, three-stage approach.

*Stage-1* is a physics-based numerical propagation model built on the construct of multiple Gaussian beams radiating from the mobile transmitter in three dimensions, refracting through the layered medium, and interacting with channel boundaries. The static seafloor absorbs some energy and scatters the rest. The dynamic sea surface scatters incident energy and imparts a Doppler smearing of spectral content. The signal obtained at an arbitrarily placed mobile receiver is the integration of contributions from all influential beams. Stage-1 output is a representative time-variant, quadrature response of the nonstationary channel, along with inferred channel characteristics such as coherence time, coherence bandwidth, multipath spread, and Doppler spread. *Stage-2* is a time-dependent simulation implemented as a Markov process. The quadrature response and underlying channel characteristics obtained from Stage-1 initiate and statistically govern Stage-2. *Stage-3* involves superposition of measured or simulated channel noise, including co-channel network multiple-access interference (MAI) and jammers.

At the end of FY 98, we have implemented a static form of the Stage-1 model. Three-dimensional Gaussian beam tracing is used to account for out-of-plane reflections from rough surfaces or sloping bathymetry. The approach is to trace, in three-dimensions, closely spaced microbeams of a finite-duration continuous wave (CW) pulse from source to receiver, accumulating travel-time, phase-shift, and Doppler-shift information for each microbeam. This information is used to construct a quadrature-detector response for each microbeam. The total quadrature-detector response is obtained by summing the responses of all component microbeams.

The environment selected for testing the channel model was that of the SubLink'98 Phase-2 experiment conducted 30 June to 2 July 1998, off the coast of San Diego. The water depth was approximately 174 m with only mild variations laterally. The source and receiver depths were both set at 170 m. Figure 2 shows a ray trace (ignoring bottom-reflected energy) along with a sound-speed profile measured during the experiment. The profile is seen to be strongly downward refracting with a slight duct forming near the bottom. Since the modeling of rough-surface scattering and source/receiver and sea-surface motion are still under development, only a refractive, flat-boundary medium is considered at this time. Figure 3 shows the quadrature-detector response as a function of time of an 8-kHz, 50-ms CW pulse for receivers located at 1-km increments from the source. For this case, the averaging time was set equal to the pulse length. Figure 3a plots the magnitude of  $R_{QD}$  while figure 3b plots the real (solid line) and imaginary (dashed line) parts. The multipath structure is clearly identifiable by the multiple peaks. Future developments of the model will focus on determining how scattering from rough surfaces, source/receiver motion, and sea-surface motion will influence these responses.

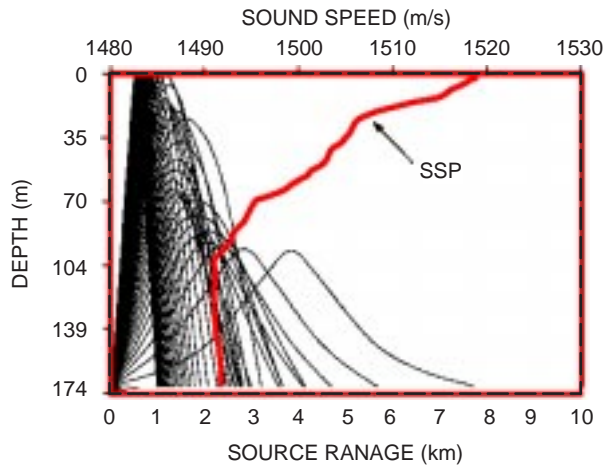


Figure 2. Sublink'98 Phase-2 sound-speed profile and ray trace (excluding bottom-reflected energy). Source depth = 170 m. Water depth = 174 m.

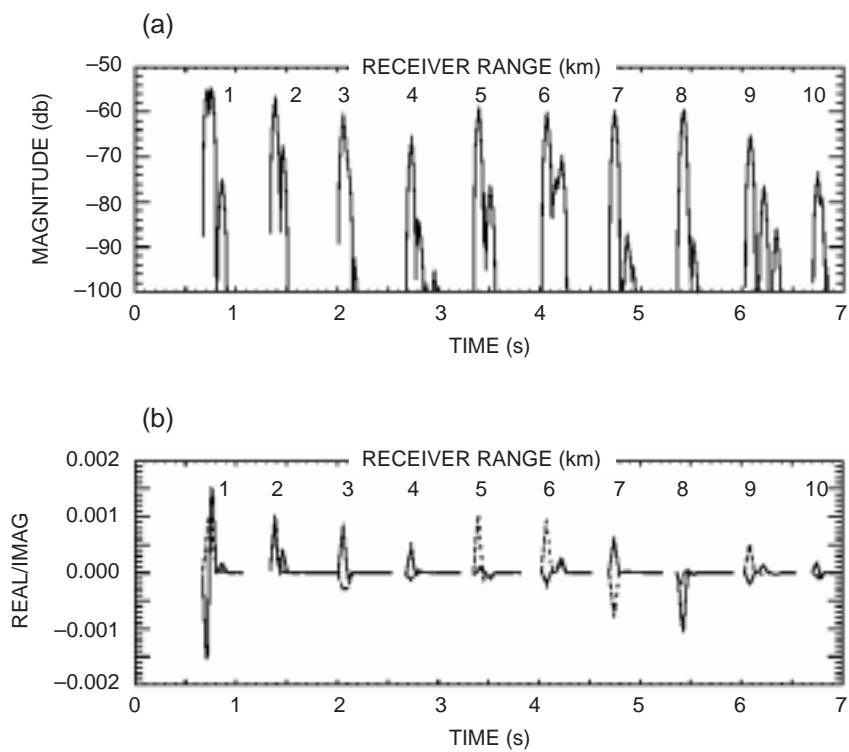


Figure 3. Quadrature detector response for 10 receivers located at 1-km increments from source for SubLink'98 Phase-2 environment. Source depth = receiver depth = 170 m. Water depth = 174 m. Frequency = 8 kHz. Pulse length = 50 ms. Averaging time (time constant) = 50 ms.

Principal Investigator:  
Joseph A. Rice  
D881

0601152N  
ZU61

Co-Investigators:  
Paul A. Baxley  
D881

Dr. Homer P. Bucker  
D881

Dr. Richard C. Shockley  
D881

Associates:  
Professors John Proakis and Milica Stojanovic, Northeastern University;  
Dale Green, Datasonics, Inc.



## Generalized Higher Order Crossings Theory and Practice

*Objective(s):* Develop an appropriate mathematical framework for extending and generalizing the theory of Higher Order Crossings (HOCs) and define novel signal/noise analysis tools, based on generalized HOC sequences, for application to detection and estimation.

*Accomplishment(s):* We investigated HOC-based methods for estimating parameters in the spectral density of a normal random process. We also investigated function-space methods and fixed-point theory for generalizing the notion of HOC. Work continued on a central limit theorem for the envelope crossings of a Chi-square process, which is a generalization of the envelope of a Gaussian process.

The Navy currently has prototype and fleet operational surveillance systems (e.g., infrared, sonar, and radar) that can produce megabytes of digital information per second. Higher Order Crossing (HOC) sequences are promising for quick classification of background/clutter data from these surveillance sensors. The sensors produce data flow rates on the order of 20 kHz (sonar), 10 mHz (radar), and 50 mHz (infrared search and track [IRST]). There is a critical need in such systems for fast, efficient methods of first classifying and then further processing (detecting and tracking) data streams from these sensors. Since real-world data can be non-Gaussian as well as spatially and temporally nonstationary, traditional signal- and data-processing methods may fail or, at best, be suboptimal for a given type of processing. Thus, new data-analysis tools that are computationally efficient and robust to nonstationary regimes are desirable.

HOCs are the level-crossing counts obtained by repeatedly filtering a time series. Generally, one deals with a zero-mean process, and thus, zero-crossing counts are of particular interest. Formulas for the average number of zero-crossings of a random process date back to the pioneering work of S. O. Rice. Explicit formulas were derived by Rice for the case of a Gaussian process since the non-Gaussian case was problematic.

The standard HOC theory has provided signal- and data-analysis tools that include fast spectral estimation, white-noise discrimination tests, and fast tests for Gaussianity, with applications in non-destructive testing and speech signal processing. Scattergram methods based on HOC sequences have proven indispensable in various nondestructive evaluation testing. Specific applications in speech processing include on-line frequency tracking and whale-vocal-sound discrimination. Generalized HOC holds the promise of a rigorous non-Fourier-based spectral analysis theory that will provide fast and efficient statistical estimators and novel discrimination metrics for use in exploratory data analyses.

During FY 98, work continued on a central limit theorem for the level crossings of the envelope of a Chi-square process. This work extends a theorem for the asymptotic normality of the level crossings of the envelope of a Gaussian process (work accomplished in FY 97).

Work also continued on infrared clutter background classifiers based on crossing counts of filtered background data.

Principal Investigator:  
Dr. John T. Barnett  
D743

0601152N  
ZU43

## Active Matched-Field Tracking

*Objective(s):* Develop new methods to automatically detect and track quiet submarines in shallow water by using matched-field tracking.

*Accomplishment(s):* We developed a method of range demodulation whereby table lookup can be used to calculate reference sound pressures. This method results in a significant reduction in the amount of required computation. We also obtained excellent results by using test data collected during the Shallow-Water Environmental Cell Experiment, 1996 (SWellEX-96) test near the Coronado bank off the coast of Southern California.

## BACKGROUND

The detection of diesel submarines operating in shallow water is a serious Navy problem. Because sound attenuates rapidly in shallow water due to bottom interaction, sonar systems (active or passive) have limited range (typically 10 km or less). Therefore, an effective antisubmarine warfare (ASW) detection system will consist of a large number of inexpensive units. By using matched-field tracking algorithms, automatic submarine detection can be made by each unit, thus providing an economical means of surveillance. Because the shallow-water sound field is a complicated mixture of multipath signals, conventional signal-processing methods (that assume a single plane-wave signal radiated by the submarine) will have degraded detection capability. In contrast, matched-field processing (MFP) [1], which matches the received signal to that calculated for a unique target location in the shallow-water environment, uses the complexity of the field to obtain a target depth. MFP requires a sound-propagation model. Because accurate shallow-water environmental data sets are not available for all possible regions of conflict, adaptive methods for improving the environmental data and detection performance were developed in the first year of this project.

## APPROACH

The basic concept of matched-field tracking was first proposed in a paper by Bucker [2]. Consider that a submarine travels from point A to point B during a period of 3 to 5 minutes. A point in seven-dimensional space represents the path (A,B). Three coordinates ( $x_A, y_A, z_A$ ) define the starting point; three more coordinates ( $x_B, y_B, z_B$ ) set the end point; and track curvature is the seventh coordinate. For convenience, it is initially assumed that  $z_A$  is the same as  $z_B$  and that the curvature is zero. During the time period, acoustic data are collected from an array of hydrophones, and elements of the covariance matrix  $g_{jkft} = \langle F_{jf} \bullet F_{kf}^* \rangle$  are formed. Here,  $F_{jf}$  is the complex Fourier transform of the signal from sensor  $j$ , in frequency bin  $f$ , and for the time interval  $t$ . The symbol  $*$  denotes complex conjugate, and  $\langle \bullet \rangle$  represents a time average. For example, if a fast Fourier transform (FFT) is used to generate 1-Hz output each second, and  $f$  represents the frequency band from 80 to 90 Hz, and  $t$  represents the time period from 30 to 40 s, then there will be 100 terms in the time average  $\langle \bullet \rangle$ . During FY 98, a method of range demodulation was developed so that table lookup could be used to calculate the reference sound pressures. This method results in a significant reduction of computer time, thereby allowing the tracking to be done in real time. Excellent results were obtained using test data collected during the Shallow-Water Environmental Cell Experiment, 1996 (SWellEX-96) test near the Coronado bank off the coast of Southern California. This work is reported in a paper [3] submitted to the *Journal of the Acoustical Society of America*. Figure 1 shows results of the

automatic algorithm. A towed source was tracked from a starting range of approximately 10 km to a point past the closest point of approach (CPA). Data from six hydrophones of a nearly vertical line array were used.

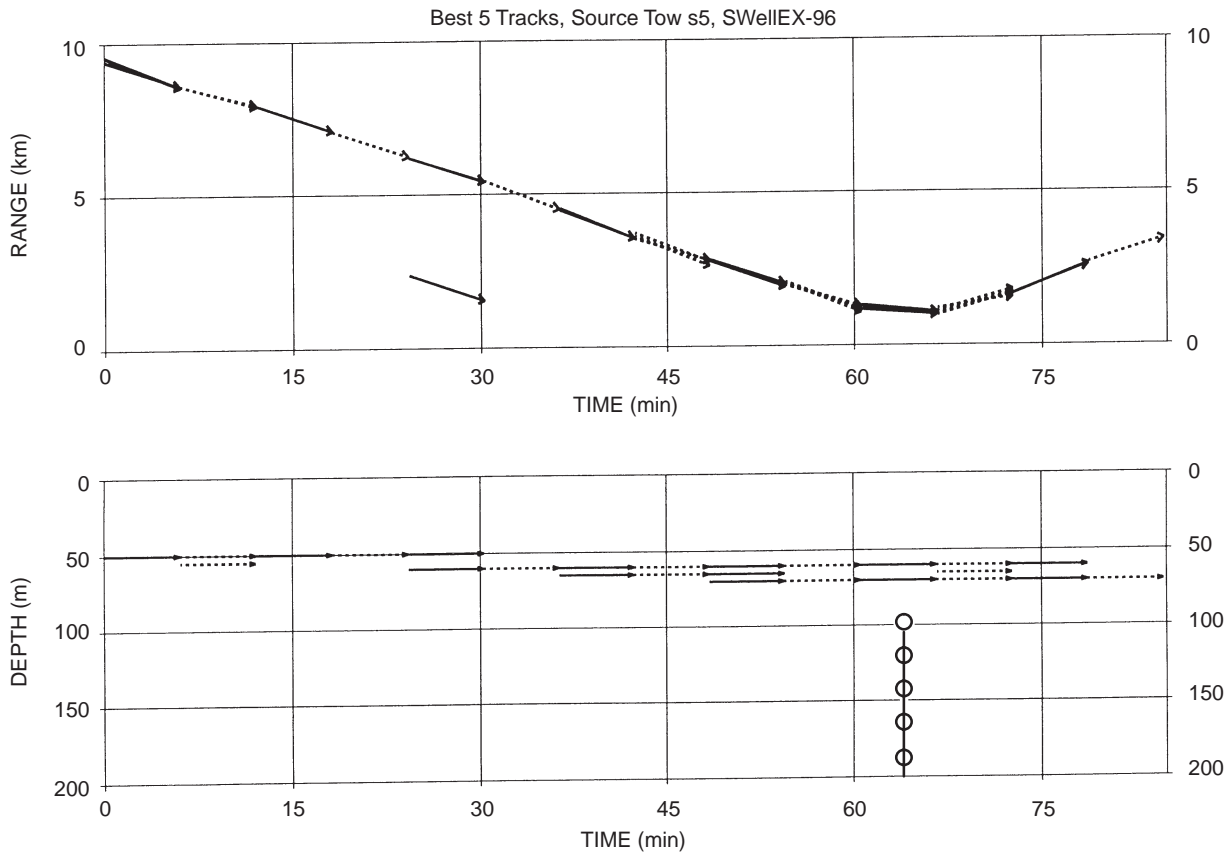


Figure 1. Results of the automatic algorithm.

## REFERENCES

1. Bucker, H. 1976. "Use of Calculated Sound Fields and Matched-Field Detection to Locate Sound Sources in Shallow Water," *Journal of the Acoustical Society of America*, vol. 59, p. 368.
2. Bucker, H. 1994. "Matched-Field Tracking in Shallow Water," *Journal of the Acoustical Society of America*, vol. 96, p. 3809.
3. Bucker, H. and P. Baxley. "Automatic Matched-Field Tracking with Table Lookup," paper submitted to the *Journal of the Acoustical Society of America*.

Principal Investigator:  
 Dr. Homer P. Bucker  
 D881

0601152N  
 ZU55

## Solid-State Blue Laser Development

*Objective(s):* Demonstrate an efficient diode-pumped Q-switched laser device at 946 nm with frequency doubling to 473 nm and determine the potential for practical underwater lidar or communication applications.

*Accomplishment(s):* Q-switched laser action at 946 nm was demonstrated in a multi-bar, diode-pumped device. A novel composite laser rod geometry was developed that improved diode-pumping brightness in an end-pumped geometry and also allowed efficient water cooling of the gain medium. Laser slope efficiencies of 20.8% and 3.4% relative to incident pump energy were achieved in long-pulse and Q-switched operation, respectively. A unique filter to suppress 1- $\mu$ m laser emission at higher pump levels was also developed but was not necessary for these experiments.

A promising approach for a simple solid-state laser source in the blue with only one nonlinear step is laser operation of the  $^4F_{3/2} - ^4I_{9/2}$  transition in neodymium (Nd) and subsequent frequency doubling. There have been significant efforts to develop low-power continuous wave (cw) blue sources for display and optical storage applications. However, other applications, such as underwater communication or laser radar, would require high-power, pulsed laser sources. The transition in Nd:YAG at 946 nm is especially promising because of the large ground-state splitting and also because 473 nm is nearly optimum for transmission in clean ocean water or Jerlov Ocean Water Types 1–3 covering much of the world's surface [1]. There is good reason to believe that coastal and ocean water generally become cleaner with increasing depth so that transmission of blue relative to green should be better with increasing depth. Nd:YAG sources at 532 nm are well developed but, in many cases, overall system efficiency would be superior in the blue if 473 nm could be generated with adequate efficiency.

There are two inherent challenges to obtain efficient laser action at 946 nm from neodymium. The gain cross section is low, (approximately 0.1 of the value at 1064 nm), and therefore, the laser performance is very sensitive to cavity losses. Also, because of the large cross section at 1064 nm, it is necessary to provide sufficient loss at 1064 nm in order to prevent parasitic lasing at that wavelength. This is more critical for Q-switched operation because the inversion is allowed to build up to high levels, and the difference in gain at 946 nm and 1064 nm becomes larger. Dielectric coatings on the cavity mirrors and the laser rod were generally adequate to suppress 1064-nm laser action. However, this is an area where improvements could be made.

Outputs of tens of mJ at repetition rates of greater than 100 Hz are expected to be required for underwater Navy applications, and therefore, multiple pump-diode bars must be used in an arrangement that maximizes pump brightness and gives high-inversion densities. A total of 20 pulsed-diode bars were used to end-pump the laser rod. All bars were configured with small antireflection (AR)-coated cylindrical lenses that collimated the emission perpendicular to the bar plane. The 1-cm bars were arranged in two stacks 1 cm wide by approximately 2 cm high, and the outputs were combined by using a polarizing beam splitter that had a half-wave plate in front of one stack. The combined pump light was then focused with a horizontal cylindrical lens and a fast f/0.67 aspherical lens onto or through the end of the laser rod. The transverse pump profile in the plane of maximum brightness was approximately 1 mm by 3 mm full width at half maximum (FWHM).

To reduce the ground-state absorption of neodymium, the total gain length must be pumped efficiently, and any length pumped below transparency must be avoided. In this work, we used a composite laser rod consisting of a short, doped section of Nd:YAG diffusion-bonded between undoped YAG sections [2]. The short gain length was matched to the pump absorption length, and the entire doped region was effectively water-cooled. The rod was 2.5 mm in diameter and had slight taper to 4 mm in diameter at the pump end. A fine polish was applied to the rod barrel so that most of the pump light transmitted through the 4-mm end would be confined by total internal reflection and concentrated in the 2.5-mm doped section.

The 4-mm rod end had a 100-cm convex radius and was coated for high reflectivity at 946 nm. Long-pulse laser experiments were conducted with a 60-cm convex output coupler and a 7.5-cm cavity length. We measured intensity profiles of the externally focused beam with a silicon charge-coupled-device (CCD) camera and obtained  $M^2$  values of 5.85 and 6.35 based on the second moments of intensity. The far-field output was nearly isotropic, which indicates that the pump absorption was very symmetric around the rod axis even though the pump profile incident on the rod was significantly asymmetric. Figure 1 shows laser performance at 20 Hz. Here, pump energy represents the measured fluence transmitted through the final focusing lens. Rods with 3-mm and 5-mm doped lengths were compared under the same conditions with a 5% output coupler. We obtained the best results with the shorter 3-mm doped rod with a maximum output of 15.5 mJ at 946 nm, which is 12.6% conversion of incident pump energy. There was a significantly higher threshold using the longer 5-mm doped rod. The maximum slope efficiency of greater than 20% was obtained with the 3-mm doped rod and a 10% output coupler, as shown. When using the 5-mm doped rod and the 10% output coupler, we did see some parasitic laser action at 1  $\mu\text{m}$ .

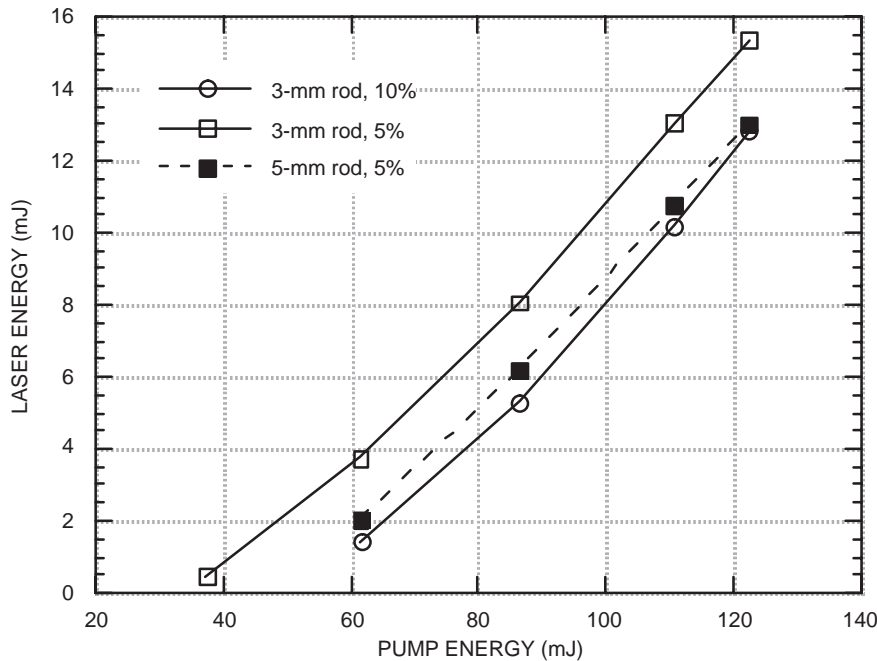


Figure 1. Long-pulse laser performance for the 3-mm rod with 10% and 5% output couplers and the 5-mm rod with a 5% output coupler.

Q-switching at 946 nm was demonstrated with a low-loss, 99%-deuterated potassium dehydrogen phosphate (KDP) Pockels cell from Quantum Technology and a polarizer consisting of two windows oriented at Brewster's angle. We were not able to Q-switch with the 10% output coupler because of insufficient transmission loss at 1064 nm. Instead, a 14.4% output coupler with higher 1- $\mu\text{m}$  loss was used with the results shown in figure 2. Here, the long-pulse performance with a bare cavity is compared with the Q-switched performance. There is significant loss associated with the polarizer and Pockels cell, which results in the lower output. The Q-switched temporal pulse was approximately 50-ns FWHM.

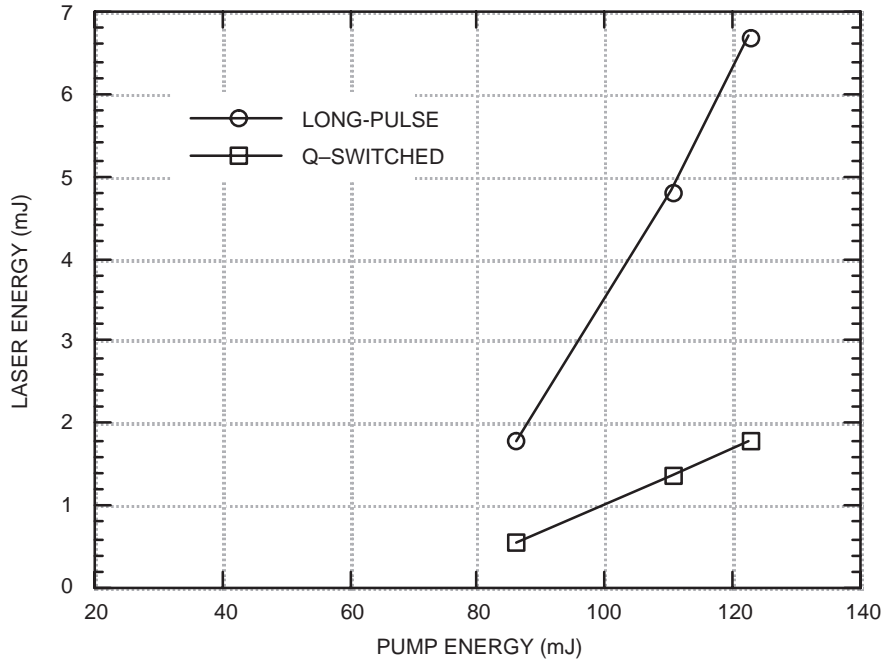


Figure 2. Laser performance for the 3-mm rod with 14.6% output coupler. Long-pulse output with a bare cavity is compared with Q-switched results using a polarizer and Pockels cell.

In conclusion, we demonstrated an approach for power scaling in Nd:YAG at 946 nm using multiple diode bars. Q-switched laser performance was significantly degraded due to cavity losses.

## REFERENCES

1. Jerlov, N. G., 1976. *Marine Optics*, Elsevier, Amsterdam.
2. Hanson, F. 1995. "Improved Laser Performance at 946 and 473 nm from a Composite Nd:Y3A15012 Rod," *Applied Physics Letters*, vol. 66, p. 3549.

Principal Investigator:  
Dr. Frank E. Hanson  
D853

0601152N  
ZU45

## Pixon-Based Image Reconstruction from Inverse Synthetic Aperture Radar Data

*Objective(s):* Modify the pixion image reconstruction method to apply to the formation of inverse synthetic aperture radar (ISAR) images and determine the improvements in image quality compared to standard Fourier inversion techniques.

*Accomplishment(s):* Although extensive quantitative evaluations could not be made in the time available, results indicated that (1) modest gains in image quality can be made by using a simple model and computationally efficient techniques, and (2) significantly better results could be obtained at the expense of a more complex model and more computationally intensive algorithms.

### BACKGROUND

The Navy is actively pursuing efforts to develop target identification systems that use inverse synthetic aperture radar (ISAR) data. Programs to identify aircraft and small ships are currently ongoing. Much of this imaging work has involved linear inversion methods using Fourier deconvolution. This approach is fast and efficient but suffers from several shortcomings. The Fourier inversion propagates the noise from the measured data into the image. It requires linear assumptions and interpolation that result in spurious responses when these linear approximations are not valid. The Fourier approach fails to achieve the maximum possible resolution because it does not take advantage of all the information available about the system.

### THE PIXION METHOD

Pixon image reconstruction is a Bayesian technique that searches for the most probable image given the measured data and a model that relates the two. In this case, the image represents a two-dimensional distribution of radio-frequency reflectivity of a target object. The model consists of the mathematical transformations necessary to predict the data that would be observed for a given image and a particular set of radar parameters. A chi-squared goodness-of-fit test determines how close the predicted data match the measured data. The probability of an image is a function of its information content and the goodness-of-fit. An iterative search technique is used to converge on the solution that maximizes this probability measure.

The pixion approach decomposes the image into a set of variably sized basis functions. Each of these functions represents a basic unit of the information content of the image and is called a pixion. These pixions form a natural coordinate system for minimizing the information content, and thereby maximizing the *a priori* probability of an image. The pixion calculator algorithm searches for the optimum size pixion for each location in the image. A larger pixion reduces the information content, thus increasing image probability. However, a smaller pixion fits the data better, increasing the goodness-of-fit, which also increases the image probability. The balance between these two factors is based on the amount of noise in the data. This occurs because the chi-squared statistic is used to determine the probability that the model produced the measured data assuming a known measurement error (i.e., noise). This also provides a natural stopping point, since improving the fit to the data only increases the probability of the image if the improvement in fit is more than would be expected from the noise.

## SCATTERING MODEL

A standard scattering model for microwave radars assumes that a target consists of a spatial distribution of point-like, isotropic scatterers. A function describing this distribution is the image to be reconstructed. Each scatterer reflects a weighted copy of the incident radar signal delayed by a time proportional to the range from the scatterer to the radar. The radar response is a superposition of the responses of all the illuminated scatterers. Under many conditions, the model can be simplified to relate the Fourier transform of the image to the frequency response of the target as measured by the radar. The conventional approach to reconstructing the image is to deconvolve the transmitted waveform from the radar data, and then apply an inverse Fourier transform to the data.

Both deconvolution and the Fourier transform amplify noise and introduce artifacts into the image. The artifacts are due to the limited region of the frequency space that is sampled by the radar measurements. Conventionally, the resolution of the reconstructed image is determined by the size of the frequency space sampled. However, information theory indicates that there is additional information in the data that is proportional to the signal-to-noise ratio of the data. The pixion method exploits this principle by allowing the pixion functions to take on sizes smaller than the conventional resolution limits set by the bandwidth of the measured data. This is only done when the smaller pixion increases the probability of the image. The increase in probability indicates that the higher resolution image is consistent with the information content of the data.

## RADAR IMAGING

The ISAR data used in this project were collected on aircraft targets by using a linear frequency modulated (LFM) chirp waveform with a bandwidth of 500 MHz. The received energy was sampled as a complex signal in the time domain. The sampled signal also contained Gaussian noise. To perform the deconvolution of the transmitted chirp signal, the data are Fourier transformed, multiplied by an inverse filter derived from the transmitted signal, and then inverse transformed. This process resulted in an image in which each scatterer on the target produced a *sinc* function response in the resulting image. The width of the *sinc* response is inversely proportional to the bandwidth of the data. This process colored the measurement noise because the frequency response of the filter did not have a uniform magnitude. That made the “compressed” data less suitable for the chi-squared goodness-of-fit than the unfiltered frequency-domain data.

Most previous applications of the pixion method have been to deconvolution problems in which the measured data were already in an image form, such as telescope data. In this case, the properties of the true underlying image are encoded locally in the data. That is, the energy from a single feature in the underlying image will be contained in a small region of the data. The pixion calculator algorithm takes advantage of this property to increase the computational tractability of the problem. However, in radar spectral data, each scatterer contributes to the response at each frequency. Ideally, a pixion calculator should be developed that performs the goodness-of-fit in the frequency domain. However, after some experimentation, it was determined that such a calculator could not be completed for this effort. Therefore, the existing pixion calculator was used to process the ISAR image after conventional Fourier processing.

## RESULTS

Conventional ISAR images were formed and used as the data for several variations of the pixon algorithms. In addition, synthetic images were used to validate the processing. In the synthetic images, white noise was added with a peak amplitude of about half that of the smallest scatterer. The pixon method was able to reduce the noise by an order of magnitude while reconstructing the scatterers. The pixon method was also able to resolve two scatterers that were one resolution distance apart.

The Quick Pixon method uses the pixon calculator to determine the optimum pixon scale at each location of the image. It assigns magnitudes to each pixon from the original data image. The Accelerated Pixon method is iterative. It optimizes the pixon size and then optimizes the magnitudes. This is repeated until the image probability no longer increases.

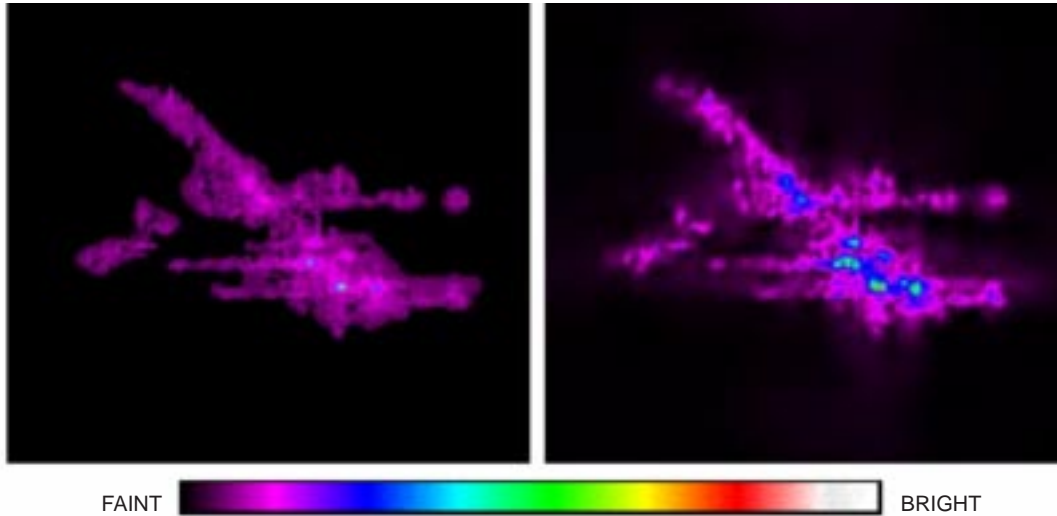
Figure 1 shows an ISAR image of a commercial jet aircraft. The fuselage extends from the nose at the upper left to the tail at the lower right. The wings extend from the middle of the fuselage. The scattering from the tail section is complicated by a “T” configuration of the horizontal and vertical stabilizers and the tail-mounted engines. The horizontal streaks to the left of the tail are caused by radar energy that is trapped in the tail and delayed before being reflected. The accelerated pixon image shows higher intensity, more concentrated scatterers. This is consistent with the scattering model, which predicts that most of the energy is scattered by surfaces normal to the radar line-of-sight and by corners such as the junction of a wing and fuselage. Such findings demonstrated significant qualitative improvements in noise reduction and elimination of spurious responses in the resulting images.

## CONCLUSIONS

Although the duration of this research did not allow for developing rigorous qualitative measures of the improvement afforded by the pixon methods, the results were encouraging. We demonstrated that improvements in image quality could be obtained by using a simplified model and computationally efficient algorithms. In addition, preliminary attempts at improving the image resolution above the bandwidth limit were effective. While these techniques can be used in their current state to gain modest improvements, additional development should result in improved techniques that take advantage of the additional information available in the frequency-domain radar data.

QUICK PIXON

ACCELERATED PIXON



FOURIER INVERSION

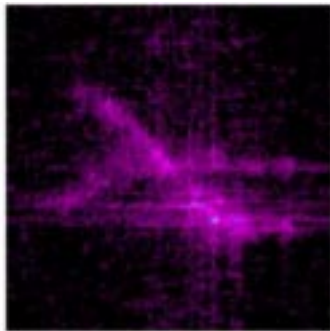


Figure 1. Comparison of the results of the Quick Pixon method and the Accelerated Pixon method. Also shown for comparison (small inset) is the result for standard Fourier inversion of the radar-imaging data. While the Quick Pixon method already is a great improvement over standard Fourier processing, the Accelerated Pixon method provides even better results (e.g., point scatterers are seen with greater spatial resolution). The improved quality of the Accelerated Pixon method results from the simultaneous optimization of image smoothness and flux. This results in a more highly simplified and optimized model for the aircraft. By contrast, the Quick Pixon method is noniterative. It uses the Fourier inversion technique to calculate the reflected radar fluxes, removes statistically unwarranted structures, but then does not reoptimize the reflected radar fluxes received.

Principal Investigator:  
Jay Trischman  
D73H

0601152N  
ZU62

### 3-D Propagation in Shallow Water Overlaying an Elastic Bottom

*Objective(s):* Provide a numerically efficient and robust acoustic model for the propagation of waves in a three-dimensional (3-D) ocean overlaying an elastic bottom.

*Accomplishment(s):* The equations of motion in an elastic waveguide were used to derive coupled mode equations for the propagation of waves in a range-dependent elastic waveguide. The coupled mode equations, which are a set of ordinary differential equations for the mode amplitudes, are coupled by the matrix of mode coupling coefficients. Unlike approaches where the wave equation is used to derive the coupled mode equations [1], the use of equations of motion results in a set of first-order, energy-conserving coupled mode equations. Using equations of motion also makes it possible to express the coupling coefficients in terms of integrals of local modes and their depth derivatives. The first use of this model would be to generate matched-field processing replicas on bottom-mounted arrays where shear wave effects are important. This model was applied to compute transmission loss in the special case of a range-dependent fluid waveguide. The results show excellent agreement with the Acoustical Society of America (ASA) benchmark solutions [2].

Matched-field processing (MFP) and matched-field tracking (MFT) have matured to where several exploratory development experiments have been conducted demonstrating passive detection, localization, and classification of submarine targets. Most experiments have been conducted in environments with high sound-speed bottoms that do not support elastic (shear) propagation. An experiment focused on MFP in elastic environments is currently being considered for FY 2000. Using MFP for source detection and localization requires the computation of replica field vectors that are solutions of the wave equation at the receiving array for a large number of hypothetical source locations. These replica vectors are then correlated with measured data to determine the location of the source. In view of the above requirement, we need a propagation model that can produce replica vectors accurately, efficiently, and rapidly. For range-independent environments, the normal mode method is the method of choice in MFP since the modes can be computed and stored. Repeated computations of the replica vectors for different source locations only require evaluation of the stored modes at those source locations. For range-dependent environments, the modes not only vary as a function of range, but range dependence forces the exchange of energy between modes through mode coupling. An accurate propagation model should also include mode coupling.

In the case of an ocean overlaying a fluid bottom, a 3-D one-way coupled mode parabolic equation (CMPE) model was developed [3] that propagates the mode amplitudes in range similarly to the way the parabolic equation (PE) method propagates the acoustic field. The exchange of energy between modes is expressed in terms of mode coupling coefficients that can be computed from the local modes and their depth derivatives. This model is well-suited for MFP in a range-dependent ocean because both the modes and the coupling coefficients as a function of range may be computed once and used in replica field computations. A realistic propagation model, however, should treat the ocean bottom as an elastic medium. In MFP applications, at low frequencies, for sources or receivers close or on the bottom, shear waves and interface modes of propagation may dominate. In ocean acoustic applications, the shear effects in the bottom may be important because conversion from compressional waves to shear waves represents a loss mechanism that can be significant. To

accommodate the MFP needs in shear supporting environments and to provide the ocean acoustic community with an accurate and robust range-dependent elastic propagation model, our objective is to extend CMPE to correctly model propagation in and over an elastic bottom.

To derive a one-way coupled mode model for the propagation of acoustic waves in and over an elastic bottom, the equations of motion in elastic media were used to obtain local mode equations for the vertical and horizontal displacements [4]. The vertical and horizontal displacement modes are coupled through the elastic mode coupling coefficients. Expressions in terms of the local modes and their depth derivatives were derived for the coupling coefficients for a waveguide made up of fluid layers, elastic layers, or a combination of both. A knowledge of the local modes and the coupling coefficients as a function of range and azimuth is enough to completely solve the elastic problem. That is, obtain all the components of the displacement vector and the stress tensor anywhere in the waveguide. To obtain the local modes, the elastic boundary value problem for the displacements, which involves four coupled, first-order ordinary differential equations, must be solved. We have solved these equations for a fluid waveguide and are currently working on finding an accurate and efficient way to solve them for an elastic waveguide. This model was applied to a range-dependent waveguide consisting of a 200-m water layer over a 1000-m bottom layer. At the 5-km range, the water depth starts decreasing at a constant rate, becoming zero at 15 km. A comparison of the transmission loss as a function of range at two different receiver depths obtained from this model and an exact two-way model shows excellent agreement (figure 1).

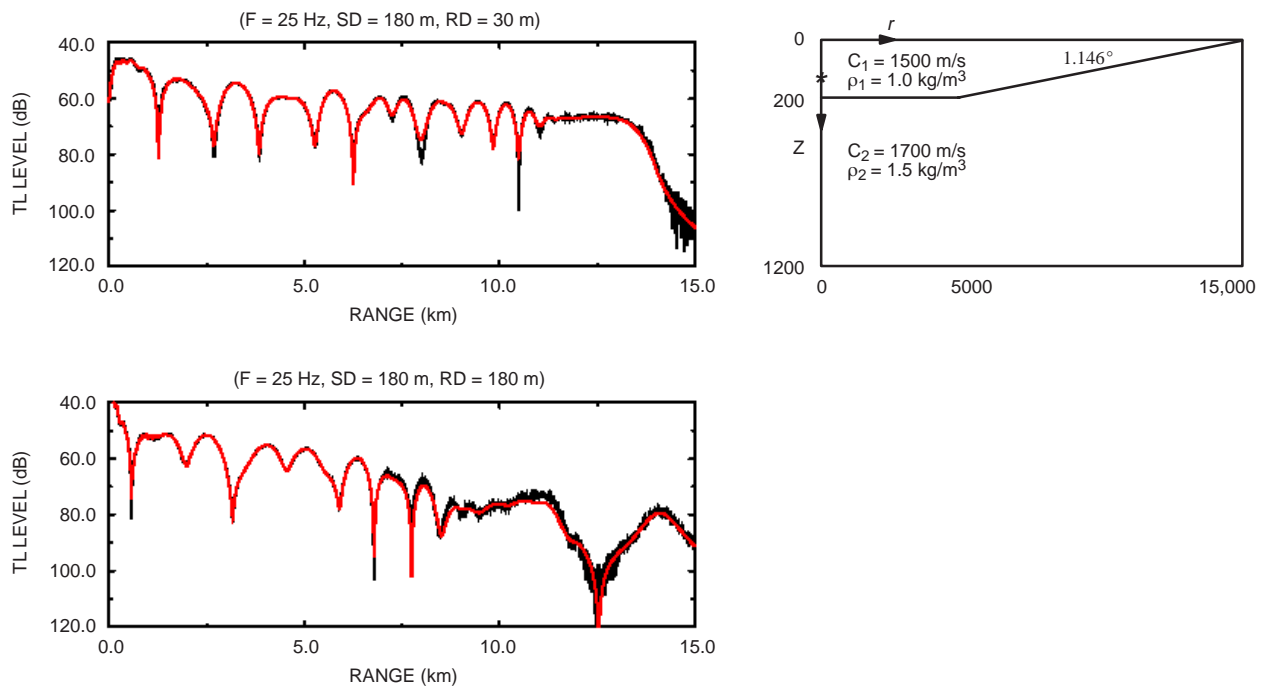


Figure 1. Transmission loss computed in a range-dependent waveguide for a source at a depth of 180 m by using an exact, two-way coupled mode model (black lines) and the energy-conserving, one-way coupled mode model developed here (red lines). The receiver is moving in range at a depth of 30 m in the top left panel and at a depth of 180 m in the bottom panel. The top right panel shows the geometry of the waveguide.

## REFERENCES

1. Pierce, A. D. 1965. "Extension of the Method of Normal Modes to Sound Propagation in Almost-Stratified Medium," *Journal of the Acoustical Society of America*, vol. 37, pp. 19–27.
2. Jensen, F. B. and C. M. Ferla. 1990. "Numerical Solution of Range-Dependent Benchmark Problems in Ocean Acoustics," *Journal of the Acoustical Society of America*, vol. 87, (April), p. 4.
3. Abawi, A. T. , W. A. Kuperman, and M. D. Collins. 1997. "The Coupled Mode Parabolic Equation," *Journal of the Acoustical Society of America*, vol. 102, (July), p. 1.
4. Tromp, J. 1994. "A Coupled Local-Mode Analysis of Surface-Wave Propagation in a Laterally Heterogeneous Waveguide," *Geophysical Journal International*, vol. 117, pp. 153–161.

Principal Investigator:

Ahmad T. Abawi

Code D881

0601152N

ZU54

## **Impulsive Snap-through Acoustic Projector (ISnAP)**

*Objective(s):* Apply analytical expressions derived during the FY 97 ILIR effort to characterize the acceleration field of an axially symmetric shell surface.

*Accomplishment(s):* Urethane and metal ISnAP prototypes were fabricated. Tests were performed, and results were compared to results from computational models.

### **BACKGROUND**

A need exists for an efficient, repeatable, impulsive source with high acoustic output over a low-frequency, broadband regime to replace present technologies (sparkers, explosive, air-gun) that use electrical/chemical/pneumatic methods for generating significant impulsive acoustic source levels. All of these technologies generate oscillating gas bubbles whose characteristics are highly dependent on hydrostatic pressure. This results in nonrepeatable effects that make processing of the received echo very challenging. Also, inherent depth dependence of gas-generating technologies greatly inhibits proper array characterization.

### **APPROACH**

Efforts were directed to develop time-domain, acoustic radiation techniques using Helmholtz integral expressions implemented by numerical computation. The time-domain acoustic model is first validated by using closed-form solutions for transient response of spheres and pistons. Then, expressions for the transient buckling of an axially symmetric shell are incorporated into the time-domain acoustic model to predict the structural-acoustic behavior of the Impulsive Snap-through Acoustic Projector (ISnAP) apparatus by numerical simulation.

### **RESULTS**

Urethane and metal ISnAP prototypes were fabricated under ONR 6.2 sponsorship (Code 321SS, Scott Littlefield and Jan Lindberg). Tests were performed at the Naval Undersea Warfare Center, Seneca Lake Detachment. This effort consisted of designing and manufacturing an ISnAP prototype and conducting an abbreviated test series to measure acoustic figures of merit and acceleration of the shell surface.

Preliminary evaluations of measured acoustic responses were performed and compared to results from computational models developed under this program. Although some agreement was found between computational and experimental results, additional resources would have been required to obtain complete quantitative agreement and predictive capability.

Principal Investigator:  
Jerome F. DeJaco  
D7102

Associate Investigator:  
Dr. George W. Benthien  
D711

0601152N  
ZU44



# OTHER LEADERSHIP AREAS

## Computational Modeling of Sediment Resuspension

*Objective(s):* Develop and computationally test models of material transport and resuspension based on the local shear stress and flow properties at the fluid–material interface computed using conditions throughout the entire domain of interest.

*Accomplishment(s):* Computations of the flow field and material transport indicate that reasonable results were obtained for the material transport, resuspension, and boundary-interface geometry. The computational method used allows for easy inclusion of various boundary conditions and resuspension models and includes a time-dependent interface technique.

The growing need to evaluate and control contaminant transport initiated by strong fluid discharges and ship wakes requires detailed understanding of the processes involved in both the transport of material and the deposit and resuspension of material, especially in a shallow-water environment.

A literature survey reveals that, in computing sediment motion in the deep ocean or along a shoreline, both empirical relationships and velocity and shear-stress approximations are used. Traditionally, models of the bottom-boundary shear stress associated with material transport provide a means to estimate the shear stress from conditions outside the bottom-boundary layer and then predict the effect it will have at the boundary. It may be postulated that the most important variable in material transport of this type is the boundary shear stress because it provides a link between the momentum and the material transport equations. Thus, the bottom-boundary shear stress determines the ability of the flow to alter the bottom. It is also known that the influence of the steady component of the bottom shear stress is difficult to estimate from a single level, and that measurements of unsteady boundary-layer flows over movable beds contain conflicting data. The important question is how does one determine the instantaneous effective bottom shear stress under flows of arbitrary form.

Considering the above difficulties in determining the boundary shear stress, we formulated a model to provide a “simple” mechanism to study the problem. It should be stated that the empirical techniques and estimates used in the past and present provide good solutions; however, we think a solution based on basic principles and Computational Fluid Dynamics (CFD) techniques would provide an alternate approach to the problem. When computing time-dependent development of the fluid–material interface geometry, methods such as front tracking or the level-set technique are not used. Rather, as part of the solution, the shape at each grid cell at each time step is computed.

For model development, we considered the two-dimensional viscous flow in a closed container. The analysis started from the Navier-Stokes equations in a vorticity-stream function formulation. We used a scalar material transport equation for each material component considered. The nondimensional equations for the vorticity  $\omega$ , stream function  $\psi$ , and transport  $C_A$  are

$$\begin{aligned} \frac{\delta\omega}{\delta t} + \frac{\delta\psi\delta\omega}{\delta y\delta x} - \frac{\delta\psi\delta\omega}{\delta x\delta y} &= \frac{1}{\text{Re}} \Delta^2\omega & \Delta^2\psi &= -\omega \\ \frac{\delta C_A}{\delta t} + \frac{\delta\psi\delta C_A}{\delta y\delta x} - \frac{\delta\psi\delta C_A}{\delta x\delta y} &= \frac{1}{\text{Pe}} \Delta^2 C_A + \frac{E_{\text{bot}} \exp(-y_{\text{ref}})}{C_2} \end{aligned}$$

where  $R_e$  is the Reynolds number,  $P_e$  is the Peclet number, and the last term in the transport equation determines the vertical distribution of material  $E_{bot}$  “picked up” or eroded from the bottom. In this formulation, the momentum and transport equations are not directly coupled. Thus, the assumption is made that the material transported does not influence the velocity field.

The transport of material at the fluid–bottom interface is determined by using an equation for the time-dependent change in bottom contour. The height of the fluid–bottom interface  $y_{bot}$  is determined using the three relationships

$$\frac{\delta y_{bot}}{\delta t} = D_{bot} - E_{bot} \quad P_u(t) = C_{P_u} \left( \frac{\theta(t) - \theta_c}{\theta_c} \right)^{1.5} \frac{1}{w_s} C_{A,bot} \quad \theta = \frac{U_\tau^2 F_R^2}{(s-1) g d}$$

where  $D_{bot}$  and  $E_{bot}$  are the amounts of material deposited and/or transported away from the bottom,  $P_u$  is a “pick up” function used to characterize how the material transported from the bottom is distributed in the vertical direction, and  $\theta$  is the Shields number. The Shields number is dependent on the boundary shear ( $U_\tau$ ), the Froude number ( $F_R$ ), the relative material density ( $s$ ), and grain size ( $d$ ). When the value of the local Shields number exceeds some critical value, material motion at the bottom is started. The boundary shear stress, and thus the Shields number, is determined by using the computed values of velocity field at the fluid–material interface.

The vorticity and material transport equations were solved by using a time-explicit, upwind, finite difference method, and Poisson’s equation for the stream function was solved by using a successive over-relaxation method. The computational method previously described was applied to several problems involving confined flows. The example shown here involves the flow over a “bump,” or mound of bottom material, located in the center of the rectangular region where the material concentration is uniform along the bottom and zero elsewhere. Figure 1a presents the geometry and the initial conditions. Figures 1b–f show the time-dependent development of the flow field, material transport, and interface contour. The “pick up” of material from the bottom is visualized via the development of the material contours and shows that the resuspension of material is occurring at various regions as the critical Shields number is reached and erosion occurs. Figure 2 presents the computed fluid–material interface and shows that the velocity field adapts to the change in bottom contour during the computation process.

The results of the model development and computations demonstrate that this is a fast and efficient method to evaluate various “pick up” functions, critical shear-stress determination techniques, and fluid–interface models. When model components have proven to be effective, they can be used in other CFD codes to solve larger and more complex problems.

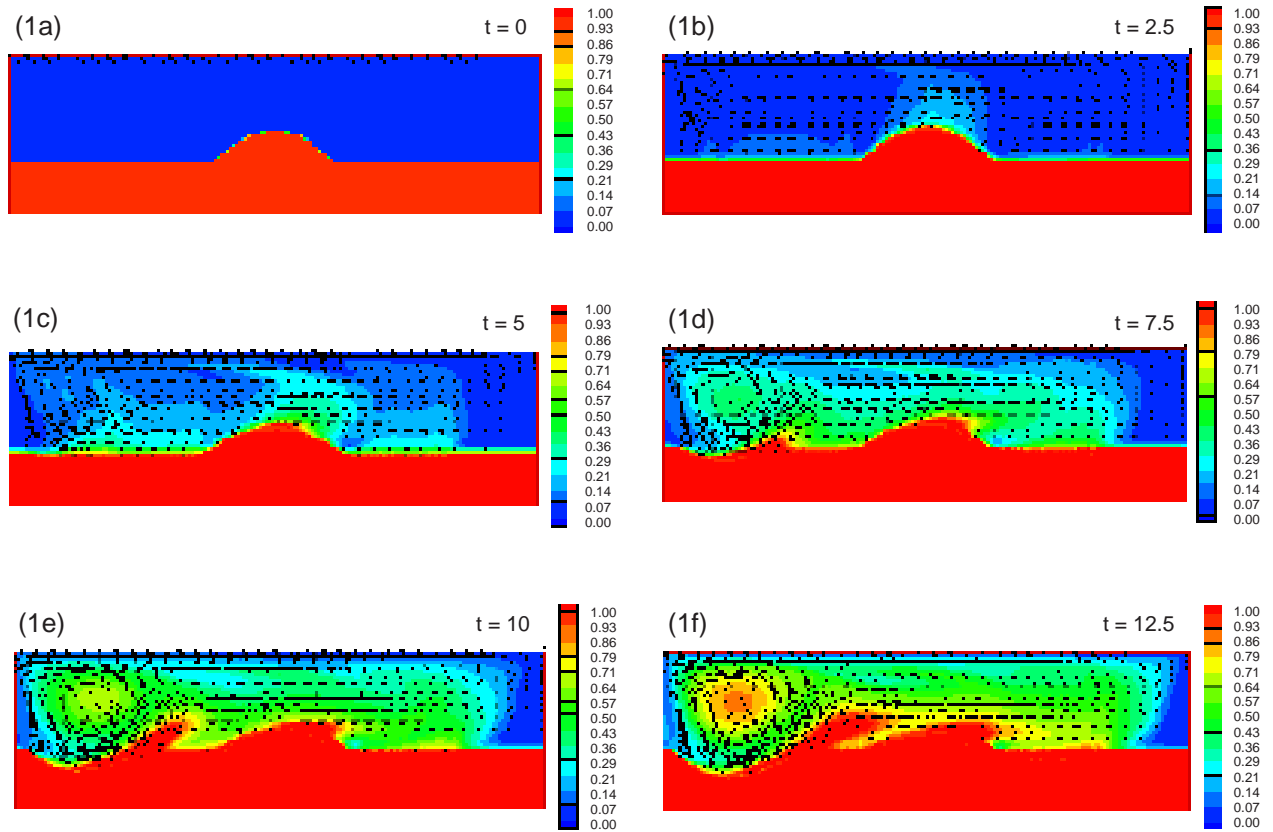


Figure 1a–f. Material concentration contours and velocity vectors for a rectangular domain with grid size 401 by 121 and  $Re = 600$  for times  $t = 0, 2.5, 5, 7.5, 10, 12.5$ .

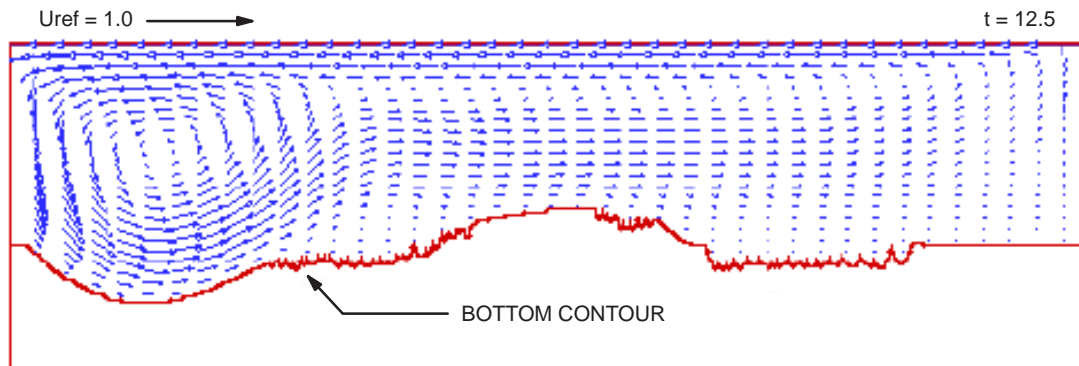


Figure 2. Computed boundary contour and velocity vectors for a rectangular domain with grid size 401 by 121 and  $Re = 600$  at time  $t = 12.5$ .

Principal Investigator:  
Dr. Tom Mautner  
D363

0601152N  
ZU52

## Anti-Ice Coatings: New Low Surface Free Energy Coatings for Easy Ice-Release

*Objective(s):* Investigate new low surface free energy materials for easy ice-release applications, (e.g., aircraft surfaces). These materials have the potential to replace or reduce the need for the conventional chemical de-icing systems of environmental concern.

*Accomplishment(s):* We designed and fabricated an apparatus for measuring ice-release properties of candidate coatings, and we developed an experimental methodology for screening potential materials and coatings. By using materials previously synthesized in this laboratory, we screened and evaluated a series of low surface free energy coatings.

This research goal is to provide an optimal coating surface upon which ice can adhere only weakly and be removed easily by minimal physical mechanisms (mechanical or thermal), rather than by environmentally unfriendly chemical processes (glycol-based freezing point depression). Chemical de-icing and anti-icing processes rely on using large quantities of chemicals that are subject to potential environmental regulation and treatment. Anti-ice coatings are an alternative to current chemical de-icing and anti-icing strategies. Such an alternative would result in a substantial decrease in chemical usage. This work addresses issues in wastewater treatment and hazardous materials management (minimization, reuse, and recycling) policies put forth by DoD agencies and the Environmental Protection Agency (EPA).

Recent advances in new low surface energy materials for use in other coating applications have resulted in a range of new materials with low surface free energies. Low surface free energy materials are known for interacting only weakly with polar liquids, are generally robust, and are capable of withstanding harsh environmental conditions for extended periods of time. For many years, U.S. Navy efforts in this area have focused on using low surface free energy as a beneficial approach to preparing materials suitable for marine fouling environments. These low surface free energy materials are designed to work by minimizing the adhesion strength between marine organisms and their substrata (*i.e.*, ship hulls, heat exchangers, power plant intakes, etc.)—an approach based on the thermodynamic work of adhesion between a solid and a liquid adherent (equation 1). The work of adhesion or work required to separate the adherent from the solid  $W_{sl}$  is the sum of the surface free energies of adherent  $\gamma_l$  and solid  $\gamma_s$ , minus the interfacial tension between the solid and adherent  $\gamma_{sl}$ . A weaker adhesion results from lowering the surface free energy of the solid.

$$(W_{sl} = \gamma_s + \gamma_l - \gamma_{sl}) \quad (1)$$

The hypothesis for ice-release is that if a liquid (water) does not wet a surface, it will not be able to adhere well when it becomes a solid (ice). An underlying mechanism for this theory may be related to a reduction of the actual contact area between the adherent and low energy surface.

Previous research in this laboratory was directed at preparing extremely low free energy surfaces for biofouling release. Useful chemistries were successfully demonstrated by preparing comb-like polymers with siloxane, polyacrylate, and polymethacrylate backbones with perfluorinated sidechains. Perfluorinated siloxanes exhibited excellent performance and properties but were considered too costly. Perfluorinated acrylate/methacrylate homopolymers exhibited low surface free energies but

had undesirable physical properties. Perfluorinated acrylate/methacrylate copolymers showed low surface free energies, good physical properties, and economic feasibility.

The technical approach of this continuing work is to utilize and transition existing knowledge, new materials and testing methods, and lessons learned from fouling-release coatings technologies into ice-release coatings. Initial efforts have focused on new low surface free energy materials developed in-house for the fouling-release coatings applications previously described. Coatings prepared and evaluated for ice-release have been screened for removal of ice under a minimal stress, or shear adhesion (release under shear due to low adhesion strength), by measuring the force required to remove ice from the coating. For this purpose, we designed and fabricated test instrumentation, and we developed a protocol for performing such measurements routinely. Ice-release screening to date has resulted in an initial down-selection of over 20 different coatings for materials previously prepared in this laboratory. We characterized coatings prepared from these materials and took ice-adhesion measurements as a function of fluorine content, polymer structure and molecular weight, surface energy, coating crystallinity, and surface roughness. Figure 1 shows the ice-release measurements for a representative series of materials differing only in fluorine content and coating type. Replicate samples of each type of coating were evaluated for initial ice-release. Additionally, each type of coating was subjected to repeated freeze-release thaw cycles to evaluate physical toughness and release reproducibility. Homopolymer coatings did not appear as robust as copolymer coatings

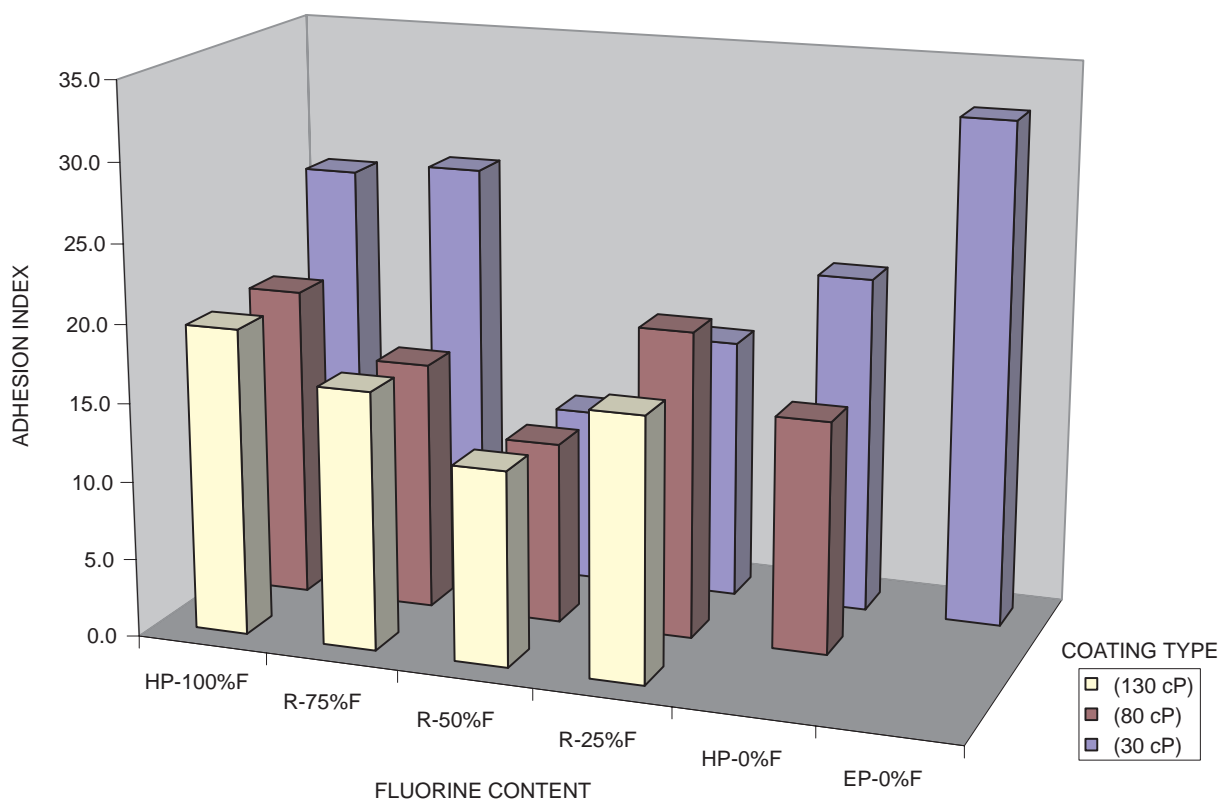


Figure 1. Ice-release properties of a low surface free energy coating series as a function of fluorine content (%F) for three types of coatings prepared with a design for varied coating crystallinity (30, 80, and 130 cP). A lower adhesion index indicates better ice-release.

when subjected to multiple ice-release cycles. In general, and as illustrated by figure 1, those coatings prepared from materials that are nominally 50% fluorinated appear to exhibit the lowest ice-adhesion values. Other preliminary work has used polarization-dependent surface infrared reflection spectroscopy to focus on surface chemical/structural characterization for this type of coating and its interaction with water.

Principal Investigator:  
Dr. Robert D. George  
D361

0601152N  
ZU57

## Surface-Plasmon Flat-Panel Display

*Objective(s):* Develop components and understand processing techniques required for a novel flat-panel display that uses the surface-plasmon effect for color generation and light modulation.

*Accomplishment(s):* We demonstrated color-selective absorption by surface plasmons and the projection of primary colors (cyan, yellow, and magenta) from a surface-plasmon tunable filter. We also demonstrated a broadband light modulator by using the surface-plasmon effect to achieve gray scales. Additionally, we designed and fabricated a prototype surface-plasmon display. This ILIR project has initiated the transition of the technology to the commercial sector through a Cooperative Research and Development Agreement (CRADA).

In the Navy, there is an increasing demand for all types of display systems. In particular, command and control requires large-screen, high-density tactical displays. Commercial systems are not yet available that can meet both the cost/performance and size/weight requirements. Established technologies such as projection cathode ray tube (CRT) and active-matrix liquid crystal devices (AMLCDs) are attempting to fill this void by incremental improvements. In addition, there are a number of emerging technologies such as plasma discharge, field emission, and the digital mirror device (DMD). However, these display technologies do not meet resolution and brightness requirements for proposed advanced displays (e.g., electronic workstations). This ILIR project, a collaborative effort with the Jet Propulsion Laboratory, proposed a new display technology that uses voltage-induced, color-selective absorption by surface plasmons at a metal/liquid crystal interface. This approach has several potential advantages: increased brightness, improved color purity, higher pixel density, lower cost, and higher reliability.

The objective of this 2-year ILIR project was to develop components and to understand processing techniques required for this novel technology and to demonstrate a proof of concept. The first-year effort focused on fabricating an active color filter (using surface plasmons) that was electrically tuned to produce the primary colors (cyan, yellow, and magenta). Figure 1 shows the theoretical and experimental tuning ability of this surface-plasmon tunable filter. Colors were generated by absorption by the surface plasmons at a silver/liquid-crystal (Merck E49) interface and tuned by applying a voltage across the liquid crystal capacitor structure. Test wafers were fabricated (NRaD\* Lot #1844 and #1963), and the wafers were subsequently used for assembly of the prism, top electrode, and liquid crystal structures. Optical coupling of the broadband light source to the surface-plasmon elements was modeled, and SF-57 Schott glass (refractive index of 1.85) was selected for display/filter assembly. Custom-fabricated SF-57 dove prisms were purchased and used for assembling the test displays.

Alternate electrode and electro-optic materials were also modeled and investigated. We completed preliminary tests on the fabrication of semi-transparent titanium silicide layers (NRaD Lot # 1953). Initial data showed that obtaining a semi-transparent silicide electrode was possible, but at a trade-off of low conductivity. Modeling of multilayered top electrodes demonstrated a rhodium-aluminum structure that produced the best broadband response in combination with nematic liquid crystals to

---

\*now SSC San Diego

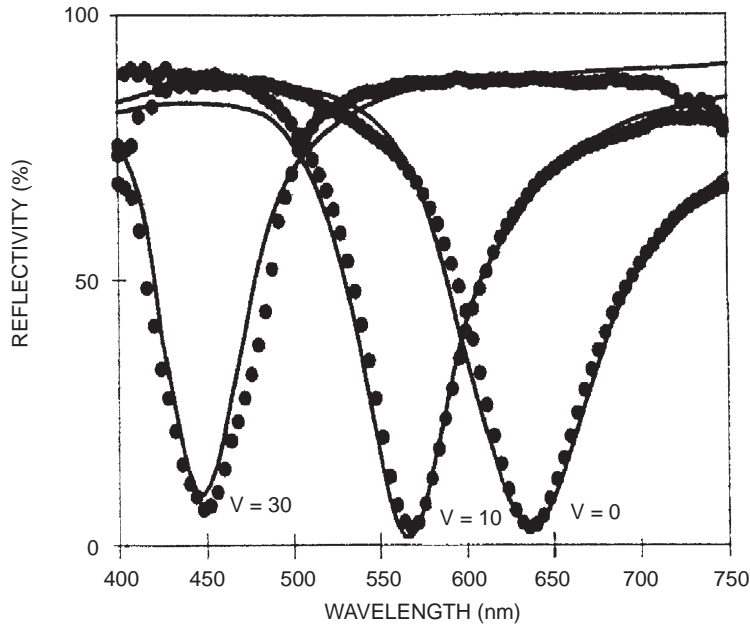


*Figure 1. Reflection properties of a surface-plasmon tunable filter for color generation at various applied voltages. Solid line is the theoretical model; dotted line is the experimental results.*

achieve gray-scale modulation. In the second year, this structure was fabricated and tested to demonstrate the ability to produce gray scales. Figure 2 shows the theoretical and experimental results for this broadband modulator or tunable mirror.

Further modeling was performed on the surface-plasmon device, including the study of angular effects, and we examined a micro-machined embodiment that would eliminate the need for liquid crystals. Patent disclosures were filed to exploit the newly discovered advantages provided by these devices.

The promising results from this ILIR project using absorption by surface plasmons as a tunable filter and/or tunable mirror for display applications have been recognized by the commercial sector. The investigation of the commercial viability of this technology will be continued under a Cooperative Research and Development Agreement (CRADA) with Optron Systems of Bedford, MA.

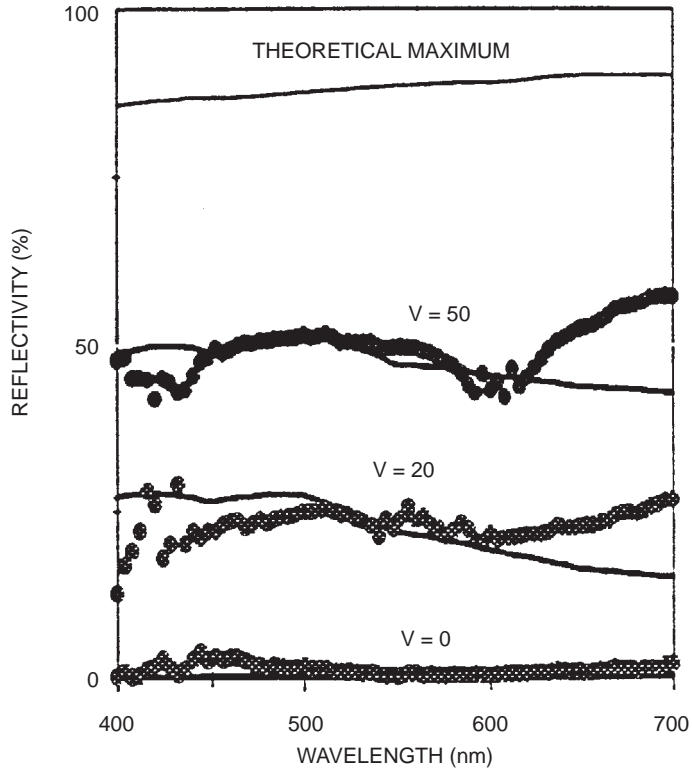


Figure 2. Reflection properties of a surface-plasmon tunable mirror for control of gray scale for various applied voltages. Solid line is the theoretical model; dotted line is the experimental results.

Principal Investigator:  
 Dr. Stephen D. Russell  
 D853

0601152N  
 ZU47

Associate Investigators:  
 Dr. Randy L. Shimabukuro  
 D893

Ayax D. Ramirez  
 D853

Dr. Yu Wang  
 Jet Propulsion Laboratory (JPL)

## Propwash/Wake Resuspension in San Diego Bay (The Grand Plan III)

*Objective(s):* Reliably estimate the resuspension of bottom sediment due to the transit of vessels through San Diego Bay. This work is important because a major portion of water pollutants are attached to fine grain sediment, and sediment transport also has implications when planning maintenance dredging operations.

*Accomplishment(s):* We built a well-characterized, closed flow channel into which sampled sediments can be introduced, and the critical shear stress and erosion rates can be measured.

The problem of estimating sediment resuspension was divided into four parts:

1. Reliably estimate the ship-induced flow field. Due to the complexity of this problem, the ship/propeller flow field has been historically modeled as a simple momentum jet. We proposed to also use the Navy's most sophisticated, ship-wake numerical simulations (CFDSHIP-IOWA and TBWAKE). In the first year of this project, Dr. Mark Hyman, Naval Coastal Systems Center (NCSC), modified these codes to include a shallow bottom and ran them for an aircraft carrier and a frigate.
2. Reliably estimate the response of the bottom sediment to the ship-induced flow field. Dr. Scott Jenkins and colleagues at Scripps Institution of Oceanography (SIO) have developed a numerical simulation (SEDXPORT) to predict the transport of cohesive fine sediments, given the hydrodynamic forcing and critical shear stress. Output of the model includes particle size and number distributions at each depth increment throughout the water column, bottom erosion and deposition patterns, and rates of change of these features. Over the last year, Dr. Jenkins has modified his code to accommodate the output of Dr. Hyman's simulation that estimates the velocity field throughout the water column and the shear stress at the bottom.
3. Determine the critical shear stress of the bottom sediment necessary to initiate resuspension. For cohesive sediments, such as are thought to be in San Diego Harbor, there is presently no way of predicting critical bed shear stress as a function of flow conditions. Consequently, we built an experimental flow channel to directly measure the onset of erosive shear stresses as a function of sediment depth. To obtain undisturbed samples of sediment, we designed and built a sampling tube that can be used both in a standard core sampler and that can be directly introduced into the flow channel. This flow channel can measure the critical shear stress of sediment core samples taken at selected locations in San Diego Bay and can also measure the rate of erosion at any shear stress.
4. Perform field tests to validate the model. Using the RV *ECOS* and associated capabilities (e.g., Acoustic Doppler Current Profiler [ADCP], conductivity, temperature, and depth [CTD], transmissometers, and Global Positioning System [GPS]), we have completed several preliminary studies showing that we can identify and track the resuspended sediment footprint of an aircraft carrier, after it had passed through the shipping channel to San Diego Harbor. Knowing the hydrodynamic forcing of the carrier (via Dr. Hyman's model) and the critical shear required for sediment resuspension (experimentally determined in the flow channel), Dr. Jenkins sediment transport model can be run and compared with field measurements.

The portion of these tasks directly funded by the ILIR program in FY 98 was the construction of the sediment flow channel (item 3). Figure 1 shows the test section of the flow channel where the sediment is introduced. The working section of the channel is rectangular: 20 mm high, 305 mm wide, and 2438 mm long. The high aspect ratio (305/20) and long entrance length (2057 mm) ensure fully developed flow at the sediment measurement station. The channel is designed to use seawater as the working medium so as not to alter the chemical properties of any cohesive sediments introduced into the working section. Wall shear stress on the channel is inferred from flow-induced pressure-drop measurements inside the channel.

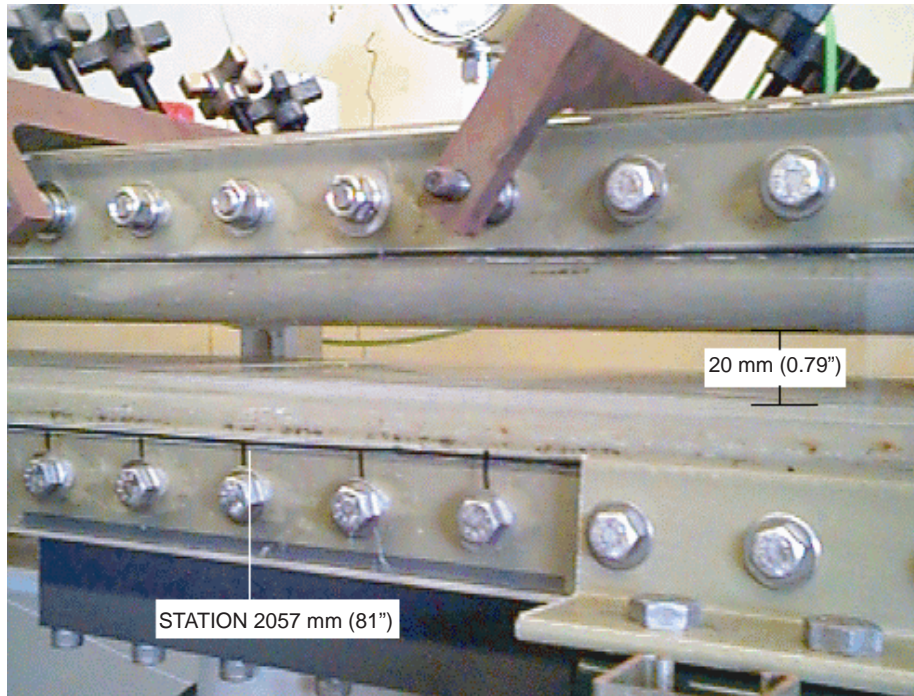


*Figure 1. Side view of flow channel. Flow is from left to right. Sediment is introduced through the bottom of the channel through a 140- by 140-mm recess. Sediment height is automatically maintained by a laser displacement sensor coupled to a computer-controlled jacking system.*

Figure 2 shows the friction factor of the channel as a function of the flow Reynolds number (based on hydraulic diameter). The results are very close to traditional measurements of smooth pipe pressure drop (corrected to channel aspect ratio). The flow in the channel can be controlled from 0.035-m/s to 1.73-m/s mean flow velocity, producing a shear stress range from 0.008 Pa to 8.0 Pa (three orders of magnitude). This is an adequate range to cover the critical shear stress for a huge range of sediment sizes and adhesion. A system is being developed to automatically control the rate of sediment introduction so that erosion rate can be calculated easily.

Great care has been taken in the channel design to preserve the integrity of sediment samples, such that valid critical shear stresses are measured. The critical shear stress measurement is a small, but critical portion of the Grand Plan (from the project title) to track sediment transport in San Diego Bay. The ultimate prediction of the fate of bay sediments is crucial to implementing Navy environmental policy and maintenance plans (e.g., dredging) for San Diego Bay.

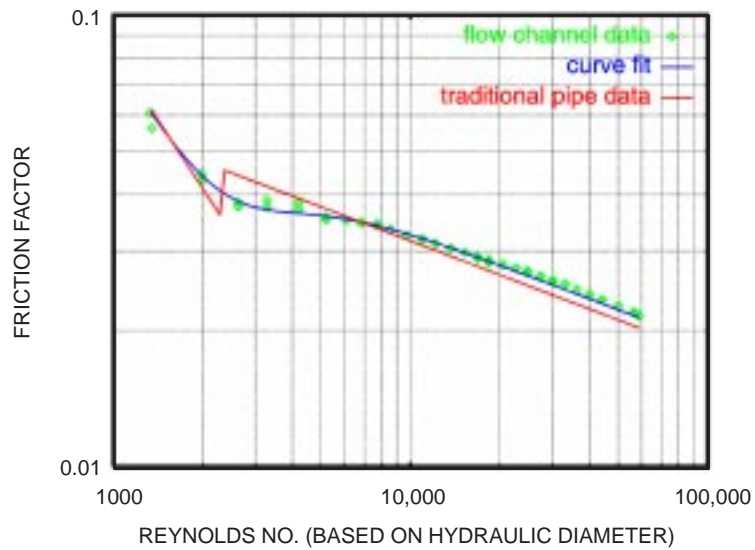


Figure 2. Darcy friction factor data for the flow channel. Curve “traditional pipe data” assume instant transition from laminar to turbulent flow at Reynolds number 2300. Actual flows have a smooth transition (as in the present data).

Principal Investigators:  
 Dr. James J. Rohr  
 D363

0601152N  
 ZU48

Daniel M. Ladd  
 D363

## Biosonar Ensonification of Buried Mines

*Objective(s):* Record the patterns and spectral composition of biosonar pulses that impinge on buried mines during routine detection and identification by the bottlenose dolphin (*Tursiops truncatus*).

*Accomplishments(s):* We developed and successfully tested a self-contained underwater computer for data acquisition, a surface computer, and an acoustic data link for communicating between them. The underwater package fits into a realistic mine simulator and records the waveforms and times of biosonar pulses that impinge on the simulator. The surface computer can command the underwater unit and receive the digitized data from the buried-mine simulator over the acoustic link.

The Navy and Marine Corps have an immediate need to improve mine countermeasures in shallow water and very shallow water (SW/VSW). The reliable detection of buried mines is the most difficult element of that task. Trained dolphins readily solve that problem, but artificial sonars have difficulty with detection, and a better understanding of the dolphins' methods could facilitate future sonar development. For example, learning how the animal controls its position and the frequency of its biosonar during detection and identification, as well as the net physical effects of those actions on the energy that impinges on a buried mine, would provide valuable insight for alternative approaches in sonar designs.

A dolphin that repeatedly detects water-column objects in predictable positions produces relatively invariant pulses that persist even when sediment is suspended between the animal and objects. However, recent findings show that when the animal is free to move and when object locations are unpredictable, the animal shows considerable variability of its biosonar output during detection and identification. An animal that searched a large field for objects in unpredictable locations in the water column used a highly variable number of pulses during object identification. Other dolphins, when searching an open-ocean field for objects in random positions on the bottom, showed high variability in both the number of pulses-on-object and the frequency content of the pulses. Such variability during detection and identification of buried objects may allow the animal to identify specific features of an object as well as control bottom penetration and backscatter.

We measured the acoustic energy that impinges on a buried mine by using a self-contained instrument pack (figure 1) that replaces the detonator canister of a realistic Manta mine simulator (figure 2). A self-contained package eliminated cables and other equipment that would provide cues to the presence of a mine and allow the animal to correctly report without having to fully use its biosonar for detection and identification. The instrumented simulator (figure 3) was buried with other simulators in an open-ocean field where trained mine-hunting dolphins were used to detect and identify them.

The battery-powered instrument pack has a broadband transducer for measuring the biosonar pulse-waveforms and a second transducer for communicating over an acoustic data link with a surface computer (figure 4) in a boat. The data link was adapted from a commercial product and uses low-speed, pulse-position coding to provide high reliability and noise immunity in VSW. Static calibration tests yielded near errorless bidirectional communication from under 2 feet of mud to the surface in a high-noise environment. To conserve power, an onboard clock wakes the unit for a short period



*Figure 1. Instrument pack and components.*



*Figure 2. Normal Manta simulator.*

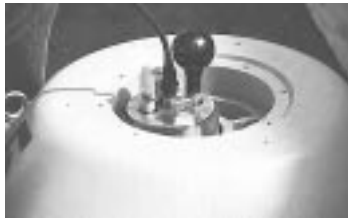


*Figure 3. Simulator with instrument pack.*



*Figure 4. Surface computer.*

every hour during each work day to listen for a command from the boat. If a command to record is received, the data acquisition components are enabled. They filter, amplify, and digitize the waveform of each impinging biosonar pulse at a rate of 500 kHz (up to 2 MHz is possible) and store up to 300 waveforms along with the time ( $\pm 0.5$  ms) of each pulse. Typically, the dolphin emits a pulse shortly after the receipt of the previous pulse's echo, and thus, the animal's distance from an ensounded object is predictable from the high negative correlation between distance and pulse rate. The surface computer (a ruggedized waterproof PC) with a compatible acoustic data link has been developed to command the underwater package and, after each detection, upload the data from the instrument pack for storage and analysis.

Initial tests were made during daylight hours with the instrument pack in 20 feet of water on, but not buried in, the bottom. The pack was allowed to "wake up" at a prescribed time and commanded from the surface to activate the recording system. Trained, mine-hunting dolphins were then directed to first detect the instrument pack (an identification pass) and then to reapproach the pack and stop at a predetermined distance from it (a stop pass). Following the stop pass, the pack was commanded to upload the digitized waveforms with their time-stamps to the surface computer. Figures 5 through 9 show example results from one animal.

The interpulse intervals on the identification pass, where the animal made a fast run up to the pack, were considerably shorter than those of the stop pass, where the animal approached more slowly and stopped at the pretrained distance (figure 5). Remarkably, both sets of interpulse intervals are considerably shorter than the putative echo-processing-time of the literature examples where more distant targets were tested with repetitive trials and static positions. The present results and other findings suggest separate functions for the biosonar at different points in time.

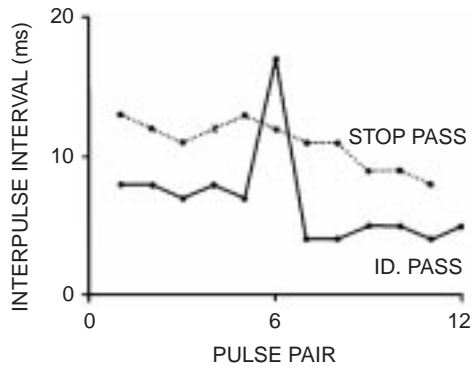


Figure 5. Interpulse intervals.

The pulses observed in this test were of low power and variability with the spectra remaining broadband throughout. The pulses of the identification pass (figures 6 and 7) were, in general, of lower power with more emphasis on the higher frequencies, whereas those of the stop pass (figures 8 and 9) were less variable with a more consistent application of low frequencies. Previous work has consistently shown a peak between 45 and 55 kHz and another between 110 and 125 kHz.

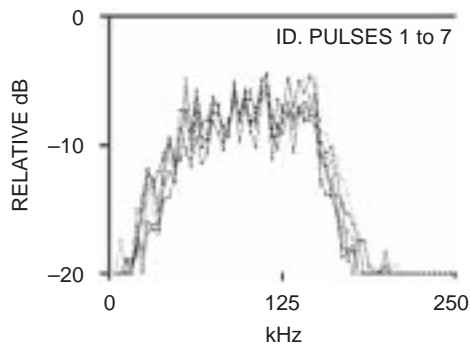


Figure 6. Power-density spectra of initial identification pulses.

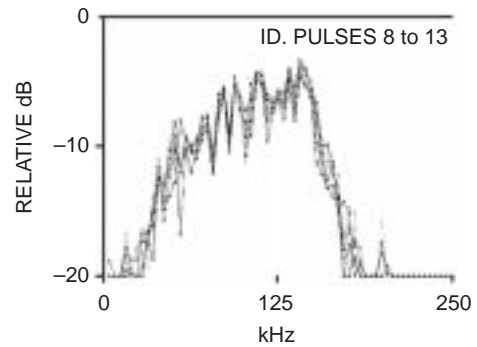


Figure 7. Power-density spectra of terminal identification pulses.

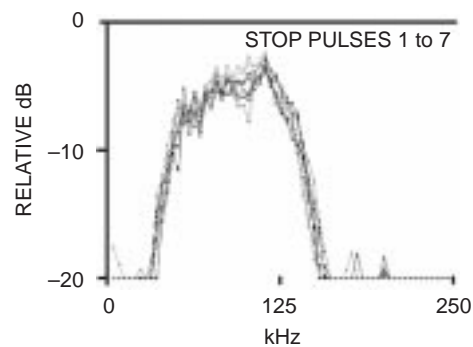


Figure 8. Power-density spectra of initial stop-pass pulses.

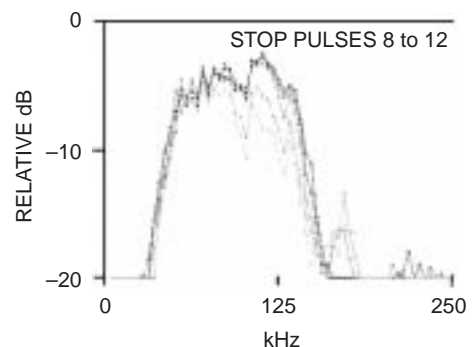


Figure 9. Power-density spectra of terminal stop-pass pulses.

This example demonstrates the system functions and analyses but does not represent the expected performance of the animals with buried targets in unknown positions and reduced visibility. There, as observed in recent related studies, considerably more pulse, power, and spectrum variability are expected during detection and identification.

Limited funding required the use of trained animals and simulators on an “as available” basis for collecting data on buried mines. That data collection was delayed because the system was completed late in the year when those animals had prior scheduling commitments.

Principal Investigator:  
Dr. John E. Sigurdson  
D351

0601152N  
ZU50

## Exact Diagonalization of Large Sparse Matrices

*Objective(s):* Develop computer code capable of diagonalizing large sparse matrices of physical interest and determine solutions other than the one associated with the lowest eigenvalue.

*Accomplishment(s):* The Density Matrix Renormalization Group (DMRG) method can provide approximate ground-state solutions for the quantum-mechanical, many body problem for a variety of one- and two-dimensional systems with a high degree of accuracy. We have developed a technique for extending DMRG to investigate arbitrary excited states. As an example, we have applied our method to describe the properties of excitons (bound electron-hole pairs) that can occur during optical excitations of low-dimensional systems. Our results show that excited-state calculations within the standard DMRG procedure give results that are both quantitatively and qualitatively incorrect.

In the DMRG method, a quantum-mechanical system of given size is divided into two pieces: a system block and an environment block. The system is chosen to be small enough so that an exact numerical solution of the ground state can be obtained. Then, the basis of this system can be represented as an outer product of the basis for the system block and the basis of the environment block. The density matrix for the system block is then formed by integrating-out the basis of the environment block. This reduced density matrix usually has dimensions that are on the order of the square root of the dimension of the original system. That allows us to completely diagonalize this matrix. The states with the lowest eigenvalues are then discarded, and only those states with the highest probability of configuration are kept. A reduced Hamiltonian for a system with two additional sites is then formed via an outer product of a complete basis for two new sites and the reduced basis of the system block. This process can be repeated over and over until the system reaches a size of interest.

Using this technique, numerical solutions of the ground state of one-dimensional systems have been obtained with excellent accuracy to almost arbitrarily large system sizes. However, as the system size is increased, the repeated pruning of the system basis gradually removes information about excited states. Our work describes a technique whereby excited states, as well as the ground state, are targeted (figure 1), and additional density matrices representing the excited states are formed. All of the density matrices are added, and the resulting matrix is diagonalized, and again, this basis is pruned. The eigenvalues do not converge as quickly, and, typically, more states must be kept to maintain the same level of accuracy, but the information describing the excited state is not lost.

Our technique for targeting excited states was worked out in some detail for a generic one-dimensional system. Optically excited states relevant to both optical absorption and third-order nonlinear optical coefficients were studied. This work is described in some detail in Chandross and Hicks, 1999, "Density Matrix Renormalization Group Method for Excited States," *Physical Review B*, vol. 59, no. 15, pp. 9699–9702.

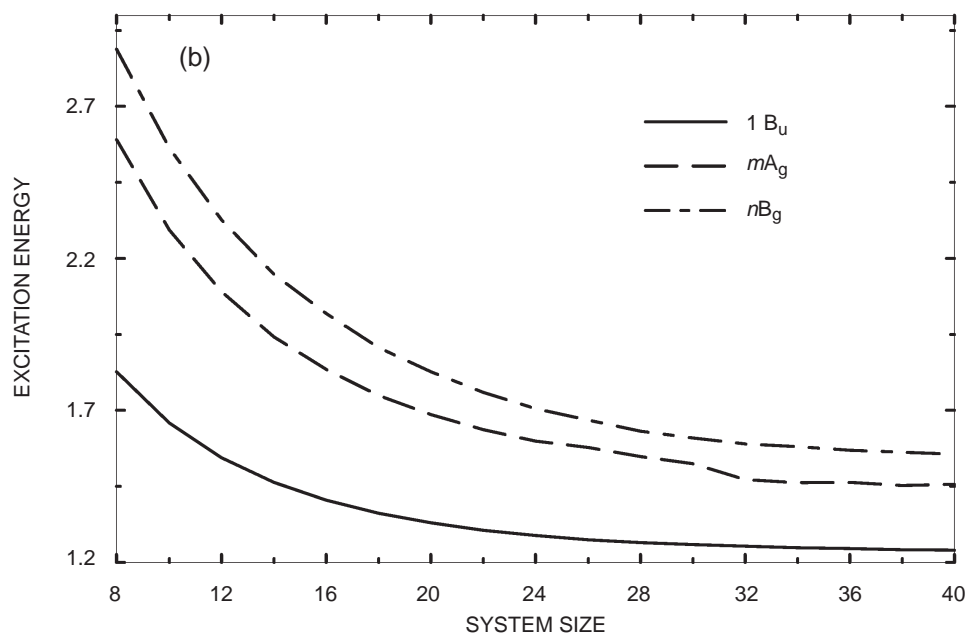
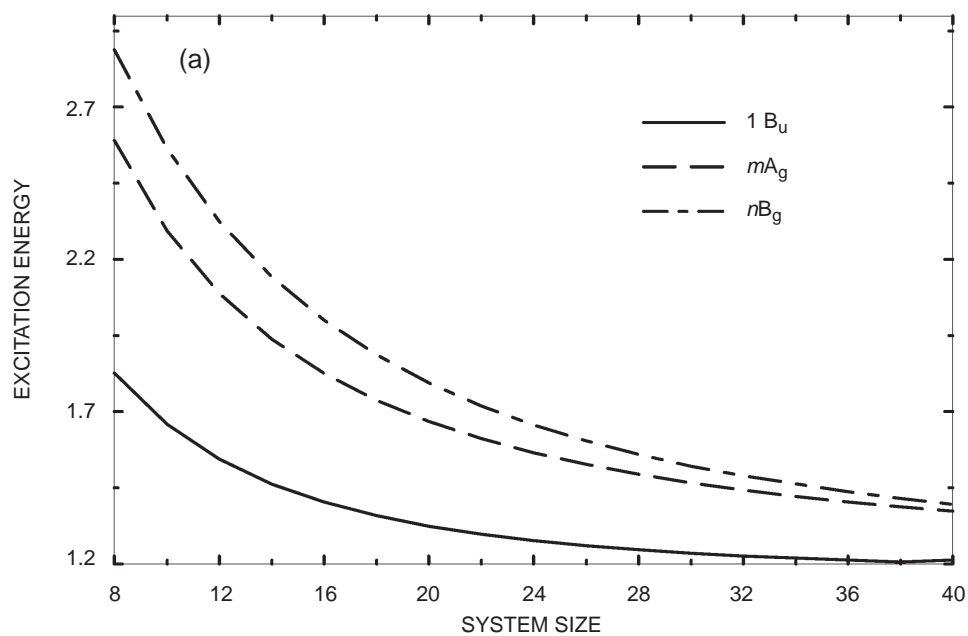


Figure 1. Excitation energies of the  $1 B_u$ ,  $m A_g$ , and  $n B_u$  optically excited states for a model system where we (a) target all of the excited states and (b) target only the ground state.

Principal Investigator:  
 Dr. Charles Hicks  
 D3604

0601152N  
 ZU53



## ACCOMPLISHMENTS AND IMPACTS

### Fiber-Optic Chemical Sensor Systems

**Principal Investigator:** Stephen Lieberman

#### ***Background:***

An ILIR project funded in FY 86 and FY 87 investigated laser-induced fluorescence generated and detected through optical fiber. The goal was to develop a method for real-time measurement of trace amounts of transition metals in seawater. As a result of that effort, a novel fiber-optic-based, laser-induced fluorescence (LIF) chemical sensor system was developed.

#### ***Scientific Accomplishments:***

To induce fluorescence, short-wavelength or ultraviolet (UV) illumination is required. Thus, optical fibers capable of transmitting UV light to the region of interest are required. Furthermore, the induced fluorescence light must be captured and returned via optical fiber, and spectroscopic analysis must be performed to identify the chemical compounds detected. The basic research performed under this ILIR project addressed these issues in order to develop successful fiber-optic LIF chemical sensor systems.

To date, more than 30 publications, 70 symposia presentations at technical conferences, and 9 patents have resulted from work initiated under this FY 86 and FY 87 ILIR project.

#### ***Technology Impacts:***

Through a collaborative effort with researchers from the U.S. Army Waterways Experiment Station, the Navy-developed LIF sensor system was subsequently adapted for use with a truck-mounted cone penetrometer for *in situ* measurements of petroleum hydrocarbons in soils. The method consists of using a hydraulic ram with a 20-ton reaction mass to push an instrumented probe into the ground. Fluorescence from aromatic hydrocarbons in the soil is excited through a sapphire window in the probe by 337-nm light generated with a pulsed nitrogen laser and transmitted down the probe over 100 meters of optical fiber. The resulting laser-induced fluorescence stimulated in the petroleum contaminated soils is returned to the surface over a second fiber where it is dispersed with a spectrograph and quantified with an intensified linear photo-diode array.

The first successful use of the Navy-developed LIF sensor at a petroleum-contaminated site in Jacksonville, FL, in 1989, led to a highly successful Tri-Service development program called Site Characterization and Analysis Penetrometer Systems (SCAPS). The Strategic Environmental Research and Development Program funded the SCAPS program. The program produced a family of direct-push sensor systems that revolutionized the way contaminated sites are characterized. Prior to developing these sensor systems, soil and water samples were collected and sent to an off-site laboratory for analysis. Results were often not available for weeks or more. Consequently, characterization of a site often required several sampling iterations. Because the LIF sensor data are available in real time, while the sensor probe is pushed into the ground, sampling plans can be modified immediately to more accurately and more cost effectively map-out subsurface contaminant plumes. An independent cost/benefit analysis conducted by the Department of Energy (DOE Report #LAUR-91-4016)

concluded that the SCAPS LIF technology could reduce the cost of site characterization by at least 25 to 35%. This has resulted in cost savings of tens of millions of dollars for the Navy and potentially hundreds of millions for the nation.

The LIF sensor system developed under the SCAPS program was subsequently transitioned to both the Navy and Army. The LIF sensor technology is now offered on a cost-reimbursable basis via penetrometer systems operated by Navy Public Works Center (PWC) Environmental Groups located in Jacksonville, FL, and San Diego, CA. In addition, three Army Corps of Engineers Field Divisions (Kansas City, MO; Tulsa, OK; and Savannah, SC) provide the same LIF sensor technology.

The fluorescence sensor technology has also been transferred to the commercial sector and is now available for sale by at least two vendors in the U.S. and Europe; the technology is also provided as a service by many vendors in the U.S. and Europe. Navy Cooperative Research and Development Agreements (CRADAs) with UNISYS Corporation and Fugro Geosciences, Inc., were used to facilitate the technology transfer of SCAPS-developed technologies. At least nine Navy-owned patents have been awarded or are pending that can be traced to the original ILIR-funded program and related SCAPS developments.

The SCAPS LIF sensor technology has been certified and verified by numerous state and Federal regulatory agencies including the California Environmental Protection Agency (EPA) Innovative Technology Certification Program; the Interstate Technology Regulatory Cooperation (ITRC) workgroup; the U.S. Environmental Protection Agency (USEPA) Superfund Innovative Technology Evaluation (SITE) program; and the USEPA Consortium for Site Characterization Technology (CSCT).

The visible success of the SCAPS program also resulted in high-level recognition. On Earth Day in 1996, the SCAPS system was prominently displayed at the Pentagon and was visited by the Secretary of the Navy, John Dalton, and the Deputy Assistant Secretary of the Navy, Environment and Safety, Elsie Munsell. SCAPS was also displayed at the California Environmental Protection Agency's Earth Day Fair in 1996 where the California Secretary for Environmental Protection, James Strock, was quoted saying "The Navy's penetrometer system is an excellent example of how a new technology can be used to improve our nation's environment."

A second significant product that evolved directly from the Navy-developed LIF sensor technology is the Oil Spill Detector System (OSDS). The OSDS makes use of a multispectral fluorometric sensor for real-time *in-situ* detection of marine petroleum spills. This system provides continuous real-time monitoring of receiving waters in the vicinity of piers and other fuel-transfer operations so as to provide early warning of oil spills or leaks. The sensor uses a compact multiwavelength fluorescence-based sensor packaged in a floating buoy that can be deployed under piers and other locations where spills or leaks might occur. Multiple sensors can be networked with a telemetry system for real-time data acquisition and display on a Web-based graphic display and telephone notification system directly linked to oil-spill responders. This system provides an improvement over traditional oil-spill detection methods currently being used at most marine facilities. Such facilities rely solely on the use of human observers to visually identify the surface sheen indicative of a petroleum spill.

This first installation of the system is currently underway at Puget Sound Naval Shipyard, Washington. There are ongoing discussions for future installations at several other facilities including Naval Station (NAVSTA) Mayport, NAVSTA San Diego, NAVSTA Norfolk, and SUBASE San Diego.

***Fleet Impacts:***

Cost savings of tens of millions of dollars have already been realized through use of SCAPS at petroleum-contaminated Navy sites requiring cleanup. An additional benefit is the national recognition this Navy technology has received.

Future Navy savings that may result from early warnings by the Oil Spill Detector System are presently incalculable, but potentially enormous in view of the litigation and remediation costs associated with oil spills. The system is far more effective and economical than relying on people to visually discover oil spills.

**Faster-Than-Real-Time Synthetic Forces (FTRT SF) Simulation**

**Principal Investigator:** Jeffrey Wallace

***Background:***

This FY 97 ILIR project investigated software architectures for realistic military-forces computer simulation at very high speed. The goal was to achieve simulation speeds that exceed real-time simulation (i.e., simulation time equal to physical time). This is referred to as faster-than-real-time simulation (e.g., execution of 2 days of simulation time within a period of several hours).

***Scientific Accomplishments:***

Over the last two decades, researchers have attempted to develop large-scale simulations spanning many levels of system resolution. These efforts to develop simulations of large parts of reality (from switching circuits to human decision making) have encompassed most of what is known about software technologies and techniques.

For example, declarative programming is typically used to model human decision making, while imperative programming languages are used for efficiency with static portions of models. However, most expert systems are designed as stand-alone packages and provide only loosely coupled interfaces to imperative languages.

The main scientific accomplishments of the Faster-Than-Real-Time Synthetic Forces (FTRT SF) FY 97 ILIR project were identification of two simulation architectures and a single software abstraction layer that enable rapid and realistic simulation of military forces and equipment. These architectures enable faster-than-real-time operation and include simulation at both the electronic-circuit-level for military equipment and the theater-level for military forces.

***Technology Impacts:***

Recent Defense Advanced Research Projects Agency (DARPA) and Department of Defense (DoD) initiatives, such as the Synthetic Theater of War (STOW) advanced technology demonstration, have goals far beyond the use of these large simulations as single-user analytical tools. Ambitious efforts are focused on providing distributed interactive simulations that use virtual reality for training, virtual prototyping of hardware, and analytical applications.

One of the simulation architectures investigated was the Synchronous Parallel Environment for Emulation and Discrete-Event Simulation (SPEEDES) framework. The SPEEDES simulation framework was the principal focus of attention since it is a Government-Off-The-Shelf (GOTS) product, and manipulation of the computer source code was allowable. Improvements were made in the areas of communications protocol design, data distribution management design, and abstraction layers to improve developer efficiency without sacrificing execution speed.

In FY 98, this ILIR program transitioned into the Joint Simulation System (JSIMS). JSIMS is a \$600M program and is currently the largest military forces simulation program. The simulation architecture identified by the FY 97 ILIR project has been adopted for use in the JSIMS program. SSC San Diego received \$6.8M in FY 98 funds under the JSIMS program. A technical point of contact for the transition is Dr. David Pratt, Technical Director, JSIMS.

The simulation architectures identified by this ILIR project have also been adopted for use in two 6.3 projects sponsored by the Director, Defense Research and Engineering (DDR&E) High Performance Computing Modernization Program (HPCMP). These projects are entitled "Forces Modeling and Simulation for Training" and "High Performance High-Level Architecture Runtime Infrastructure." The funding amounts for these projects at SSC San Diego were \$1.2M in FY 98 and are \$1.4M in FY 99 and \$700K in FY 00.

The Parallel Discrete Event Simulation (PDES) Framework User Group (of which SPAWAR is one of the founding members, due to the fundamental work on FTRT SF under this ILIR project) was established in May 1997 under the auspices of the Joint National Test Facility (JNTF) Wargaming & Simulation (WS) Deputate.

***Fleet Impacts:***

This research has improved the effectiveness of computer simulations in Navy and Joint Service war games and warfare training.



## **FY 98 TRANSITIONED PROJECTS**

### **Applications of Stochastic Nonlinear Dynamics to Communications**

**Principal Investigator:** Dr. Adi Bulsara

**Co-Principal Investigator:** Dr. Brian Meadows

SSC San Diego project ZU65, completed in FY 98, investigated the control and optimization of electronic communication systems and devices via nonlinear dynamics. Specifically, the nonlinear model of the analog phase-locked loop (PLL) does benefit from the optimization of the system noise at low signal-to-noise ratios (SNRs). This intriguing cooperative effect arises out of the coupling between deterministic and random dynamics in a nonlinear system and is known as Stochastic Resonance (SR). There are two distinct application areas in which nonlinear dynamics can be expected to improve PLL-based communication systems. The first application is at the component level by tuning the amount of noise present in an individual PLL. Here, the cycle slip problem (the sudden noise-induced jump from one stable state to the next) is recast as a time-dependent shot noise process that exhibits SR. The second application for improving PLL-based communication systems is when nonlinear elements form arrays. By employing the nonidentical oscillator theory, “tuning” the spatial disorder, the SNR of an array of PLLs improves, as well as the frequency and phase locking across the array. Analytical and numerical studies of noise in nonlinear arrays were complemented by a series of experiments on coupled microelectronic elements.

Due to the progress achieved during FY 98, this ILIR project was completed and transitioned to direct ONR 6.1 funding. The new program is titled “Applications of Stochastic Resonance in Communications,” and the SSC San Diego principal investigator (PI) is Dr. Brian Meadows (Co-PI on the ILIR project; contact information listed above). The cognizant ONR program officer is Mike Shleshinger, ONR 331.

### **Fiber-Optic Add/Drop Multiplexers Produced by Writing Gratings on Fused-Fiber Tapered Couplers**

**Principal Investigator:** Dr. Richard Orazi

This SSC San Diego project (ZU59) is a continuing effort studying a novel way to produce add/drop multiplexers for fiber-optic systems operating with multiple, closely spaced wavelengths of signal light. The approach is to create Bragg gratings within fused-fiber biconical tapered couplers. This is done by producing spatial variations in the refractive index while using interference-patterned ultraviolet illumination. This project explores the effects of material, fabrication, and device design.

Due to the progress achieved during FY 98, the FY 99 research effort has received more than 50% support from ONR 6.2 funding under a program to improve wavelength division multiplexers used in undersea surveillance systems. The sponsor is ONR 321, and the ONR program officer is Don Davison. SSC San Diego project number SUBD is managed locally by Ken Rogers.

## **Surface-Plasmon Flat-Panel Display**

**Principal Investigator:** Dr. Stephen D. Russell

SC San Diego project ZU47, completed in FY 98, investigated the possibility of developing a novel flat-panel display technology by using the surface-plasmon effect for color generation and light modulation. Accomplishments included demonstration of color-selective absorption by surface plasmons and the projection of primary colors (cyan, yellow, and magenta) from a surface-plasmon tunable filter; demonstration of a broadband light modulator that uses the surface-plasmon effect to achieve gray scales; and the design and fabrication of a prototype surface-plasmon display.

The transition of surface-plasmon-based light modulation technology to the commercial sector is proceeding via an existing Navy-issued Cooperative Research and Development Agreement (NCRADA-NRaD-95-042, modified to include this project) between SSC San Diego and Optron Systems, Inc., of Bedford, Massachusetts. The point of contact at Optron Systems is Ali Ersen.

## **Telesonar Channel Models**

**Principal Investigator:** Joseph A. Rice

SSC San Diego project ZU61 was initiated in FY 98 and is continuing in FY 99. This project seeks to understand undersea acoustic communication channels through theoretical and numerical modeling of the propagation physics.

“Telesonar” is undersea acoustic signaling for wireless networks of distributed sensors in shallow and very shallow water. Telesonar technology relies on signal-processing techniques to overcome the deleterious aspects of the physical channel and to exploit advantageous channel features. The technology employs various spread-spectrum modulation techniques with signal energy, typically in the 8- to 16-kHz acoustic band. Propagation of acoustic signals in shallow water is impaired by a complex multipath structure and the nonhomogeneous, nonstationary nature of the medium and its boundaries. This project is developing a physics-based numerical propagation model that attempts to account for these effects.

Results from this project are being transitioned into a new Small Business Innovation Research (SBIR) program initiated in FY 99. SBIR Topic N99-011, “Directional Underwater Acoustic Communications Transducer,” is supported by ONR SBIR funds. The program is incorporating results from the Telesonar Channel Model research via technology transfer to the winning contractor. The ONR SBIR program manager is Doug Harry, ONR 362.

In addition, results from the ILIR project are being transitioned into an ONR 6.2 program, “Modem Performance Measurements,” under the cognizance of Tom Curtin, ONR 322. This project, SSC San Diego number MA11, has \$80K in funding for FY 99.



## REFEREED PAPERS (PUBLISHED OR ACCEPTED)

- Barnett, J. T. and B. Kedem. 1998. "Zero-Crossing Rates of Mixtures and Products of Gaussian Processes," *IEEE Transactions on Information Theory*, vol. 4, July, pp. 1672–1677.
- Boss, P. 1999. "Feasibility Studies for the Detection of Volatile Organic Compounds in the Gas Phase Using Microelectrode Sensors," *Journal of Electroanalytical Chemistry*, vol. 460, pp. 105–118.
- Chandross, M. and J. C. Hicks, 1999. "Density-Matrix Renormalization-Group Method for Excited States," *Physical Review B*, vol. 59, no. 15, pp. 9699–9702.
- Goodman, I. R. and G. F. Kramer. 1999. "Homomorphic-Like Random Set Representations for Fuzzy Logic Models Using Exponentiation with Applications to Data Fusion," *Information Sciences*, vol. 113, pp. 85–112.
- Goodman, I. R. and H. T. Nguyen. 1999. "Probability Updating Using Second Order Probabilities and Conditional Event Algebra," *Information Sciences*, to appear.
- Inchiosa, M. E. and A. R. Bulsara. 1998. "DC Signal Detection Via Dynamical Asymmetry in a Non-linear Device," *Physical Review E*, vol. 58, no. 1, pp. 115–127.
- Inchiosa, M. E., A. R. Bulsara, K. A. Wiesenfeld, and L. Gammaitoni. 1999. "Nonlinear Signal Amplification in a 2D System Operating in Static and Oscillatory Regimes," *Physics Letters A*, vol. 252, pp. 20–26.
- Kevorkian, A. K., D. Barach, and G. W. Benthien. 1998. "Bistatic Target Strength Prediction from Limited Data," *High Performance Computing Contributions to DoD Mission Success*, May, p. 121.
- Reuter, M. and J. Zeidler. 1999. "Nonlinear Effects in LMS Adaptive Equalizers," *IEEE Transactions on Signal Processing*, vol. 47, June, no. 6.
- Rohr, J., M. I. Latz, S. Fallon, J. C. Nauen, and E. Hendricks. 1998. "Dolphin Stimulated Bioluminescence," *Nature*, vol. 393, June, pp. 731–732.
- Rohr, J., M. I. Latz, S. Fallon, J. C. Nauen, and E. Hendricks. 1998. "Dolphin Stimulated Bioluminescence," *Pour La Science* (French edition of *Scientific American*), Juin, pp. 26–27.
- Stein, D. W. J. 1999. "Robust Implementations of an Exponential Mixture Detector with Applications to Radar," *IEEE Transactions on Aerospace and Electronic Systems*, to appear.
- Vu, T. T., R. J. Orazi, and M. N. McLandrich. 1998. "Four Channel Fused Fibre Mux/Demux Couplers and Add/Drop Filters in the 1300 and 1550 nm Regions," *Electronics Letters*, 19 March, vol. 43, no. 6, pp. 583–584.
- Wallace, J. et al. 1999. "IMPORT v2.0 Beta 1: A Tool for Large-Scale, Complex System Simulation," *High Performance Computing 1999: Grand Challenges in Simulation*, ISBN# 1-56555-166-4, Adrian Tenter, ed., Society for Computer Simulation International, San Diego, CA, pp. 261–266.

Welstand, R. B., S. A. Pappert, C. K. Sun, J. T. Zhu, Y. Z. Liu, and P. K. L. Yu. 1996. "Dual-Function Electroabsorption Waveguide Modulator/Detector for Optoelectronic Transceiver Applications," *IEEE Photonics Technology Letters*, vol. 8, pp.1540–1543.

## REFEREED PAPERS (SUBMITTED)

Barnett, J. T. and B. Kedem. "Asymptotic Normality of Level-Crossings for the Envelope of a Gaussian Process with Applications to Radar Detection," submitted to the *Journal of Fourier Analysis and Applications*.

Bucker, H. and P. Baxley. "Automatic Matched-Field Tracking with Table Lookup," submitted to the *Journal of the Acoustical Society of America*.

Freund, R. F., M. Gherrity, S. Ambrosius, M. Campbell, M. Halderman, D. Hensgen, E. Keith, T. Kidd, M. Kussow, J. Lima, F. Mirabile, L. Moore, B. Rust, and H. J. Siegel. "Scheduling Resources in Multi-User, Heterogeneous, Computer Environments," submitted to the *Journal of Parallel and Distributed Computing*.

Lorincz, K., Z. Gingl, L. Kiss, and A. Bulsara. "Higher Order Stochastic Resonance in a Level Crossing Detector," submitted to *Physical Review E*.

Wahlen, B. E. and C. T. Mai. "Turbo Code Applied to Pragmatic Trellis-Coded Modulation," submitted to *IEEE Communication Letters*.

## BOOKS/CHAPTERS

Barnett, J. T. 1999. "Zero-Crossing Problems for Random Processes with Applications," *Sampling Theory and Practice*, (Farokh Marvasti, ed.), Plenum Press, to appear.

Edelblute, D. J. 1999. "Correlation Theory," *Wiley Encyclopedia of Electrical and Electronics Engineering*, (John G. Webster, ed.), John Wiley & Sons, Inc., New York, vol. 4, pp. 365–379.

Goodman, I. R. and H. T. Nguyen. 1999. "Fuzziness and Randomness," invited Chapter 1 for book *Statistical Modeling, Analysis, and Management of Fuzzy Data*, (D. A. Ralescu, C. Bertoluzza & M. A. Gil, eds.), Springer-Verlag, New York, to appear.

## IN-HOUSE PUBLICATIONS

Pappert, S. A., R. J. Orazi, C. J. Dempsey, S. T. Li, and J. Feist. 1996. "Shipboard Electromagnetic Environment Measurements Using a Wideband Photonic Probe," TR 1731 (December), Naval Command, Control and Ocean Surveillance Center RDT&E Division,\* San Diego, CA.

Rohr, J. J., E. W. Hendricks, L. Quiqley, F. E. Fish, J. W. Gilpatrick, and J. Scardina–Ludwig. 1998. "Observations of Dolphin Swimming Speed and Strouhal Number," TR 1769 (April), SSC San Diego, CA.

---

\*now SSC San Diego

## PROCEEDINGS

- Baxley, P. 1998. "Experimental Investigation of Matched-Field Processing in a Wedgelike Shallow-Water Environment," *Proceedings of the 16<sup>th</sup> International Congress on Acoustics and the 135<sup>th</sup> Meeting of the Acoustical Society of America*, vol. 4, pp. 2437–2438.
- Baxley, P. A., H. P. Bucker, and J. A. Rice. 1998. "Shallow-Water Acoustic Communications Channel Modeling Using Three-Dimensional Gaussian Beams," *Proceedings of the Ocean Community Conference*, November.
- Chou, S., M. Pollock, and M. Soumekh. 1998. "On Target Resolvability from Single Tone Fringe Patterns of Digitally-Spotlighted SAR Image," *Proceedings of SPIE International Symposium on Optical Science, Engineering and Instrumentation*, July, pp. 586–593.
- Goodman, I. R. 1998. "New Perspectives on Deduction in Data Fusion," *Proceedings of the 1998 (Open) Symposium on Multisensor Data Fusion*, March, pp. 79–96.
- Goodman, I. R. 1998. "Applications of Fréchet and Other Random Set Averaging Techniques to Fusion of Information," *Proceedings of SPIE Signal Processing, Sensor Fusion & Target Recognition VII*, (I. Kadar, ed.), vol. 3374, pp. 108–118.
- Goodman, I. R. 1998. "Random Set and Fuzzy Sets: A Special Connection," *Proceedings of the International Conference on Multisource-Multisensor Information Fusion (Fusion '98)*, vol. 1, pp. 93–100.
- Goodman, I. R. 1999. "New Applications of Conditional Event Algebra and Relational Event Algebra to Fusion Information," *Proceedings of the 32<sup>nd</sup> Asilomar Conference on Signals, Systems & Computers*, to appear.
- Goodman, I. R. and G. F. Kramer. 1998. "Recent Use of Relational Event Algebra, Including Comparisons, Estimations and Deductions for Probability-Functional Models," *Proceedings of the 1998 IEEE International Symposium on Intelligent Control*, September, pp. 543–548.
- Goodman, I. R. and H. T. Nguyen. 1998. "Adams' High Probability Deduction and Combination of Information in the Context of Product Probability Conditional Event Algebra," *Proceedings of the International Conference on Multisource-Multisensor Information Fusion (Fusion '98)*, vol. 1, pp. 1–8.
- Green, M. D. and J. A. Rice. 1997. "Error-Correction Coding for Communication in Adverse Underwater Channels," *Proceedings of IEEE OCEANS '97 Conference*, October, pp. 854–861.
- Green, M. D. and J. A. Rice. 1997. "Noncoherent Communication for Adverse Channels," 134<sup>th</sup> Meeting of the Acoustical Society of America, *Journal of the Acoustical Society of America*, vol. 102, pp. 3118–3119 (abstract).\*
- Green, M. D. and J. A. Rice. 1998. "Robust Communications in Adverse Channels," *Proceedings of the Oceanology International '98 Conference*, vol. 2, pp. 271–283.

---

\* No proceedings, just abstracts were published for the 134<sup>th</sup> Meeting of the Acoustical Society of America.

- Green, M. D. and J. A. Rice. 1998. "Low-Probability-of-Detection Communications in Adverse Underwater Acoustic Channels," *Proceedings of the 16<sup>th</sup> International Congress on Acoustics and the 135<sup>th</sup> Meeting of the Acoustical Society of America*, June, pp. 307–308.
- Green, M. D. and J. A. Rice. 1998. "Handshake Protocols for Underwater Communications Networks," *Proceedings of the IEEE OCEANS '98 Conference*, vol. 1, pp. 487–491.
- Green, M. D., J. A. Rice, and S. Merriam. 1998. "Underwater Acoustic Modem Configured for Use in a Local Area Network," *Proceedings of the IEEE OCEANS '98 Conference*, vol. 2, pp. 634–638.
- Green, M. D., J. A. Rice, and S. Merriam. 1998. "Implementing an Undersea Wireless Network for Shallow-Water Acoustic Modems," *Proceedings of the Ocean Community Conference*, November.
- McDonald, V. K., J. A. Rice, and C. L. Fletcher. 1998. "An Underwater Communication Testbed for Telesonar RDT&E," *Proceedings of the IEEE OCEANS '98 Conference*, vol. 2, pp. 639–643.
- McDonald, V. K., J. A. Rice, and C. L. Fletcher. 1998. "Telesonar Testbed Engineering and Sea Trials," *Proceedings of the Ocean Community Conference*, November.
- McDonald, V. K., R. C. Shockley, J. A. Rice, and M. D. Green. 1997. "Probe Signals for Obtaining Impulse Response of Doubly Spread Channels," 134<sup>th</sup> Meeting of the Acoustical Society of America, *Journal of the Acoustical Society of America*, vol. 102, p. 3118 (abstract).\*
- Neff, J. D., B. K. Meadows, W. L. Ditto, G. N. Patel, and S. P. DeWeerth. 1998. "Spatiotemporal Dynamics of a Stochastic VLSI Array," *Proceedings of the 1998 IEEE International Symposium on Circuits and Systems, ISCAS '98*, vol. 3, pp. 542–545.
- Proakis, J. G., M. Stojanovic, and J. A. Rice. 1998. "Design of a Communication Network for Shallow-Water Acoustic Modems," *Proceedings of the Ocean Community Conference*, November.
- Rice, J. A. and M. D. Green. 1998. "Adaptive Modulation for Undersea Acoustic Modems," *Proceedings of the Ocean Community Conference*, November.
- Rice, J. A. and R. C. Shockley. 1998. "Battery-Energy Estimates for Telesonar Modems in a Notional Undersea Network," *Proceedings of the Ocean Community Conference*, November.
- Rice, J. A., R. C. Shockley, V. K. McDonald, M. D. Green, and J. G. Proakis. 1997. "Long-Range Signaling in Shallow Ocean Transmission Channels," 134<sup>th</sup> Meeting of the Acoustical Society of America, *Journal of the Acoustical Society of America*, vol. 102, p. 3118 (abstract).\*
- Shockley, R. C., J. G. Proakis, M. Stojanovic, and J. A. Rice. 1998. "Spectral Shaping in MFSK Modulation for Underwater Acoustic Communications," *Proceedings of the 16<sup>th</sup> International Congress on Acoustics and the 135<sup>th</sup> Meeting of the Acoustical Society of America*, June, pp. 315–316.
- Shockley, R. C., J. A. Rice, and V. K. McDonald. 1997. "Spreading, Coherence, Fading, and Noise in Shallow-Water Channels," 134<sup>th</sup> Meeting of the Acoustical Society of America, *Journal of the Acoustical Society of America*, vol. 102, p. 3118 (abstract).\*

---

\* No proceedings, just abstracts were published for the 134<sup>th</sup> Meeting of the Acoustical Society of America.

Shockley, R. C., J. A. Rice, V. K. McDonald, M. D. Green, J. G. Proakis, and J. Newton. 1998. "Observations of Coherence Time and Amplitude Fluctuations in a Shallow-Water Acoustic Communications Channel," *Proceedings of the 16<sup>th</sup> International Congress on Acoustics and the 135<sup>th</sup> Meeting of the Acoustical Society of America*, June, pp. 303–304.

Stojanovic, M., J. G. Proakis, J. A. Rice, and M. D. Green. 1998. "Spread-Spectrum Methods for Underwater Acoustic Communications," *Proceedings of the IEEE OCEANS '98 Conference*, vol. 2, pp. 650–654.

Wallace, J. W. 1998. "Implementing Neural Networks and Fuzzy Logic Using the IMPORT Simulation Language," *Object-Oriented Simulation 1998* (Proceedings of the 1998 Object-Oriented Simulation Conference), ISBN#1-56555-142-7, (J. Wallace and J. Steinman, eds.), Society for Computer Simulation International, pp. 171–176.

Wang, Y., S. D. Russell, and R. L. Shimabukuro. 1998. "Electronically Tunable Mirror Using Surface Plasmons," *SPIE Proceedings*, vol. 3292, pp. 103–106.

## PRESENTATIONS TO PROFESSIONAL MEETINGS

Abawi, A. T. 1999. "An Energy Conserving One-Way Coupled Mode Propagation Mode," Joint Meeting of the European and American Acoustical Societies, 15 to 19 March, Berlin, Germany.

Baxley, P. 1998. "Experimental Investigation of Matched-Field Processing in a Wedgelike Shallow-Water Environment," 16<sup>th</sup> International Congress on Acoustics and the 135<sup>th</sup> Meeting of the Acoustical Society of America, 20 to 26 June, Seattle, WA.

Baxley, P. A., H. P. Bucker, and J. A. Rice. 1998. "Shallow-Water Acoustic Communications Channel Modeling Using Three-Dimensional Gaussian Beams," Ocean Community Conference, 16 to 18 November, Baltimore, MD.

Chou, S., M. Pollock, and M. Soumekh. 1998. "On Target Resolvability from Single Tone Fringe Patterns of Digitally-Spotlighted SAR Image," SPIE International Symposium on Optical Science, Engineering and Instrumentation, July, San Diego, CA.

Goodman, I. R. 1997. "Can a Fuzzy Analogue Be Developed Relative to Adams' High Probability Deduction Logic?" invited presentation, Berkeley Information & Soft Computing (BISC) Seminar, 6 November, University of California at Berkeley.

Goodman, I. R. 1998. "New Results on High Probability Deduction and Combination of Information," 36<sup>th</sup> Annual Bayesian Research Conference, 19 to 20 February, Los Angeles, CA.

Goodman, I. R. 1998. "New Perspectives on Deduction in Data Fusion," (Open) Symposium on Multisensor Data Fusion, 30 to 31 March, Georgia Tech. Research Institute, Marietta, GA.

Goodman, I. R. 1998. "Applications of Fréchet and Other Random Set Averaging Techniques to Fusion of Information," SPIE Signal Processing, Sensor Fusion & Target Recognition VII, 13 to 15 April, Orlando, FL.

Goodman, I. R. 1998. "Random Set and Fuzzy Sets: A Special Connection," International Conference on Multisource-Multisensor Information Fusion (Fusion '98), 6 to 9 July, Las Vegas, NV.

- Goodman, I. R. 1998. "New Applications of Conditional Event Algebra and Relational Event Algebra to Fusion Information," 32<sup>nd</sup> Asilomar Conference on Signals, Systems & Computers, 1 to 4 November, Pacific Grove, CA.
- Goodman, I. R. and G. F. Kramer. 1998. "Recent Use of Relational Event Algebra, Including Comparisons, Estimations and Deductions for Probability-Functional Models," IEEE International Symposium on Intelligent Control, 14 to 17 September, National Institute of Standards & Technology (NIST), Gaithersburg, MD.
- Goodman, I. R. and H. T. Nguyen. 1998. "Adams' High Probability Deduction and Combination of Information in the Context of Product Probability Conditional Event Algebra," International Conference on Multisource-Multisensor Information Fusion (Fusion '98), 6 to 9 July, Las Vegas, NV.
- Green, M. D. and J. A. Rice. 1997. "Error-Correction Coding for Communication in Adverse Underwater Channels," IEEE OCEANS '97 Conference, October, Halifax, Nova Scotia, Canada.
- Green, M. D. and J. A. Rice. 1997. "Noncoherent Communication for Adverse Channels," 134<sup>th</sup> Meeting of the Acoustical Society of America, November, San Diego, CA.
- Green, M. D. and J. A. Rice. 1998. "Robust Communications in Adverse Channels," Oceanology International '98 Conference, March, Brighton, UK.
- Green, M. D. and J. A. Rice. 1998. "Low-Probability-of-Detection Communications in Adverse Underwater Acoustic Channels," 16<sup>th</sup> International Congress on Acoustics and the 135<sup>th</sup> Meeting of the Acoustical Society of America, June, Seattle, WA.
- Green, M. D. and J. A. Rice. 1998. "Non-Coherent Acoustic Communication in Adverse Channels: Requirements, Simulation, Experiments, and Models," invited presentation, ONR 3210A Workshop on High-Frequency Acoustics for Communications, August, University of Delaware.
- Green, M. D. and J. A. Rice. 1998. "Handshake Protocols for Underwater Communications Networks," IEEE OCEANS '98 Conference, September, Nice, France.
- Green, M. D., J. A. Rice, and S. Merriam. 1998. "Underwater Acoustic Modem Configured for Use in a Local Area Network," IEEE OCEANS '98 Conference, September, Nice, France.
- Green, M. D., J. A. Rice, and S. Merriam. 1998. "Implementing an Undersea Wireless Network for Shallow-Water Acoustic Modems," Ocean Community Conference, November, Baltimore, MD.
- Hicks, C. 1998. "Density-Matrix Renormalization-Group Method for Excited States," invited talk, American Physical Society, 16 to 20 March, Los Angeles, CA.
- Kevorkian, A. K. 1998. "Sparse Matrix Ordering for the Parallel Computation of Cholesky Factors," software demonstration at Supercomputing (SC) '98: High Performance Networking and Computing Conference, 7 to 13 November, Orlando, FL, High Performance Computing Modernization Office (HPCMO) booth.
- Mautner, T. 1999. "Modeling of Material Transport in a Closed Container," to be presented at the 30<sup>th</sup> AIAA (American Institute of Aeronautics and Astronautics) Fluid Dynamics Conference, June, Norfolk, VA.

- McDonald, V. K., J. A. Rice, and C. L. Fletcher. 1998. "An Underwater Communication Testbed for Telesonar RDT&E," IEEE OCEANS '98 Conference, September, Nice, France.
- McDonald, V. K., J. A. Rice, and C. L. Fletcher. 1998. "Telesonar Testbed Engineering and Sea Trials," Ocean Community Conference, 16 to 18 November, Baltimore, MD.
- McDonald, V. K., R. C. Shockley, J. A. Rice, and M. D. Green. 1997. "Probe Signals for Obtaining Impulse Response of Doubly Spread Channels," 134<sup>th</sup> Meeting of the Acoustical Society of America, November, San Diego, CA.
- Neff, J. D., B. K. Meadows, W. L. Ditto, G. N. Patel, and S. P. DeWeerth. 1998. "Spatiotemporal Dynamics of a Stochastic VLSI Array," IEEE International Symposium on Circuits and Systems, ISCAS '98, 31 May to 3 June, Monterey, CA.
- Orazi, R. J., M. N. McLandrich, T. T. Vu, A. Nelson, and D. Ferrell. 1998. "WDM Couplers for Erbium-Doped Fiber Amplified Spontaneous Emission Sources," Optical Society of America Annual Meeting, 4 to 9 October, Baltimore, MD.
- Proakis, J. G., M. Stojanovic, and J. A. Rice. 1998. "Design of a Communication Network for Shallow-Water Acoustic Modems," Ocean Community Conference, 16 to 18 November, Baltimore, MD.
- Rice, J. A. 1998. "Sensor-to-Sensor Acoustic Communications," invited presentation, ONR Workshop on Airborne ASW-Surveillance and Search, January, Patuxent River, MD.
- Rice, J. A. 1998. "Telesonar Channel Models, Measurements, and Adaptive Modulation," invited presentation, ONR 3210A Workshop on High-Frequency Acoustics for Communications, August, University of Delaware.
- Rice, J. A. 1998. "Undersea Internet," NDIA Undersea Warfare Division Meeting on "Network-Centric Warfare—USW Implications and Challenges," September, Groton, CT.
- Rice, J. A. and M. D. Green. 1998. "Adaptive Modulation for Undersea Acoustic Modems," Ocean Community Conference, 16 to 18 November, Baltimore, MD.
- Rice, J. A. and R. C. Shockley. 1998. "Battery-Energy Estimates for Telesonar Modems in a Notional Undersea Network," Ocean Community Conference, 16 to 18 November, Baltimore, MD.
- Rice, J. A., R. C. Shockley, V. K. McDonald, M. D. Green, and J. G. Proakis. 1997. "Long-Range Signaling in Shallow Ocean Transmission Channels," 134<sup>th</sup> Meeting of the Acoustical Society of America, November, San Diego, CA.
- Shockley, R. C. and P. A. Baxley. 1997. "Telesonar Channel Measurements and Modeling," invited presentation, ONR Acoustic Communications Workshop, November, Arlington, VA.
- Shockley, R. C., J. G. Proakis, M. Stojanovic, and J. A. Rice. 1998. "Spectral Shaping in MFSK Modulation for Underwater Acoustic Communications," 16<sup>th</sup> International Congress on Acoustics and the 135<sup>th</sup> Meeting of the Acoustical Society of America, June, Seattle, WA.

- Shockley, R. C., J. A. Rice, and V. K. McDonald. 1997. "Spreading, Coherence, Fading, and Noise in Shallow-Water Channels," 134<sup>th</sup> Meeting of the Acoustical Society of America, November, San Diego, CA.
- Shockley, R. C., J. A. Rice, V. K. McDonald, M. D. Green, J. G. Proakis, and J. Newton. 1998. "Observations of Coherence Time and Amplitude Fluctuations in a Shallow-Water Acoustic Communications Channel," 16<sup>th</sup> International Congress on Acoustics and the 135<sup>th</sup> Meeting of the Acoustical Society of America, June, Seattle, WA.
- Stojanovic, M., J. G. Proakis, J. A. Rice, and M. D. Green. 1998. "Spread-Spectrum Methods for Underwater Acoustic Communications," IEEE OCEANS '98 Conference, September, Nice, France.
- Wallace, J. W. 1998. "Implementing Neural Networks and Fuzzy Logic Using the IMPORT Simulation Language," Object-Oriented Simulation Conference, Society for Computer Simulation International, San Diego, CA.
- Wang, Y., S. D. Russell, and R. L. Shimabukuro. 1998. "Electronically Tunable Mirror Using Surface Plasmons," SPIE "Photonics West" Conference, 29 January, San Jose, CA.



## HONORS AND AWARDS

## HONORS AND AWARDS



**Dr. Stephen Russell**, Head of the Advanced Technology Branch at SSC San Diego, has over 20 years' experience in lasers, optics, electronics, sensors, and display technologies. While working for 10 years in the Solid-State Electronics Division's Integrated Circuit Fabrication Facility, he served as Manager of the Laser Processing Laboratory and also as a Lead Engineer for diffusion and chemical-vapor deposition, ultraviolet reflectometry, and secondary ion mass spectroscopy. His contributions have ensured the success of many Navy projects and have resulted in an excess of 40 patents issued or pending. Dr. Russell has established a reputation of technical excellence with the publication of numerous journal articles and conference proceedings. In addition, he has initiated three Cooperative Research and Development Agreements (CRADAs) with private

companies and has teamed with industry, government laboratories, and universities on many projects that expand SSC San Diego's leadership role in C<sup>4</sup>ISR (command, control, communications, computers, intelligence, surveillance, and reconnaissance) systems. Dr. Russell's most recent work includes research and development of novel displays and optical filters and excimer laser processing of microelectronic devices.

On 1 May 1998, Dr. Russell, Dr. Randy L. Shimabukuro, and Dr. Yu Wang received a Certificate of Recognition from the National Aeronautics and Space Administration (NASA) for "the creative development of a technical innovation." On 23 October 1997, they also received NASA's Class 1 Technical Brief Award. Dr. Russell serves as a referee for *Physical Review B* and *Physical Review Letters* and was selected as a National Research Counsel Advisor in 1995. Dr. Russell is a member of the American Physical Society, Society for Information Display, Optical Society of America, and the Materials Research Society. A dedicated supporter of SSC San Diego's New Professional (NP) program, he has served as a recruiter and as a department representative to the NP and Co-Op hiring committee. Recently, he has also served as a technical consultant and contracting officer's representative for the Defense Advanced Research Projects Agency (DARPA) and the Ballistic Missile Defense Organization (BMDO).

His FY 97 and FY 98 ILIR project, Surface-Plasmon Flat-Panel Display, was done in collaboration with Dr. Yu Wang of NASA's Jet Propulsion Laboratory and with SSC San Diego colleagues Dr. Randy Shimabukuro (D893) and Ajax Ramirez (D853). The project proposed a new display technology that uses voltage-induced color-selective absorption by surface plasmons at a metal/liquid crystal interface. This approach has several potential advantages over existing and emerging display technologies: increased brightness, improved color purity, higher pixel density, lower cost, and higher reliability. Test wafers were fabricated at the Center's Integrated Circuit Fabrication Facility, and the wafers were subsequently used for assembly of the prism, top electrode, and liquid-crystal structures. In FY 97, an active color filter using surface plasmons was electrically turned to produce the primary

colors (cyan, yellow, and magenta). Modeling of multilayered top electrodes demonstrated a rhodium-aluminum structure that produced the best broadband response in combination with nematic liquid crystals to achieve gray-scale modulation.

In FY 98, this structure was fabricated and tested to demonstrate the ability to produce gray scales. Further modeling was performed on the surface-plasmon device, the angular effects were studied, and a micro-machined embodiment was examined that would eliminate the need for liquid crystals. Patent disclosures were filed to exploit the newly discovered advantages provided by these devices. The commercial sector has recognized the promising results from Dr. Russell's project, and an investigation of the commercial viability of this technology will be continued under a CRADA with Optron Systems of Bedford, MA.

In February 1999, **Dr. John Barnett** was selected as Editor, Electro-Optic and Infrared Systems, for the *IEEE Transactions on Aerospace and Electronic Systems*. During FY 98, Dr. Barnett was also selected to be a member of the Industrial Liaison Committee for the Center for Applied Mathematical Sciences at the University of Southern California (USC), Los Angeles, CA.

**Paul Baxley** continues as President of the San Diego Chapter of the Acoustical Society of America (ASA). He is Chairman of the ASA Public Relations Committee, a Member of the ASA External Affairs Committee, and Co-Chair of the ASA Home Page Committee. He is the creator and web-master of the "ASA World Wide Press Room" on the WWW (World Wide Web).

**Dr. I. R. Goodman**, in addition to having his work cited by peers in various scientific publications, received multiple requests for review of professional papers and has been appointed to the review editorial board of *Information Sciences*. Dr. Goodman has also been invited to serve on the founding panel for the new Data Fusion Society and to co-chair a special session on Conditional Event Algebra and Random Set Theory for the April 1999 SPIE Session on Signal Processing, Sensor Fusion and Target Recognition VIII.

**Richard Orazi** received an SSC San Diego Publication Excellence Award as one of the authors of the SSC San Diego technical report TR 1724, "Manufacturing Science and Technology for Polarization Independent Narrow Channel (PINC) Wavelength Division Multiplexing (WDM) Fiber Couplers." He also received an SSC San Diego Publication Award of Merit as one of the authors of TR 1731, "Shipboard Electromagnetic Environment Measurements Using a Wideband Photonic Probe."

**Joseph Rice** was one of five panelists chosen by the Acoustical Society of America (ASA) to lead a discussion during a special session on underwater acoustic communications at the 16th International Congress on Acoustics and the 135th Meeting of the ASA in Seattle (June 1998). He was also consulted by Dr. Jeffrey Simmen (ONR 321OA) on aspects of a future 6.1 Program in Underwater Acoustics for Communications and participated in the resulting workshop sponsored by ONR 321OA at the University of Delaware (August 1998). Mr. Rice will co-host the second such workshop to be held at Scripps Institution of Oceanography in FY 99.

**Dr. James Rohr** received an SSC San Diego Distinguished Publication Award for Open Literature for the article he coauthored entitled “The Use of Bioluminescence as a Flow Diagnostic,” *Physics Letters A*, vol. 228, pp. 408–416. Also, a figure from a journal article he coauthored entitled “Dolphin Stimulated Bioluminescence” appeared on the cover of the *Journal of Experimental Biology*, vol. 201, no. 9, and on the cover of the publication *Biophotonics International*.

**Jeffrey Wallace** is now the Associate Vice President (Standards) for the Society for Computer Simulation International.

PATENT ACTIVITY

## **INDEPENDENT RESEARCH**

### **Patents Issued**

**Aram K. Kevorkian**

**“Method and Apparatus for Pre-Processing  
Inputs to Parallel Architecture Computers”**

This invention provides an advanced computer user with an automated means to find hidden parallelism in a wide range of problems of interest to both government and industry. With hidden parallelism exposed, the computer is able to partition the original problem into a suite of independently solvable smaller tasks that are then executed in parallel on different processors.

Patent 5,655,137 Navy case 76,956 (Serial 08/409,256) filed 23 March 1995; issued 5 August 1997 (continuation of Patent 5,446,908).

**Howard L. Dyckman**

**“Spread Spectrum Modulation Using  
Time-Varying Linear Filtering”**

This method for transmitting information by radio over a wide bandwidth comprises the following steps: inputting a data signal into a time-varying filter modulator; spreading the data signal in time and in frequency to produce a wideband signal; modulating the sideband signal onto an RF carrier to provide an RF output signal; and transmitting the RF output signal. This step of spreading includes performing a series of linear transformations to the data signal.

Patent 5,748,667 Navy case 77,685 (Serial 08/621,400) filed 25 March 1996; issued 5 May 1998.

**Richard Scheps**

**“Laser Diode Wavelength and  
and Beam Homogenizer”**

A laser-diode power combiner comprises a dye laser operably coupled to an array of laser diodes for combining optical power from the laser diodes into a single, coherent laser beam.

Patent 5,764,677 Navy case 77,221 (Serial 08/572,828) filed 14 December 1995; issued 9 June 1998.

**Adi R. Bulsara  
William L. Ditto  
Mario E. Inchiosa  
John F. Lindner  
Brian K. Meadows**

**“Noise and Coupling Tuned Signal  
Processor with Arrays of Nonlinear  
Dynamic Elements”**

This invention exploits the phenomenon of stochastic resonance in a nonlinear dynamic system to enhance the system’s response to a weak periodic signal corrupted by background noise.

Patent 5,789,961 Navy case 77,854 (Serial 08/671,909) filed 28 June 1996; issued 4 August 1998.

**Stephen D. Russell**

**“System That Uses Porous Silicon for  
Down-Converting Electromagnetic Energy to an  
Energy Level within the Bandpass of an  
Electromagnetic Energy Detector”**

This invention describes an optical element made of porous silicon on a transparent substrate for converting light of an incident energy to that of a lower emitted energy. This invention may be used for the efficient detection of normally invisible and undetectable wavelengths and has applications in imaging, surveillance, and reconnaissance.

Patent 5,828,118 Navy case 76,947 (Serial 08/812,680) filed 6 March 1997; issued 27 October 1998.

**INDEPENDENT RESEARCH  
Claims Allowed; Notice of Allowance**

**Steven D. Russell  
Shannon Kasa  
Howard W. Walker**

**“Chemical Sensor Using  
Ring-Oscillator Thermometry”**

This invention describes a novel structure using ring-oscillator thermometry for use as a chemical or biological sensor. Combustible gas sensors based on thermal sensors have been demonstrated in the prior art. These sensors, called pellistors, depend on a rise in temperature at a catalytic surface due to catalytic oxidation of the combustible gas. The pellistor measures this rise in temperature with a thermistor. The novel gas sensor incorporates a catalytic platinum layer deposited on top of a ring oscillator. Combustible gases will be catalytically oxidized at the platinum surface. The heat released by the reaction will cause local heating of the ring oscillator and thus, affect its frequency.

Navy case 76,462; (Serial 08/977,720) filed 25 November 1997; Notice of Allowance 22 November 1998.

**Jerome F. DeJaco  
Willard F. Rask**

**“Impulsive Snap-through  
Acoustic Projector (ISnAP)”**

An impulsive snap-through acoustic pulse generator may be used to generate an acoustic pulse in an aqueous environment without gas bubbles. The impulsive snap-through acoustic pulse generator includes a support structure having an open end, a resilient shell mounted to the support structure to define a chamber, and a gas vent in fluid communication with the chamber through which a gas passes for changing the pressure in the chamber so that the resilient shell transitions from a first stable state to a second stable state, thereby generating an acoustic pulse.

Navy case 77,245 (Serial 08/955,339) filed 21 October 1997; Notice of Allowance 8 July 1998.

**Allen Shum**

**“Asynchronous Transfer Mode Cell  
Loss Estimation Algorithms”**

A software program for estimating traffic loss of an asynchronous transfer mode (ATM) statistical multiplexer comprises a communication channel having traffic sources and a buffer. Traffic is generated by the traffic sources and removed by the communication channel. When total traffic exceeds the capacity of the communication channel, excess traffic is stored in the buffer. When the buffer is full, excess traffic is lost. Estimating the amount of traffic that will be lost by an ATM statistical multiplexer, therefore, has application in the design of ATM networks.

Navy case 77,443 (Serial 08/707,284) filed 3 September 1996; Notice of Allowance 12 May 1998.

**David W. J. Stein**

**“Coherent Hidden-  
Markov Detector”**

This method for processing coherent radar-return data detects targets in nonstationary radar clutter. Advantages and new features of this method over Doppler processing include modeling the clutter using Markov models and applying a phase-coherent detection statistic based on a likelihood ratio that allows for the clutter level to fluctuate over the duration of the time series being analyzed.

Navy case 78,933 (Serial 09/112,906) filed 9 July 1998; Notice of Allowance 17 December 1998.

**INDEPENDENT RESEARCH  
Patent Applications Filed**

**Stanislaw J. Szpak  
Pamela A. Boss**

**“Electrode and Method for Preparation of  
Electrode for Electrochemical Compression  
of Deuterium into a Metal Lattice”**

This invention provides an electrode and method for preparing the electrode that may be employed to electrochemically compress deuterium into a metal lattice of the electrode. An electrochemical cell is constructed that includes an electrolyte solution comprising a metallic salt and a supporting electrolyte. The metallic salt, when in a reduced state, absorbs deuterium. Both the electrolytic solution and supporting electrolyte are dissolved in heavy water. An anode and cathode are immersed and stable within the electrolytic solution. The anode is stable when polarized. A voltage is applied across the anode and cathode while a constant potential is maintained at the cathode. The constant potential is measured with respect to a reference electrode immersed within the electrolytic solution so that deposition of metallic ions occurs in the presence of evolving deuterium during electrolysis of the electrolytic solution. By this method, the cathode is transformed into the electrode.

Navy case 73,311 (Serial 07/632,896) filed 24 December 1990; pending.

**Stanislaw J. Szpak  
Pamela A. Boss**

**“Electrochemical Cell Having a  
Beryllium Compound Coated Electrode”**

This invention describes a procedure to modify metal-hydride electrodes so as to increase hydrogen storage capabilities as well as increase the cycling lifetime of the electrode. Such an invention improves the performance of fuel cells and/or rechargeable metal-hydride batteries.

Navy case 76,707 (Serial 08/969,175) filed 12 November 1997; pending.

**Stephen M. Hart**

**“Optoelectronically Controlled Waveguide”**

An optoelectronically controlled waveguide (OCW) is composed of a metallic waveguide, a finline, and a PVFET. (A PVFET is a field-effect transistor with a gate controlled by a photo-voltaic cell.) The finline is inserted into the waveguide making electrical contact, and the PVFET is affixed to the finline in a shunt configuration. The resulting device is capable of attenuating the energy propagating in the waveguide to any desired degree. In this fashion, the OCW can function as an attenuator or a switch.

Navy case 76,916 (Serial 09/093,849) filed 28 May 1998; pending.

**Richard Scheps**

**“Underwater Imaging Technique for the  
Detection of Shallow Submerged Objects”**

This high-resolution underwater imaging and ranging device scans an area underwater with a pulsed laser and records the reflected signal from the illuminated area with a gated photomultiplier.

Navy case 77,222 (Serial 08/908,778) filed 7 August 1997; pending.

**Michael J. Winton  
Stephen D. Russell**

**“Method of Making Improved  
Electrical Contact to Porous Silicon”**

This is an improved method of making electrical contact to porous silicon and porous silicon device structures by controlling the global or large-scale surface morphology. The inventive process uses the supply of holes, ions of other charged species to control the etching dynamics of the porous silicon formation. The intensity of the light emitted by porous silicon layers and devices can therefore be increased by the improved electrical interconnection between the mechanically, chemically, and thermally fragile porous silicon and the device electrodes.

Navy case 77,603 (Serial 08/944,746) filed 6 October 1997; pending.

**Monti E. Aklufi  
Stephen D. Russell**

**“Thin-Film Improvement Method  
and Apparatus”**

This invention provides a novel apparatus and an improved method by using a contoured laser beam to improve the electrical, optical, and material properties of thin films.

Navy case 77,921 (Serial 08/934,037) filed 19 September 1997; pending.

**Adi R. Bulsara  
Mario E. Inchiosa  
Luca Gammaitoni  
Frank E. Gordon**

**“Detector of Weak Signals Based on  
Noise-Controlled Resonance Behavior in Nonlinear  
Dynamic Systems with Broken Symmetry”**

This device exploits the dynamical symmetry-breaking property of a weak dc signal in an *a priori* symmetric nonlinear dynamic device, to detect and quantify the dc signal. Simultaneously, the technique offers a novel way to circumvent detector low-frequency noise constraints by shifting the detection to a more acceptable part of the frequency spectrum.

Navy case 78,154 (Serial 08/917,655) filed 25 August 1997; pending.

**Parviz Soltan  
John A. Trias  
Weldon J. Dahlke  
Robert V. Belfatto  
Frank Sanzone  
Christopher J. Poulos  
Neil P. Acantilado**

**“Computer-Controlled  
Three-Dimensional  
Volumetric Display”**

A three-dimensional display system comprises a display volume selectively partitioned into distinct display regions: a display surface for scattering light beams from the display volume; at least two optical scanners for modulating the light beams and for directing the light beams to the display surface within each distinct display region, respectively; and a display controller. The display controller comprises a world-coordinate interface for inputting world coordinates, a data processor for transforming the world coordinates into view coordinates and device coordinates, and an optical-scanner controller for sensing and controlling the motion of the display surface and for outputting the device coordinates to the optical scanners to generate a three-dimensional image within the display volume.

Navy case 78,445 (Serial 08/926,854) filed 10 September 1997; pending.

**Stephen D. Russell  
Randy L. Shimabukuro  
Yu Wang**

**“Transmissive Surface-  
Plasmon Light Valve”**

The invention provides a light valve or optical modulating device that exploits color-selective absorption at a metal-dielectric interface by surface plasmons. The invention includes an electrode layer formed of an optically transparent substrate. A layer of electro-optic material is formed on the electrode. The electro-optic material has an index of refraction that may be modulated by an electrical bias. A second electrode is formed over the electro-optic material. Changes in a voltage bias across the electrodes modulate the index of refraction of the electro-optic material so that it selectively absorbs light (at different wavelengths) that passes through the light valve, depending on the index of refraction. The electrodes are made of a transparent or semitransparent material, such as indium tin oxide. Multiple light valves may be arranged in an array to form a flat-screen video display.

The novelty of the invention is that it provides a new mode of operation in that it is a transmissive device, rather than a reflective device.

Navy case 78,518 (Serial 09/172,581) filed 14 October 1998; pending.

**Gregory A. Theriault  
Leonard J. Martini  
Leon V. Smith**

**“A Translation System  
for Directing an Optical Signal  
to Predetermined Coordinates”**

A translation system for directing an optical signal through predetermined coordinates of a window mounted in a soil penetration probe includes a tube having a sidewall and an aperture through said sidewall; an optically transparent window mounted in said aperture; an optical system for emitting an optical signal through said aperture; and a translation mechanism mounted within said tube. The translation mechanism may be selectively operated to translate independently and simultaneously the optical system along two orthogonal vectors so that the optical signal scans across the window. Scanning the optical signal extends the useful life of the window before its transmissibility becomes too impaired by damage caused from the optical signal.

Navy case 78,881 (Serial 09/015,431) filed 29 January 1998; pending.

**Carol A. Becker**

**“Light-Activated  
Polymeric Actuators”**

Visible light causes a pH charge *in situ* to the polymer backbone. The pH charge expands and contracts the polymeric actuator in a timeframe suitable for robotics. A mechanism is provided for reversible dissipation of any heat produced by the light.

Navy case 78,990 (Serial 09/137,008) filed 20 August 1998; pending.

**INDEPENDENT RESEARCH  
Invention Disclosures Authorized**

**Willard M. Cronyn**

**“Compact, Phasable, Multioctave,  
Planar, High-Efficiency Spiral-Mode  
Antenna”**

The antenna consists of eight planar windings, each one of which is an exponential spiral. The windings are connected in groups of three to a balanced transmission line, with a “floating” winding between each of the two groups. For the purpose of phasing elements together for directional-beam control, the particular grouping of windings can be changed. A sinuous variation is imposed on the spiral windings to increase the path length for each winding rotation so that the circumference through which the phase increases by 360 degrees is correspondingly decreased. This element integrates a planar structure, wideband compact design, and phasability into a single physical structure.

Navy case 76,188; authorized for preparation of patent application 30 April 1997.

**Stephen M. Hart**

**“Optoelectronically Controlled  
Frequency-Selective Surface”**

A photovoltaic field-effect transistor (PVFET) is used to control the impedance, scattering frequency, and scattering cross-section of the scattering elements on a Frequency-Selective Surface. The PVFETs are implanted in the arms of either wire or slot scatterers to make their scattering properties adjustable. The resulting Optoelectronically Controlled Frequency-Selective Surface (OCFSS) becomes a programmable electromagnetic shield or pattern control device.

Navy case 76,915; authorized for preparation of patent application 26 March 1996.

**Frank E. Hanson  
Peter M. Poirier**

**“Technique for Operating High-  
Energy Q-switched 0.9- $\mu\text{m}$   
Neodymium Lasers”**

This invention describes a wavelength discriminating filter and procedure to efficiently operate a Q-switched neodymium laser on the  $4F_3/2$  to  $4I_9/2$  transition near  $0.9 \mu\text{m}$  by suppressing the higher gain emissions near  $1 \mu\text{m}$ . The invention applies in general to all neodymium-based lasers operating at  $0.9 \mu\text{m}$  and, in particular, to neodymium-doped yttrium aluminum garnet (Nd:YAG) operating at  $0.0946 \mu\text{m}$ .

Navy case 79,523; authorized for preparation of patent application 3 February 1996.

## **INDEPENDENT RESEARCH Invention Disclosures Submitted**

**Thomas W. Schlosser**

**“A Spherical Coordinate Algorithm for the  
Detection of Collisions between Three-  
Dimensional Objects in Computer Models”**

This invention describes an algorithm for collision detection between three-dimensional objects in computer models that is more efficient and simpler than current algorithms. Current collision-detection algorithms rely either on testing for polygon intersections or attempt to solve multiple simultaneous polynomial equations to test for collision between surface patches on a three-dimensional model. All algorithms rely on Cartesian representations of the objects. A method using spherical coordinates, based on the relatively simple test for collision between spheres, provides a more efficient means of testing for collisions and is simple to calculate and implement after multiple rotations of the model.

Navy case 77,771; disclosure submitted 18 April 1996.

**Stephen D. Russell  
Philip R. Kesten**

**“Interactive Display Device”**

This invention is a monolithically integrated display and sensor array that provides for interactive real-time changes to the display image.

Navy case 78,287; disclosure submitted 24 October 1996.

**Pamela A. Boss  
Stephen H. Lieberman**

**“The Use of Microelectrode  
Arrays for the Detection of  
Volatile Organic Contaminants  
in the Air”**

The invention is used to detect organic contaminants in the gas phase. The invention comprises a working electrode separated from an auxiliary electrode by an insulator. The electrodes are coated with self-assembled monolayers, and a voltage bias is applied across the electrodes while the resulting current is measured. The electrode materials and monolayers are selected so that when a gaseous analyte of interest contacts the electrodes, the current changes by a detectable amount. Multiple microelectrodes may be configured into arrays whereby each microelectrode is responsive to a particular analyte. In this way, many different gaseous contaminants may be detected with a single instrument. The microelectrodes may be fabricated onto chips using photo-lithographic techniques.

An important novelty of the invention is that it provides an instrument capable of monitoring contaminants over time and provides the real-time detection of drugs and explosives. The use of the self-assembled monolayers as a coating to enhance the response of the electrodes is novel.

Navy case 78,928; disclosure submitted 1 December 1997.

**Stephen D. Russell**  
**Randy L. Shimabukuro**  
**Yu Wang**

**“Microdynamic Optical Device”**

This invention describes a light valve, display, optical modulating device or optical filter that uses a microdynamic construction to exploit the color-selective absorption at a metal-dielectric interface by surface plasmons. This invention has applications for displays in command and control, for multispectral imaging in surveillance and reconnaissance, and for filtering in optical communications and scientific instrumentation.

Navy case 78,968; disclosure submitted 19 November 1997.

**Richard Scheps**

**“Compact Solid-State Dye Laser”**

This invention describes a compact solid-state dye laser that is diode-pumpable. The laser in its preferred embodiment consists of a monolithic state of materials including a solid-state  $l$ - $\mu$ -emitting laser gain element, a passive Q-switch, a second-harmonic doubling crystal, and the solid-state dye gain element.

Navy case 79,094; disclosure submitted 12 January 1998.

**Ayax D. Ramirez**  
**Stephen D. Russell**  
**Randy L. Shimabukuro**

**“Resonance-Tunable Optical Filter”**

This invention exploits color-sensitive absorption at a metal dielectric interface by surface plasmons. The invention provides a resonance-tunable optical filter that includes a dielectric and a metal layer through which electromagnetic radiation may be transmitted or reflected. A beam-steering apparatus is used to change the incident angle of the electromagnetic radiation whose optical properties are modified by choice of incident angle. The incident medium and exit medium are optically transmissive.

Unlike the prior art, the invention device does not require spacers, alignment layers, and seals previously used to make liquid crystal filled surface-plasmon devices.

Navy case 79,095; disclosure submitted 26 February 1998.

**David W. J. Stein**

**“Hidden-Markov  
Amplitude Detector”**

This invention provides a means of detecting incoherent signals in non-Gaussian noise.

Navy case 79,280; disclosure submitted 17 December 1997.

**Stephen D. Russell**  
**Randy L. Shimabukuro**  
**Yu Wang**

**“Solid-State Light  
Valve and Tunable Filter”**

This invention describes an all solid-state light valve, optical modulating device or optical filter that uses color-selective absorption at a metal-dielectric interface by surface plasmons. The invention has applications for displays in command and control, for multispectral imaging in surveillance and reconnaissance, and for filtering in optical communications and scientific instrumentation.

Navy case 79,542; disclosure submitted 3 November 1997.

**Stephen D. Russell**

**“Spatially Conformable Tunable Filter”**

The invention provides a flexible or pliable optical modulating device, light-valve or optical filter. It uses a sheet of polymer-dispersed liquid crystal (PDLC) material and specifically selected thin metal electrodes on either side of the PDLC to form a capacitor structure. When a voltage is applied to the capacitor, the refractive index of the liquid crystal changes since it is an electro-optic material. The optical properties of one of the thin metal electrodes are selected in combination with the PDLC to have a surface-plasmon resonance that is either narrow band or broadband depending on the application. The surface plasmon is then used to selectively absorb incident light at the metal-PDLC interface, while the remaining light gets reflected (or transmitted). By varying the applied voltage, and its corresponding change in PDLC refractive index, we can modulate the light valve or tune the filter. The improvement over the prior art is that this can be configured conformably over a surface to improve the acceptance angle for the filter and to simplify the fabrication of the device as compared to conventional liquid crystals.

Navy case 79,545; disclosure submitted 1 June 1998.

**Pamela A. Boss**  
**Stephen H. Lieberman**

**“Spectroelectrochemical Device  
to Detect Airborne Contaminants”**

The invention is a gas sensor that combines the sensitivity of electrochemistry with the specificity of spectroscopy for detecting organic contaminants in the gas phase. The sensing unit consists of a micro-electrode assembly comprising an inner working disk electrode and an outer auxiliary ring electrode. The inner working disk electrode is coated with a thiol coating. The micro-electrode portion of the sensor is used to continuously monitor the environment. When current flow between the two electrodes of the sensor occurs, a spectrum of the working electrode can be obtained to identify the electro-active species. The invention can operate in either a flowing stream or a quiescent environment. It can also be used to monitor for dangerous volatile organics, explosives, or drugs. The invention may also be used to perform surface-enhanced Raman spectroscopy (SERS).

An important novelty of the invention is that it incorporates micro-electrodes and SERS, which combine to have the capability of detecting organic contaminants in the ppm level. The micro electrodes can be arranged in arrays and require reduced capacitive charging currents. Micro-electrodes exhibit reduced signal-to-noise characteristics over standard-sized electrodes and can be configured into a variety of shapes.

SSC SD-322; disclosure submitted 5 August 1998.

**Stanislaw Szpak**  
**Pamela A. Boss**

**“Power Conversion Unit”**

This invention describes a power-conversion unit consisting of a working electrode and counter electrode. Palladium and deuterium are co-deposited on the working electrode. During co-deposition, nuclear events of unknown origin occur resulting in enormous heat release. This heat can be used to provide power for a number of applications.

SSC SD-327; disclosure submitted 17 September 1998.

**Pamela A. Boss**  
**Roger D. Boss**  
**Stephen H. Lieberman**

**“Method of Preparing Durable  
Gold or Silver Film Substrates  
for Surface-Enhanced Raman  
Spectroscopy (SERS)”**

This invention describes a process to prepare durable gold or silver films on substrates containing metal-oxide bonds for use in SERS. Steps in the process are (1) roughen the surface of the substrate, (2) react the roughened surface with a silanization agent such as (3-mercaptopropyl) trimethoxy silane, (3) vacuum-deposit silver or gold onto the silanized surface, and (4) react with thiol coating. Depending upon the thiol coating used, these substrates can be used to detect VOCs, metal ions, and anions. Substrates prepared in this manner exhibit excellent adherence between the substrate surface and the metal film. The films can be immersed in water over extended periods of time. The silver or gold metal film can be used as the sensing layer of an optical waveguide device.

SSC SD-328; disclosure submitted 8 October 1998.

**David F. Schwartz**  
**J. William Helton**  
**Jeffery C. Allen**

**“Predictor for Optimal Broadband Matching”**

A predictor for optimal broadband matching of the present invention comprises a computer program that inputs samples of load reflectance normalized to characteristic line impedance, the frequencies associated with the normalized reflectance samples, and a parameter specifying the number of frequency increments for calculation. The program calculates and outputs the highest power gain obtainable by any matching circuit and two associated system parameters: the power mismatch and the voltage standing wave ratio.

SSC SD-341; disclosure submitted 1 December 1998.

**INDEPENDENT EXPLORATORY DEVELOPMENT  
Patent Issued**

**Everett W. Jacobs  
Roger D. Boss  
Yuval Fisher**

**“Method of Encoding a  
Digital Image by Using Adaptive  
Partitioning in an Iterated  
Transformation System”**

This invention is a new adaptive method for partitioning an image, resulting in efficient encoding by using the iterated transformation image-compression technique.

Patent 5,862,262 Navy case 74,198 (Serial 07/859,782) filed 30 March 1992; issued 19 January 1999.

**INDEPENDENT EXPLORATORY DEVELOPMENT  
Claims Allowed; Notice of Allowance**

**Neil P. Acantilado**

**“Computer Program for a Three-  
Dimensional Volumetric Display”**

This method for transforming world coordinates into device coordinates comprises the following steps: inputting a set of world coordinates to be displayed; scaling the world coordinates into view coordinates bounded by a display volume; finding a control memory location of a light-beam deflector corresponding to a Y-axis position for each of the view coordinates; calculating X-axis and Z-axis device coordinates from the view coordinates for deflecting a light beam to a selected point within the display volume, corresponding to each of the view coordinates; and loading the device coordinates into the control memory locations corresponding to the Y-axis position for each of the view coordinates, to cause the light beam to be deflected to each selected point.

Navy case 77,782 (Serial 08/726,305) filed 2 October 1996; Notice of Allowance 4 January 1999.

**INDEPENDENT EXPLORATORY DEVELOPMENT  
Patent Application Filed**

**Pamela A. Boss  
Roger D. Boss**

**“Versatile, Thin-Layer Cell for  
*In-Situ* Spectroelectrochemistry”**

This invention describes the design of a low-volume, thin-layer cell constructed of chemically resistant materials capable of performing spectroelectrochemistry. Such a cell can be used as a flow-through cell to continuously monitor manufacturing processes.

Navy case 77,803 (Serial 08/900,983) filed 25 July 1997; pending.



### SSC San Diego FY 98 ILIR Database

SSC SD PROJ #	DTIC DN#	Project Title	Principal Investigator	SSC SD Code		ONR SE#	DoD MA1	DoD MA2	JMA	DoD CT	FY 97 \$K	FY 98 \$K	Planned FY 99 \$K	Keywords
ZU54	307777	3-D Propagation in Shallow Water Overlaying an Elastic Bottom	Dr. A. T. Abawi	D881		14	ASW	OSV	2	19	0	80	75	propagation; parabolic equation model; coupled mode
ZU43	306750	Generalized Higher Order Crossings Theory and Practice	Dr. J. T. Barnett	D743		14	MWT	CCC	4	6	93	110	0	level crossing; higher order crossing; parametric filtering; fixed-point theory
ZU25	305519	Array Processing with 3-D Bathymetry	P. A. Baxley	D881		31	ASW	OSV	3	19	66	60	0	array processing; underwater acoustic propagation; matched-field processing
ZU30	305524	Development of Ultramicroelectrode (UME) Arrays for Use in a Remote Probe	Dr. P. A. Boss	D363		13	FSO		7	12	82	60	0	UME array; gas phase; sensors; electrochemistry
ZU55	307778	Environmentally Adaptive Autonomous Matched-Field Tracking	Dr. H. P. Bucker	D881		14	OSV	ASW	3	19	0	68	70	underwater sound; signal processing
ZU65	307790	Stochastic Resonance for Communications	Dr. A. R. Bulsara	D364		14	CCC		4	6	0	130	0	stochastic resonance; receivers
ZU44	306749	Impulsive Snap-through Acoustic Projector (ISnAP)	J. F. DeJaco	D7102		11	OSV	ASW	3	19	88	55	0	impulsive acoustic source; snap-through
ZU56	307779	Robust Control and Identification of Multiclass Queuing Systems for C4I	Dr. R. F. Freund	D4223		15	CCC		4	7	0	187	0	distributed computing; scheduling; multiclass queuing
ZU57	307780	Anti-Ice Coatings: New Low Surface Free Energy Coatings for Easy Ice-Release	Dr. R. D. George	D361		13	MOB		8	17	0	90	35	polymers; coatings; ice-release; environmental; anti-ice
ZU58	307781	Algebraic Estimation of Multivalued Phenomena with Applications to Data Fusion	Dr. I. R. Goodman	D44215		14	CCC		4	6	0	185	115	data fusion; expectation of random sets; generalized estimation; relational event algebras
ZU45	306755	Solid-State Blue Laser Development	Dr. F. E. Hanson	D853		11	CCC		3	19	83	70	0	lasers; nonlinear optics; neodymium
ZU53	306770	Exact Diagonalization of Large Sparse Matrices	Dr. C. Hicks	D364		11	MWT	CCC	4	6	27	40	35	high-performance computing; large matrix diagonalization

**NOTES:** SE = Subelement (codes); MA = Mission Area; JMA = Joint Mission Area (codes); CT = Critical Technology (codes)  
See Glossary for numbered codes and other abbreviations.

### SSC San Diego FY 98 ILIR Database (contd)

SSC SD PROJ #	DTIC DN#	Project Title	Principal Investigator	SSC SD Code	ONR SE#	DoD MA1	DoD MA2	JMA	DoD CT	FY 97 \$K	FY 98 \$K	Planned FY 99 \$K	Keywords
ZU35	305529	Sparse QR Factorization with Column Pivoting as Applied to Target-Strength Prediction	Dr. A. K. Kevorkian	D714	14	ASW		3	22	99	84	35	least squares; sparse matrices; indefinite systems; linear and nonlinear programming
ZU52	306759	Determination of the Boundary Shear Stress Required for Sediment Resuspension	Dr. T. Mautner	D363	23	FSO	MWT	7	12	45	80	0	sediment; shear stress
ZU59	307782	Fiber-Optic Add/Drop Multiplexers Produced by Writing Gratings on Fused-Fiber Tapered Couplers	R. J. Orazi	D895	11	CCC		4	6	0	90	94	wavelength division multiplexing; Bragg gratings; fused-fiber couplers
ZU60	307783	Performance Analysis of Single and Multichannel Adaptive Equalizers	M. Reuter	D855	14	CCC		4	6	0	105	0	adaptive equalization; line-of-sight digital radio; multichannel equalization; channel fading; interference
ZU61	307784	Telesonar Channel Measurements and Models	J. A. Rice	D881	31	CCC		4	19	0	105	115	underwater acoustic propagation; transmission channels; propagation models; telesonar; sound scattering
ZU48	306760	Propwash/Wake Resuspension in San Diego Bay—The Grand Plan	Dr. J. Rohr	D363	23	FSO	MWT	7	12	76	80	90	critical shear stress; resuspension
ZU47	306756	Surface-Plasmon Flat-Panel Display	Dr. S. D. Russell	D853	15	CCC		4	6	137	135	0	flat-panel display; surface plasmon
ZU21	305515	H <sup>∞</sup> Impedance Matching Broadband Antennas	Dr. D. F. Schwartz	D7213	21	CCC	FSO	4	6	117	105	0	H <sup>∞</sup> methods; antenna design; impedance estimation
ZU50	306762	Biosonar Ensonification of Buried Mines	J. Sigurdson	D351	11	MIW		2	19	63	35	0	biosonar; detection; mines
ZU39	306758	Resonantly Enhanced EHF Electroabsorption Modulator with a Novel Back-to-Back Diode Structure	Dr. C. K. Sun	D895	11	CCC	MWT	4	6	123	115	0	fiber-optic link; optoelectronic transceiver
ZU62	307785	Pixon-Based Image Reconstruction from Inverse Synthetic Aperture Radar Data	J. Trischman	D73H	14	OSV		3	19	0	90	0	radar; ISAR; imaging; pixion; Bayesian; target identification

**NOTES:** SE = Subelement (codes); MA = Mission Area; JMA = Joint Mission Area (codes); CT = Critical Technology (codes)  
See Glossary for numbered codes and other abbreviations.

### SSC San Diego FY 98 ILIR Database (contd)

SSC SD PROJ #	DTIC DN#	Project Title	Principal Investigator	SSC SD Code		ONR SE#	DoD MA1	DoD MA2	JMA	DoD CT	FY 97 \$K	FY 98 \$K	Planned FY 99 \$K	Keywords
ZU63	307786	Development and Analysis of Turbo Codes for Navy Applications	Dr. B. E. Wahlen	D855		14	CCC		4	6	0	105	105	forward error correction; turbo codes; trellis-coded modulation
ZU64	307787	Using IMPORT to Implement Complex Behaviors in Simulations	J. W. Wallace	D44201		15	CCC		4	7	0	187	0	modeling and simulation forces

**NOTES:** SE = Subelement (codes); MA = Mission Area; JMA = Joint Mission Area (codes); CT = Critical Technology (codes)  
See Glossary for numbered codes and other abbreviations.

### SSC San Diego FY 99 ILIR Database

SSC SD PROJ #	DTIC DN#	Project Title	Principal Investigator	SSC SD Code	ONR SE#	DoD MA1	DoD MA2	JMA	DoD CT	FY 97 \$K	FY 98 \$K	Planned FY 99 \$K	Keywords
ZU54	307777	3-D Propagation in Shallow Water Overlaying an Elastic Bottom	Dr. A. T. Abawi	D881	14	ASW	OSV	2	19	0	80	75	propagation; parabolic equation model; coupled mode
ZU78	308521	Detection of Ionic Nutrients in Aqueous Environments Using Surface-Enhanced Raman Spectroscopy (SERS)	Dr. P. A. Boss	D363	13	MWT		8	12	0	0	95	sensors; surface-enhanced Raman spectroscopy
ZU69	308519	Public-Key Cryptosystems Based on Groups on Elliptic Curves	Dr. V. P. Broman	D712	15	CCC		4	7	0	0	110	cryptosystems; public key; elliptic curve; discrete logarithm; cryptanalysis
ZU55	307778	Environmentally Adaptive Autonomous Matched-Field Tracking	Dr. H. P. Bucker	D881	14	OSV	ASW	3	19	0	68	70	underwater sound; signal processing
ZU79	308522	Frequency-Mixing in Nonlinear Dynamic Devices	Dr. A. R. Bulsara	D364	14	CCC		4	6	0	0	80	heterodyne signal; nonlinear device; target frequency
ZU72	308510	Geolocation Error Modeling and Reduction	Dr. S. I. Chou	D73A	14	INT	ELW	4	19	0	0	75	time difference of arrival; time of arrival; constant pulse repetition interval
ZU73	308513	In-Fiber Polarizers Using Blazed Fiber Gratings	D. Evans	D746	11	CCC		3	6	0	0	80	fiber optics
ZU57	307780	Anti-Ice Coatings: New Low Surface Free Energy Coatings for Easy Ice-Release	Dr. R. D. George	D361	13	MOB		8	17	0	90	35	polymers; coatings; ice-release; environmental; anti-ice
ZU58	307781	Deduction in Data Fusion Based upon Algebraic Representation of Probabilistic Models	Dr. I. R. Goodman	D4223	14	CCC		4	6	0	185	115	data fusion; expectation of random sets; generalized estimation; relational event algebras
ZU80	308516	Coherent Mid-IR Optical Parametric Oscillator	Dr. F. E. Hanson	D853	11	AAW		3	19	0	0	110	lasers; nonlinear optics; laser radar
ZU53	306770	Exact Diagonalization of Large Sparse Matrices	Dr. C. Hicks	D364	11	MWT	CCC	4	6	27	40	35	high-performance computing; large matrix diagonalization
ZU74	308509	Evaporation Duct Assessment from Meteorological Buoys	H. V. Hitney	D883	21	OSV		3	19	0	0	85	radar; evaporation ducting; propagation
ZU75	308527	Floating Antenna Propagation	B. R. Hunt	D7303	21	ELW	INT	4	10	0	0	100	RF propagation; floating antennas

**NOTES:** SE = Subelement (codes); MA = Mission Area; JMA = Joint Mission Area (codes); CT = Critical Technology (codes)  
See Glossary for numbered codes and other abbreviations.

### SSC San Diego FY 99 ILIR Database (contd)

SSC SD PROJ #	DTIC DN#	Project Title	Principal Investigator	SSC SD Code	ONR SE#	DoD MA1	DoD MA2	JMA	DoD CT	FY 97 \$K	FY 98 \$K	Planned FY 99 \$K	Keywords
ZU84	308530	Speech Enhancement	R. R. Johnson	D44213	15	CCC		4	6	0	0	150	speech enhancement; noise reduction
ZU35	305529	Parallel Sparse Factorizations through Recursive Bordered Block Diagonalization	Dr. A. K. Kevorkian	D714	14	MWT		3	22	99	84	35	least squares; sparse matrices; indefinite systems; linear and nonlinear programming
ZU48	306760	Propwash/Wake Resuspension in San Diego Bay—The Grand Plan	D. M. Ladd	D363	23	FSO	MWT	8	12	76	80	90	critical shear stress; resuspension
ZU66	308507	Integration of Complex Information	D. Lange	D4221	15	CCC		3	6	0	0	64	hypermedia; knowledge base; plan
ZU70	308511	Wireless Network Resource Allocation with QoS Guarantees	S. K. Lopic	D882	21	CCC		3	6	0	0	110	communications; wireless networks
ZU81	309260	Electronic Properties of Cubic Boron Nitride	Dr. W. C. McGinnis	D364	21	MWT		3	9	0	0	55	semiconductors; electronics
ZU71	308514	Applications of Stochastic Nonlinear Dynamics to Communication Arrays	Dr. B. K. Meadows	D02P	14	CCC		3	6	0	0	60	command and communications; nonlinear dynamics; stochastic
ZU67	308520	Innovative Methods for Alertness Management	S. A. Murray	D374	15	CCC		4	15	0	0	98	alertness; human factors; human-computer interaction; psychophysiology
ZU82	308524	Laser Optical Parametric Oscillator for mid-IR	J. Myers	D743	11	CCC		3	6	0	0	100	laser; optical; oscillator
ZU59	307782	High-Isolation Fiber-Optic Add/Drop Multiplexers for Shipboard Networking Applications	R. J. Orazi	D895	11	CCC		4	6	0	90	94	wavelength division multiplexing; Bragg gratings; fused fiber couplers
ZU61	307784	Telesonar Transmission Channel Modes	J. A. Rice	D881	11	CCC		4	19	0	105	115	underwater acoustic propagation; transmission channels; propagation models; telesonar; sound scattering
ZU83	308518	Sensitivity of Marine Mammals to Low-Frequency Acoustic Pressure and Particle Motion	Dr. S. H. Ridgway	D3503	31	ASW	MIW	3	19	0	0	60	marine mammals; acoustics; particle motion
ZU68	309262	Robust Control of Information-Flow for Network-Centric Warfare	Dr. S. Sritharan	D73H	15	CCC		4	6	0	0	125	C4I; network-centric warfare; optimal control; information

**NOTES:** SE = Subelement (codes); MA = Mission Area; JMA = Joint Mission Area (codes); CT = Critical Technology (codes)  
See Glossary for numbered codes and other abbreviations.

### SSC San Diego FY 99 ILIR Database (contd)

SSC SD PROJ #	DTIC DN#	Project Title	Principal Investigator	SSC SD Code		ONR SE#	DoD MA1	DoD MA2	JMA	DoD CT	FY 97 \$K	FY 98 \$K	Planned FY 99 \$K	Keywords
ZU76	308523	Advanced Hyperspectral Data Processing	Dr. S. Stewart	D743		14	MWT		3	19	0	0	90	hyperspectral data; data processing; stochastic; linear unmixing; detection
ZU77	308532	Super Composite Slotted Cylinder Projector	Dr. P. Y. Tang	D746		11	ASW		3	19	0	0	100	laminated composite materials; actuator; active materials; wall-driven projector; slotted cylinder projector
ZU63	307786	Development and Analysis of Turbo Codes for Navy Applications	Dr. B. E. Wahlen	D855		21	CCC		4	6	0	0	105	forward error correction; turbo codes; trellis-coded modulation

**NOTES:** SE = Subelement (codes); MA = Mission Area; JMA = Joint Mission Area (codes); CT = Critical Technology (codes)  
See Glossary for numbered codes and other abbreviations.



## GLOSSARY

AC	Alternating Current
A/D	Add/Drop
ADCP	Acoustic Doppler Current Profiler
AMGSSS	Air-Mobile Ground Surveillance and Security System
AMLCD	Active-Matrix Liquid Crystal Device
AODS	All-Optical Deployable System
APL	Applied Research Laboratory
Ar	Argon
AR	Antireflection
ASA	Acoustical Society of America
ASTO	Advanced Submarine Technology Office
ASW	Antisubmarine Warfare
ATM	Asynchronous Transfer Mode
Au	Gold
BISC	Berkeley Information and Soft Computing
BMPO	Ballistic Missile Defense Organization
btsp	Bistatic Target-Strength Prediction
C	Carbon
C <sup>4</sup> I	Command, Control, Communications, Computers, and Intelligence
CAOTA	Common All-Optical Towed Array
CBF	Conventional Beamformer
CCD	Charge-Coupled Device
CFD	Computational Fluid Dynamics
CMPE	Coupled Mode Parabolic Equation
COTS	Commercial Off-the-Shelf
CPA	Closest Point of Approach
CPM	Continuous Phase Modulation
CPU	Central Processing Unit
CRADA	Cooperative Research and Development Agreement
CRT	Cathode Ray Tube
CSCT	Consortium for Site Characterization Technology
CTD	Conductivity, Temperature, and Depth
Cu	Copper
CW	Continuous Wave
DARPA	Defense Advanced Research Projects Agency
DC	Direct Current
DDR&E	Director, Defense Research and Engineering
DFE	Decision Feedback Equalizer
DISA	Defense Information Systems Agency
DMD	Digital Mirror Device
DMRG	Density Matrix Renormalization Group
DoD	Department of Defense

DoD CT	Department of Defense Critical Technology
Codes	
1	Aerospace Propulsion and Power
2	Air Vehicles
3	Space Vehicles
4	Chemical and Biological Defenses
5	Clothing, Textiles, and Food
6	Command, Control, and Communications
7	Computers
8	Conventional Weapons
9	Electronics
10	Electronic Warfare
11	Directed Energy Weapons
12	Environmental Quality
13	Civil Engineering
14	Battlespace Environments
15	Human-System Interfaces
16	Manpower, Personnel, and Training
17	Materials, Processes, and Structures
18	Biomedical
19	Sensors
20	Surface/Undersurface Vehicles
21	Ground Vehicles
22	Software
23	Manufacturing Science and Technology
24	Simulation and Modeling Technology

DoD MA	Department of Defense Mission Area
AAW	Anti-Air Warfare
AMW	Amphibious Warfare
ASU	Anti-Surface Ship Warfare
ASW	Anti-Submarine Warfare
CCC	Command, Control, and Communications
ELW	Electronic Warfare
FSO	Fleet Support Operations
INT	Intelligence
LOG	Logistics
MIW	Mine Warfare/Mine Countermeasures
MOB	Mobility
MWT	Multi-Warfare Technology
OSV	Ocean Surveillance
PMD	Personnel/Medical
SBS	Sea-Based Strategic Warfare
SPW	Special Warfare
STW	Strike Warfare
TNG	Training

DOE	Department of Energy
DOME	Declarative Object Management Environment
DSP	Digital Signal Processors
EA	Electroabsorption
EHF	Extremely High Frequency
EMI	Electromagnetic Interference
EPA	Environmental Protection Agency
EW	Electronic Workstation
FFT	Fast Fourier Transform
FTRT SF	Faster Than Real-Time Synthetic Forces
FWHM	Full Width at Half Maximum
FY	Fiscal Year
GOTS	Government-Off-The-Shelf
GPS	Global Positioning System
HDR	High Data Rate
HF	High Frequency
HLA	Horizontal Line Array
HOC	Higher Order Crossing
HPCMP	High Performance Computing Modernization Program
IEEE	Institute of Electrical and Electronic Engineers
IFOG	Interferometric Fiber-Optic Gyroscope
ILIR	In-house Laboratory Independent Research
IMA	Institute of Mathematics and its Applications
IMPORT	Integrated Modular Persistent Objects and Relations Technology
INTL	Interleaver Length
IRST	Infrared Search and Track
ISAR	Inverse Synthetic Aperture Radar
ISCAS	International Symposium on Circuits and Systems
ISI	Intersymbol Interference
ISnAP	Impulsive Snap-through Acoustic Projector
ITRC	Interstate Technology Regulatory Cooperation
JIEO	Joint Interoperability Engineering Organization
JMA	Joint Mission Area
Codes	
1	Joint Strike
2	Joint Littoral Warfare
3	Joint Surveillance
4	Joint Space and Electronic Warfare/Intelligence
5	Strategic Deterrence
6	Strategic Sealift and Protection

7	Forward Presence
8	Readiness, Support, and Infrastructure
9	Manpower and Personnel
JNTF	Joint National Test Facility
JPL	Jet Propulsion Laboratory
JSIMS	Joint Simulation System
KDP	Potassium Dehydrogen Phosphate
LAPACK	Linear Algebra PACKage
LFM	Linear Frequency Modulated
LIF	Laser-Induced Fluorescence
MAI	Multiple-Access Interference
MFP	Matched-Field Processing
MFT	Matched-Field Tracking
mJ	milliJoules
MMIC	Monolithic Microwave Integrated Circuit
MMWS	Multi-Modal Watch Station
MSE	Mean-Square Error
NASA	National Aeronautics and Space Administration
NAVSEA	Naval Sea Systems Command
NAVSTA	Naval Station
NCSC	Naval Coastal Systems Center
Nd	Neodymium
Nd:YAG	Neodymium: Yttrium Aluminum Garnet
Ni	Nickel
NP	New Professional
NRL	Naval Research Laboratory
NUWC	Naval Undersea Warfare Center
OCFSS	Optoelectronically Controlled Frequency-Selective Surface
OCW	Optoelectronically Controlled Waveguide
ONR	Office of Naval Research
ONR SE	Office of Naval Research Subelement
Codes	
11	General Physics
12	Radiation Sciences
13	Chemistry
14	Mathematics
15	Computer Science
21	Electronics
22	Materials
23	Mechanics

24	Energy Conversion
31	Ocean Sciences
32	Ocean Geophysics
33	Atmospheric Sciences
34	Astronomy and Astrophysics
35	Environmental Science
41	Biological and Medical Sciences
42	Cognitive and Neural Sciences
52	Multidisciplinary Support
OSDS	Oil Spill Detector System
PCTCM	Parallel Concatenated Trellis-Coded Modulation
Pd	Palladium
PDES	Parallel Discrete Event Simulation
PDLC	Polymer-Dispersed Liquid Crystal
PE	Parabolic Equation
PID	Photo Ionization Detector
PINC	Polarization Independent Narrow Channel
PLL	Phase-Locked Loop
Pt	Platinum
PTCM	Pragmatic Trellis-Coded Modulation
PVFET	Photovoltaic Field-Effect Transistor
PWC	Public Works Center
QPSK	Quadrature Phase Shift Keying
QVI	Quasi-Variational Inequalities
RF	Radio Frequency
RSC	Recursive Systematic Convolutional
SAIC	Science Applications International Corporation
SAM	Self-Assembled Monolayers
SAW	Surface Acoustic Wave
SBIR	Small Business Innovation Research
SCAPS	Site Characterization and Analysis Penetrometer System
SCS	Society for Computer Simulation
SERS	Surface-Enhanced Raman Spectroscopy
SIO	Scripps Institution of Oceanography
SITE	Superfund Innovative Technology Evaluation
S/N	Signal to Noise
SNR	Signal-to-Noise Ratio
SPAWAR	Space and Naval Warfare
SPEEDES	Synchronous Parallel Environment for Emulation and Discrete-Event Simulation

SPIE	Society of Photo-Optical Instrumentation Engineers (also known as the International Society for Optical Engineering)
SR	Stochastic Resonance
STOW	Synthetic Theater of War
SUBASE	Submarine Base
SURTASS	Surveillance Towed Array Sensor System
SWellEX	Shallow-Water Environmental Cell Experiment
SW/VSW	Shallow Water and Very Shallow Water
TCM	Trellis-Coded Modulation
TCPTCM	Turbo-Coded Pragmatic TCM
TCTCM	Turbo-Coded TCM
UCSD	University of California, San Diego
UME	Ultramicroelectrode
USC	University of Southern California
USEPA	U.S. Environmental Protection Agency
UV	Ultraviolet
VLA	Vertical Line Array
VOC	Volatile Organic Compound
VSWR	Voltage Standing Wave Ratio
WDM	Wavelength Division Multiplexer
WS	Wargaming & Simulation
WWW	World Wide Web
YAG	Yttrium Aluminum Garnet

# REPORT DOCUMENTATION PAGE

*Form Approved*  
OMB No. 0704-0188

Public reporting burden for this collection of information is estimated to average 1 hour per response, including the time for reviewing instructions, searching existing data sources, gathering and maintaining the data needed, and completing and reviewing the collection of information. Send comments regarding this burden estimate or any other aspect of this collection of information, including suggestions for reducing this burden, to Washington Headquarters Services, Directorate for Information Operations and Reports, 1215 Jefferson Davis Highway, Suite 1204, Arlington, VA 22202-4302, and to the Office of Management and Budget, Paperwork Reduction Project (0704-0188), Washington, DC 20503.

1. AGENCY USE ONLY <i>(Leave blank)</i>	2. REPORT DATE  April 1999	3. REPORT TYPE AND DATES COVERED <b>Final: October 1997 through September 1998</b>	
4. TITLE AND SUBTITLE <b>SSC SAN DIEGO IN-HOUSE LABORATORY INDEPENDENT RESEARCH 1998 ANNUAL REPORT</b>		5. FUNDING NUMBERS  In-house	
6. AUTHOR(S)		8. PERFORMING ORGANIZATION REPORT NUMBER	
7. PERFORMING ORGANIZATION NAME(S) AND ADDRESS(ES)  SSC San Diego San Diego, CA 92152-5001		10. SPONSORING/MONITORING AGENCY REPORT NUMBER  TD 3049	
9. SPONSORING/MONITORING AGENCY NAME(S) AND ADDRESS(ES) Office of Naval Research 800 North Quincy Street Arlington, VA 22217-5000		11. SUPPLEMENTARY NOTES	
12a. DISTRIBUTION/AVAILABILITY STATEMENT  Approved for public release; distribution is unlimited.		12b. DISTRIBUTION CODE	
13. ABSTRACT <i>(Maximum 200 words)</i>  The work detailed in this report was carried out in FY 98 as part of the Office of Naval Research In-house Laboratory Independent Research (ILIR) program.  Summaries of the projects are presented, and three projects are described in detail: Development of Ultramicroelectrode (UME) Arrays for Use in a Remote Probe; Underwater Acoustic Array Processing in High-Slope Shallow-Water Environments; and A New Sparse Complete Orthogonal Factorization Method as Applied to Bistatic Target-Strength Prediction.			
14. SUBJECT TERMS AND MISSION AREAS  In-house Laboratory Independent Research (ILIR) command and control                      communications intelligence, surveillance, and reconnaissance                      other leadership areas			15. NUMBER OF PAGES  182
17. SECURITY CLASSIFICATION OF REPORT  UNCLASSIFIED			16. PRICE CODE
18. SECURITY CLASSIFICATION OF THIS PAGE  UNCLASSIFIED	19. SECURITY CLASSIFICATION OF ABSTRACT  UNCLASSIFIED	20. LIMITATION OF ABSTRACT  SAME AS REPORT	

## AUTHOR INDEX

<b>Code</b>	<b>Contributor</b>	<b>Page</b>	<b>Code</b>	<b>Contributor</b>	<b>Page</b>
D881	Abawi, Ahmad T.	90	D363	Mautner, Tom	97
D743	Barnett, John T.	79	D895	Orazi, Richard J.	66
D881	Baxley, Paul A.	19	D855	Reuter, Michael	56
D363	Boss, Pamela A.	7	D881	Rice, Joseph A.	72
D881	Bucker, Homer P.	81	D363	Rohr, James J.	106
D364	Bulsara, Adi R.	53	D853	Russell, Stephen D.	103
D7102	DeJaco, Jerome F.	93	D721	Schwartz, David F.	69
D4223	Freund, Richard F.	49	D351	Sigurdson, John E.	109
D361	George, Robert D.	100	D895	Sun, Chen-Kuo	62
D44215	Goodman, I. R.	43	D73H	Trischman, Jay	86
D853	Hanson, Frank E.	83	D855	Wahlen, Bruce E.	59
D3604	Hicks, Charles	113	D44201	Wallace, Jeffrey W.	48
D714	Kevorkian, Aram K.	31			

## EXTERNAL DISTRIBUTION

Air Force Office of Scientific Research  
Bolling AFB, DC 20332-0001

Center for Naval Analysis  
Alexandria, VA 22302-0268

Coastal Systems Station  
Panama City, FL 32407-7001

Defense Advanced Research  
Projects Agency  
Arlington, VA 22203-1700

Defense Research and Engineering (3)  
Washington, DC 20301-3030

Defense Technical (2)  
Information Center  
Fort Belvoir, VA 22060-6218

Deputy Assistant Secretary of the Navy  
Washington, DC 20350-1000

Federal Contracts Research Center  
Ft. Monmouth, NJ 07703-5027

Government-Industry Data Exchange  
Program (GIDEP) Operations Center  
Corona, CA 91718-8000

Naval Air Warfare Center  
Aircraft Division  
Patuxent River, MD 20670-1161

Naval Air Warfare Center  
Weapons Division  
China Lake, CA 93555-6001

Naval Facilities Engineering Service Center  
Port Hueneme, CA 93043-4370

Naval Medical Research and  
Development Command  
Bethesda, MD 20889-5606

Navy Personnel Research and  
Development Center  
San Diego, CA 92152-6800

Naval Postgraduate School (6)  
Monterey, CA 93943-5001

Naval Research Laboratory  
Washington, DC 20375-5320

Naval Sea Systems Command  
Arlington, VA 22242-5160

Naval Surface Warfare Center  
Arlington, VA 22242-5160

Naval Surface Warfare Center  
Carderock Division  
West Bethesda, MD 20817-5700

Naval Surface Warfare Center  
Carderock Division Detachment  
Annapolis, MD 21402-1198

Naval Surface Warfare Center  
Dahlgren Division  
Dahlgren, VA 22448-5100

Naval Undersea Warfare Center  
Newport, RI 02841-1708

Naval Undersea Warfare Center Division  
Newport, RI 02841-5047

Navy Acquisition, Research and Develop-  
ment Information Center (NARDIC)  
Arlington, VA 22214-5114

Office of Naval Research (24)  
Arlington, VA 22217-5660

Office of the Secretary of Defense (4)  
Washington, DC 20301-8000

Space and Naval Warfare Systems (2)  
Command  
San Diego, CA 92110-3127

SSC San Diego Liaison Office  
Arlington, VA 22202-4804

U.S. Army Laboratory Command  
Ft. Monmouth, NJ 07703-5302

U.S. Naval Academy  
Annapolis, MD 21402-5000



TD 3049  
April 1999

SSC San Diego  
San Diego, CA 92152-5001

Approved for public release;  
distribution is unlimited.